Attractor dynamics in perceptual decision making: from theoretical predictions to psychophysical experiments

Genís Prat Ortega

Attractor dynamics in perceptual decision making: from theoretical predictions to psychophysical experiments

Tesis doctoral.

Programa de doctorat en Matemàtiques,

Universitat Autònoma de Barcelona

Genís Prat Ortega

Directors Tutor

Jaime de la Rocha Alex Roxin Tomás Alarcón

Setembre 2019

Agraïments

M’agradaria agrair als meus supervisor, el Jaime i l’Alex, pel seu suport durant tots aquests anys i al Klaus que ha estat involucrat en la meva tesis desde el primer dia.

També m'agradaria agrair al Tobias i al Niklas per ajudar-me a realitzar els experiments del capítol 4.

A tots els companys del IDIBAPS, CRM i UKE que m’han fet la vida molt més fàcil.

També els meus pares i la meva germana, que sempre, sempre estan allà i mai fallen!

Table of contents

Summary

From time to time humans and animals must respond to a certain stimulus that can be ambiguous. In the old days, before the creation of video assistant referee, football referees had a very hard life. One of the most popular plays in football history is the so-called "La mano de dios" where Maradona used his hand to score a goal in the quarter-final match of the 1986 World Cup. Based on what he saw, the referee incorrectly decided that Maradona had not touched the ball with his hand and Argentina ended up winning the World Cup. The decisions based on external stimuli (in this case visual) are what we call perceptual decision making.

In this thesis, we studied how the brain makes perceptual decisions in experimental settings where subjects have to make a categorical decision about a certain feature of the presented stimulus. We studied the case where the stimulus is presented for a certain time controlled by the experimenter. During the stimulus presentation, the subjects have to accumulate evidence and when the stimulus ends, they need to choose between two possible alternatives. These experiments are typically called 2-alternative forced choice tasks (2AFC).

From a computational point of view the accumulation of stimulus evidence in 2AFC tasks has been studied intensively in the last decades. Canonical approaches to model this cognitive function are based on diffusion processes that assume bounded or unbounded perfect stimulus evidence accumulation. However, the relationship of such models with the underlying neural circuitry is unclear. In this thesis, we study the accumulation process in neurobiological models with attractor dynamics. Such models can actually be reduced to a nonlinear diffusion process, which in the case of binary categorizations can be described by a double well potential (DW). Despite the fact that the canonical and the neurobiological models rely on different mechanisms, they can account for various behavioral aspects such as performance or reaction time.

The first aim of this thesis was to derive behaviourally testable predictions of attractor dynamics during a 2AFC task and compare them with models that assume other kinds of dynamics (e.g. perfect integration). We found two signatures of attractor dynamics that can be tested in behavioural experiments. Specifically, we found that: 1) The DW model had

different integration regimes, from transient (primacy) to leaky (recency) as the magnitude of the stimulus fluctuations (σ_s) or the stimulus duration (T) increased and 2) the DW had a non-monotonic relation between the accuracy and the stimulus fluctuations.

The second final aim of this thesis is to qualitatively and quantitatively test the existence of attractor dynamics. To this aim, we designed an experiment where we systematically modified the magnitude of the stimulus fluctuations. Qualititatively, we could not identify obvious signatures of attractor dynamics that allow us to distinguish between different models. However, we quantitatively assessed the attractor dynamics and other plausible neural mechanisms by developing a model-based analysis. Preliminary results suggest that attractor dynamics can be important to explain the behavioural results in at least a fraction of subjects.

1. Introduction

I would like to start my thesis with an insight: humans make decisions. Some of them are important, whereas others are less important. For example, today while I was writing this paragraph I made a critical decision for my life: I decided that it was time to clean up the blankets that were on a chair in my bedroom for the last three months. It is funny because today (September 6, 2019) was the first day during these three months that it was actually a little bit chilly at night. But do not blame me, humans do not make optimal decisions (Barth, Cordes, and Patalano 2018), or maybe they do (Brunton, Botvinick, and Brody 2013), who knows? Well, I should probably stop procrastinating and start writing the introduction.

Spain has not had a government since the last elections in April. Today, two parties that in principle want to implement similar progressive policies are negotiating to form it. It seems, however, that they will not reach an agreement before the deadline to call for new elections. If this finally happens, many former voters from the two parties are going to vote for the party that they consider is not responsible for this disaster. Thus, they will have to decide based on very little and manipulated information which of the two parties is more responsible for not reaching an agreement. Although studying this type of decision is a very interesting problem, it is not well suited for studying how brain circuits carry out these computations because voters can base their decision on multiple sources of information which are hard to control experimentally. In contrast, in perceptual decision making, subjects must base their decisions on sensory information that is completely controlled by the experimenter. A famous experiment is the motion discrimination task where subjects must decide if a cloud of dots is moving towards the right or the left. Because experimenters can control all the details of the stimuli, the subject's responses, etc, we can try to infer how the brain is using these stimuli to make a choices.

The canonical approaches to model perceptual decision making describe the dynamics of the decision process with a simple heuristical linear equation. In contrast, biophysical attractor models are complex and high dimensional but they explain the dynamics of the decision process based on realistic neural circuits. Here, we explain that attractor biophysical models can be reduced to a one dimensional nonlinear equation. The main goal of the thesis is to find experimentally testable signatures of non-linear attractor dynamics in perceptual

decision making and test them in a psychophysical experiment. To analyze the psychophysical experiments, we are extending the attractor models to include different plausible neural mechanisms and we are developing a fitting procedure to fit all these mechanisms by maximum likelihood.

In this introduction, we first summarize the canonical and biophysical models for perceptual decision making. Then, we explain what a psychophysical kernel is and why it is important for understanding how the brain uses the stimulus to make decisions. Finally, we discuss why the findings of our work are important.

Canonical models of perceptual decision making

In perceptual decision making, the standard approaches to model the dynamics of sensory evidence accumulation during two alternative forced choice tasks (2AFC) are one-dimensional drift diffusion processes. Specifically, the diffusion process describes the dynamics of the decision variable (X). This decision variable represents the moment-by-moment evidence for one alternative over the other. The mean sensory evidence is generally modeled as a constant drift in this integration which also has a noise term, reflecting fluctuations in the sensory input and internal noise in the decision process. We define the canonical models as three drift diffusion models with different boundary mechanisms: 1) The drift diffusion model with absorbing boundaries (DDMA) integrates the stimulus evidence until the decision variable reaches an absorbing boundary. 2) The drift diffusion model with reflecting bounds (DDMR) integrates the stimulus evidence with an upper limit to the accumulated evidence for one of the choices imposed 3) The perfect integrator (PI) perfectly integrates the stimulus evidence without bounds. In the three models, the choice is given by the sign of the decision variable at the end of the trial (figure 1a). The decision variable X therefore obeys the simple stochastic equation

$$\tau \frac{dX}{dt} = \mu + \sigma\xi(t) \qquad (1)$$

where μ is the drift and σ is the standard deviation of the noise, modeled as Gaussian stochastic process ξ with zero mean, unit variance and without temporal correlations (white noise). For the purpose of this thesis, we separate the noise in two sources: 1) the internal noise (σ_i) produced by the intrinsic variability of neurons as and inputs to the decision circuit from other brain regions and 2) the stimulus fluctuations (σ_S), which are proportional

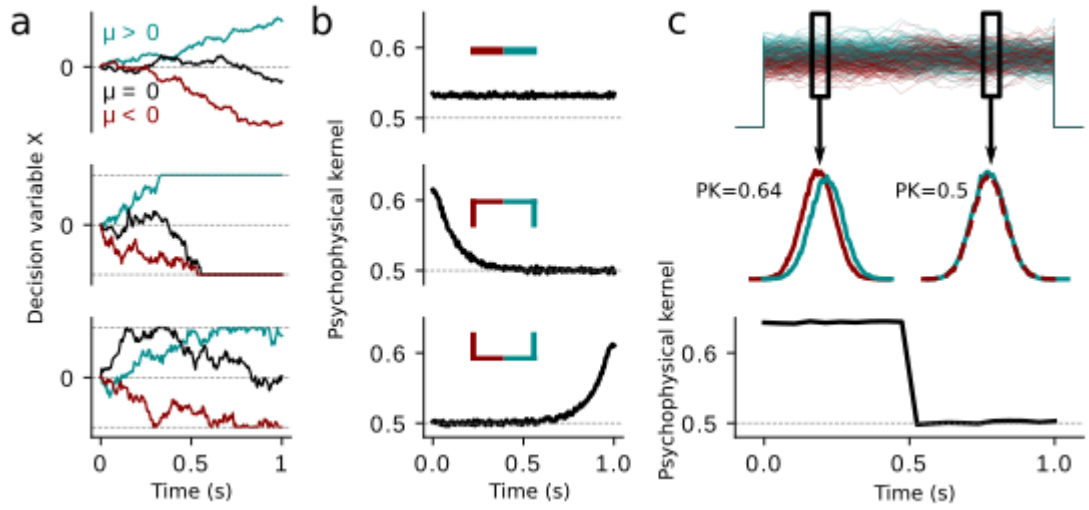

Figure 1 | Canonical models of perceptual decision making
a) Example of single traces of the decision variable for the canonical models: Top: in the perfect integration model the decision variable is simply the integral of the stimulus. Middle: The drift diffusion model with absorbing (DDMA) barrier perfectly integrates the evidence until it commits to a decision when the decision variable reaches one of the bounds. Bottom: The drift diffusion model with reflecting barrier perfectly integrates the evidence during the entire trial but the reflecting boundaries introduces an upper limit to the accumulated evidence towards one of the choices. **b)** Psychophysical kernels for the three diffusion models. Without bounds the model weights all the evidence equally. With bounds the model shows primacy for absorbing and recency for reflecting boundaries. **c)** Psychophysical kernel diagram for a toy model that perfectly integrates the evidence of the first half of the trial but it omits the second half. Top: In red (blue) stimuli that give rise to a left (right) choice. Note that in the first half of the trial, the blue stimuli tend to be positive whereas the red stimuli tend to be negative. This structure is lost in the second half. Middle: The distributions of the left and right stimuli during the first half are separable (area under the ROC curve 0.64) whereas during the second half, both distributions are equal.

to the variance of the stimulus and thus are controlled by the experimenters. We write the total noise as the sum of a stimulus-dependent term and internal noise: $\sigma\xi(t) = \sigma_S\xi_S + \sigma_I\xi_I$.

The dynamics in equation 1 can be recast as the motion of a particle in a potential $\varphi(X)$:

$$\tau \frac{dX}{dt} = -\frac{d\varphi}{dX} + \sigma\xi(t) \qquad (2)$$

where $\varphi(X) = -\mu X$ (figure 1a). The conceptual advantage of using a potential relies on the fact that, ignoring the noise term, the dynamics of the decision variable always leads the potential to decrease in time. Therefore, starting with an initial position on the potential, the

decision variable will always “roll downward” with only the noise fluctuations causing possible motion upward along the potential. For the canonical models described in equation 2, the potential is a linear ramp. In the case of absorbing boundaries, it has two vertical cliffs and for reflecting boundaries two vertical walls (figure 1b insets). It is worth noting that the form of the potential depends both on the properties of the stimulus and the intrinsic dynamics of the integration process itself. Specifically, the steepness of the linear ramp μ is just the mean evidence in favor of one of the two possible choices; it is therefore an exogenous parameter. On the other hand, the potential boundaries are a property of the intrinsic dynamics of the model and hence do not depend, in principle, on the stimulus. To explain the effect of the bounds in the decision process dynamics, we first need to define what a psychophysical kernel is.

Psychophysical kernel

In perceptual decision tasks, subjects make choices based on stimulus evidence. One of the goals in systems neuroscience is to reveal how the brain uses the stimulus evidence to guide our behaviour. A useful analytical tool for this purpose is the psychophysical kernel (PK) (Neri and Heeger 2002). In tasks where the stimulus duration is controlled by the experimenters, the PK measures the average time-course of the impact of stimulus fluctuations on choice. Classically, the PK has been computed by averaging the stimuli that give rise to a right and left choice separately and subtracting them (Roozbeh Kiani, Hanks, and Shadlen 2008; Okazawa et al. 2018). We are going to compute the PK as the temporal evolution of the separability between the stimulus distributions that give rise to left and right choices. This method has the advantage that the magnitude of the PK is interpretable and comparable between different experiments (see methods, figure 2). To illustrate how the PK works, we build a toy model that perfectly integrates the evidence of the first half of the stimulus but it omits the second half. For this simple example, the PK is able to recover the integration dynamics of the model (figure 1c).

In psychophysical experiments where the duration of the stimulus is controlled by the experimenters, three qualitative classes of PK have been mainly reported: primacy (Roozbeh Kiani, Hanks, and Shadlen 2008; Nienborg and Cumming 2009) or recency (Wyart, Myers, and Summerfield 2015; Cheadle et al. 2014) when the subjects tend to give more weight to early or late evidence and flat PK when the subjects equally weight the stimulus (Brunton, Botvinick, and Brody 2013). The PK is a powerful analytical tool and it can be

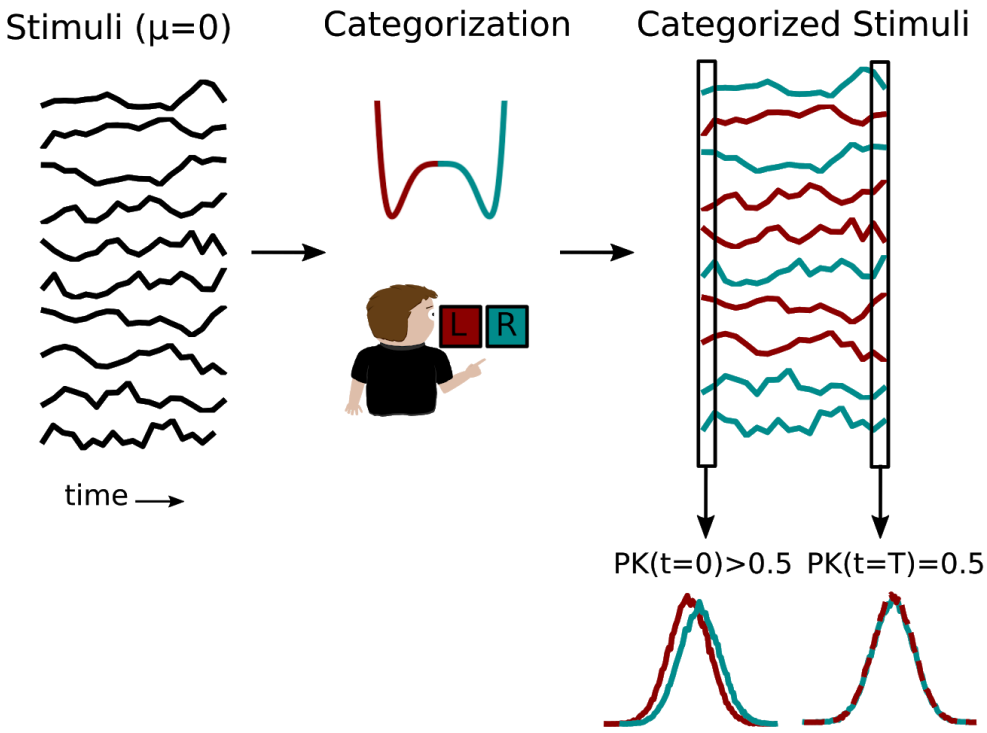

Figure 2 | Psychophysical kernel method
First the stimuli are categorized by the model or by a subject, then we compute the distribution for left and right stimuli in each frame. The psychophysical kernel is the temporal evolution of the separability between the right and left stimuli. We compute this separability with the area under the ROC curve.

useful for different analysis. For instance, it has been used to study the temporal evolution of the stimulus fluctuations impact in confidence choices (Zylberberg, Barttfeld, and Sigman 2012). Other studies have used the PK to postulate their hypothesis. For example in (Wimmer et al. 2015), the authors propose top-down signals as a possible mechanism to explain primacy PK but constant choice probabilities in sensory areas. In another study, PK from high and low confidence trials have been used to compare different models (Kawaguchi et al. 2018). Finally, in a more recent study, PKs were used to show that rats can optimally discount information in a dynamic environment where the old information may no longer be relevant of the state of the world (Piet, El Hady, and Brody 2018).

All these examples show the potential of the PK to reveal the dynamics of the decision making process, but the limitations of the PK have also been pointed out in (Okazawa et al. 2018). For example, the PK reflects both sensory and decision dynamics processes and they can not be distinguished with the PK. Thus, a PK showing primacy can be explained by adaptation in sensory neurons (Yates et al 2017) or by decision related mechanisms such as

the accumulation to bound (Yates et al. 2017; Wimmer et al. 2015; Roozbeh Kiani, Hanks, and Shadlen 2008).

Here, we are going to use the PK to understand how the statistical properties of the stimulus and the model parameters can change the dynamics of the decision making process. We start by explaining the impact of the decision boundaries in the canonical models on the PK.

Psychophysical Kernel for the canonical models

In the canonical models described above, the differences in the intrinsic dynamics introduced by imposing absorbing or reflecting bounds, or removing the bounds altogether, strongly influence the way the stimulus impacts the upcoming decision. Using the PK, we can unequivocally characterize the integration dynamics resulting from each of the canonical models: 1) the perfect integrator for which there are no bounds (figure 1a, top), 2) the DDM with absorbing boundaries (figure 1a, middle) and 3) the DDM with reflecting boundaries (figure 1a, bottom). In the case of the perfect integrator, the stimulus fluctuations are weighted equally during the entire duration of the trial, leading to a flat PK (figure 1b, top). When there are absorbing boundaries fluctuations late in the trial are unlikely to affect the decision and therefore the PK shows a “primacy” effect (figure 1b, middle). On the other hand, a “recency” effect is seen when boundaries are reflecting because early fluctuations are largely forgotten once a boundary is reached (figure 1b, bottom).

Drift diffusion model with absorbing bounds: the standard cognitive model

Canonical models such as the DDM have proven very successful in fitting key features of animal behavior in perceptual decision making tasks. The most common diffusion model is the version with absorbing bounds (DDMA). The bounds provide a mechanism to commit to a decision which it is useful to model reaction time tasks. In this type of task, the stimulus is present until subjects make a choice. The reaction time is the time from the stimulus onset until the decision is made.

The DDMA can be viewed as an implementation of the sequential probability ratio test (Wald and Wolfowitz 1948). This test minimizes the number of random variables that need to be observed to distinguish the true generative distribution between two possible options with a certain level of accuracy controlled by the bounds. For each observed random variable, the

decision variable is updated with the difference between the log-likelihood of the two alternatives until the decision variable reaches the upper or the lower bound. In the DDMA, the decision variable is updated at each time step with the instantaneous evidence from the stimulus until the decision variable reaches one of the bounds. The two processes are equivalent if the stimulus is the difference between the log-likelihoods probabilities of the left and right choices.

Thus in the DDMA, larger bounds produce more accurate but slower decisions. This property makes the DDMA a suitable model to study the speed-accuracy trade-off. It has been shown that under time pressure, subjects can trade accuracy for speed, something that can be accounted for in the DDM by decreasing the bounds (Duncan Luce 1991; Smith and Ratcliff 2004).

One of the great advantages of the DDM is that, due to its simplicity (e.g. the small number of parameters) it can easily be fitted to reproduce the responses of a subject (Ratcliff and Rouder 1998; Ratcliff and Tuerlinckx 2002). In order to correctly fit the accuracy and reaction time distributions (for Reaction Time tasks) for error and correct trials with the DDMA, we need to add two extra parameters. The first one is a non-decision time that models the stimulus encoding time. It is an additive lag parameter that is added to the diffusion reaction time. The second one is a bias in the starting point which is the value of the decision variable before the stimulus onset. In addition, we also need to introduce trial-to-trial variability in three different parameters: 1) the drift rate (μ) which produces longer reaction times for error trials (Ratcliff 1978) 2) the starting point which produces faster reaction time in errors trials (Ratcliff and Rouder 1998) and 3) the non-decision time which helps to fit the distributions of reaction times (Ratcliff and Tuerlinckx 2002). An urgency signal mechanism (e.g. collapsing bounds or a gain parameter) has also been proposed as a possible mechanism to account for the reaction time distributions (Drugowitsch et al. 2012; Thura et al. 2012) but see also (Hawkins et al. 2015).

Although the absorbing bounds are a mechanism originally proposed to capture the moment in which subjects commit to a decision in reaction time tasks, the DDMA has also been applied in fixed duration task (Roozbeh Kiani, Hanks, and Shadlen 2008). Consistent with the DDMA, in a motion discrimination task in which stimulus duration (T) is variable and monkeys have to wait for stimulus offset to respond, the accuracy increases with the square root of T for short trials but it plateaus when the trials are long enough (figure 4). For short

trials, the evidence is perfectly integrated because the decision variable never reaches the bounds. In this case, the accuracy increases with the square root of the T because the mean accumulated evidence increases with T whereas the standard deviation increases with the square root of T. For long stimuli, the decision variable reaches the bounds easily and the accumulation of evidence finishes before the stimulus. Consequently the accuracy tends to plateau (Roozbeh Kiani, Hanks, and Shadlen 2008).

The popularity of the DDMA has been growing in the last two decades. Not only because it can fit the accuracy and the mean reaction time but also because the activity of neurons in decision areas resembles a diffusion process with absorbing bounds. Various studies (Roitman and Shadlen 2002; Roozbeh Kiani, Hanks, and Shadlen 2008), have shown that the firing rate of neurons in several associative brain areas ramps up with the stimulus presentation and it plateaus after $400-500\ ms$. Similar to the bound in the DDMA, the saturation firing rate is independent of the stimulus strength. Nevertheless, the DDMA is still a cognitive model and it can not explain from a mechanistic point of view how the ramping and the plateaus of the firing rate are produced.

Despite this limitation, many studies have used the DDMA to perform model based analysis and try to relate the model parameters with different mechanisms. For instance, several experiments have shown that the drift, the non-decision time or the bounds can change with the age (Ratcliff, Thapar, and McKoon 2004; Thapar, Ratcliff, and McKoon 2003; Starns and Ratcliff 2010). Different mechanisms of bias such as an initial offset or an asymmetric drift rate have also been compared under the DDMA framework (Gold et al. 2008; Urai et al. 2019; Mulder et al. 2012). Finally, confidence judgements (Roozbeh Kiani, Corthell, and Shadlen 2014) or changes of mind (Resulaj et al. 2009) have been studied with different versions of the DDMA. For all these reasons, the drift diffusion model with absorbing barriers is the standard cognitive model in perceptual decision making because it is simple, can be easily fit to data and can be related to neuronal activity. However the relation between the DDMA and the neural mechanisms remains at best heuristic and biophysical models are needed to uncover the neural mechanisms underlying perceptual decision making.

Biophysical models of perceptual decision making

During the last two decades many studies have addressed the question of how a circuit made of neurons with a time constant of tens of milliseconds can give rise to cognitive

processes such as working memory or decision making which operate on a time scale of seconds (Amit and Brunel 1997; Compte et al. 2000; Brunel and Wang 2001; Wang 2002). In these studies, it has been proposed that this could be solved by strong recurrent connections mediated by NMDA receptors. For illustration purposes, let us study a simple linear network model with a single neural population described by its averaged firing rate *r*. Without recurrent connections, the firing rate decays with the synaptic time constant and its dynamics are governed by:

$$\tau_{syn}\frac{dr}{dt} = -r \qquad (3)$$

When we introduce recurrent connections the firing rate evolves according to the equation

$$\tau_{syn}\frac{dr}{dt} = -(1 - w_{rec})r \qquad (4)$$

The effective time scale of the network can be estimated by $\tau_{net} = \tau_{syn}/(1 - w_{rec})$ where w_{rec} is the strength of the recurrent connections. If the strength of the recurrent connections is $w_{rec} = 1$ then all the possible firing rates are stable and the system becomes a line attractor. In the case where $w_{rec} < 1$, the network evolves towards an attractor state of *r* =0 with the effective time constant τ_{net}. If we consider NMDA receptors with long synaptic time constants $(\tau_{syn} = 100\ ms)$ and $w_{rec} = 0.9$ the effective time scale is $\tau_{net} = 1s$ (Wang 2008; Goldman, Compte, and -J. Wang 2009).

A popular biophysical model for perceptual decision making with slow attractor dynamics was published in the early 2000s (Wang 2002). Wang's attractor network consists of two pools of excitatory spiking neurons and one pool of inhibitory spiking neurons. Each of the excitatory pools is selective to one of the possible choices and has strong recurrent connections (figure 3a). These two populations compete through the third pool of untuned inhibitory neurons. Before the stimulus presentation, the firing rate of the two excitatory

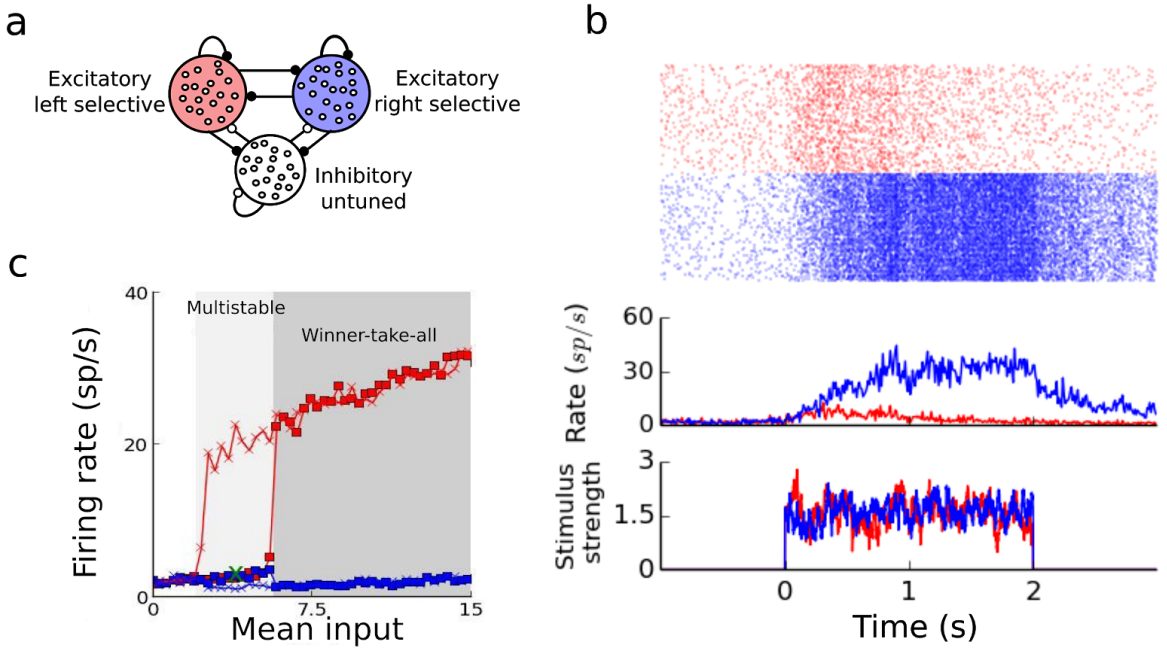

Figure 3 | Standard biophysical model for perceptual decision making

a) The standard biophysical model for perceptual decision making consists of two populations of excitatory neurons with strong recurrecnt activity and an untuned inhibitory population. Each of the excitatory population represents a possible choice and they compete through the inhibitory population. **b)** Example of a single trial in the biophysical network. Bottom: Each of the excitatory populations receives an input proportional to the instantaneous stimulus evidence for the choice that it represents. Middle: When the stimulus is presented the two excitatory populations start increasing their firing rate until one of them wins the competition and shuts down the other one. Top: Raster plot of each population of **c)** Stable Firing rates for the excitatory populations when we slowly increase (squares) or decrease (crosses) the mean input. Note that there are symmetric stable firing rate where the blue population win the competition in the winner-take-all regime (not shown).

populations is similar. With the stimulus presentation, the two excitatory populations receive an input proportional to the evidence for left or right choice according to its selectivity. The firing rate of both populations ramps up until one of the populations wins the competition. When the stimulus ends, the network is able to maintain the decision in working memory (figure 3b). To illustrate this dynamics, it is convenient to plot the rate of the stable states by slowly increasing and decreasing the mean input to the network (figure 3c). When we compute the stable states by increasing the inputs (squares in figure 3), the undecided stable state where the firing rates of both populations are similar becomes unstable for strong enough inputs. In contrast, when we compute the stable states by decreasing the inputs (crosses in figure 3c), the decision states disappear. Critically, they do not disappear for the same value of the input. As occurs in a system showing histeresis, there is a multistable region where the decision and the undecided states are both stable. Without the

stimulus Wang's attractor network is in the multistable region (green cross figure 3). With the stimulus the network crosses the bifurcation to the winner-take-all region and it evolves towards one of the decision states. When the stimulus is removed the network returns to the original input but it remains in the decision state. Thanks to recurrent connections mediated by NMDA with a long synaptic time scale, Wang's attractor network has an effective long time scale that allows for the integration of stimuli during hundreds of milliseconds. The integration of the stimulus ends when the network reaches one of the attractors. This is consistent with the experimental results where the accuracy of two monkeys performing a direction discrimination task does not increase indefinitely with the stimulus duration (figure 4a) (Roozbeh Kiani, Hanks, and Shadlen 2008; Roitman and Shadlen 2002). Wang's model is also compatible with the empirical result that reaction times are longer for error than correct trials (Roxin and Ledberg 2008; Roitman and Shadlen 2002) and the primacy psychophysical kernels seen in motion discrimination tasks (Roozbeh Kiani, Hanks, and Shadlen 2008; Nienborg and Cumming 2009). The advantage of the biophysical models is that we can study the neural mechanisms underlying the behaviour results. Similar to neurons in the lateral intraparietal cortex (LIP), the two populations of excitatory selective neurons first ramp up together when the stimulus is presented until one of the population wins the competition and shuts down the other one (Roozbeh Kiani, Hanks, and Shadlen 2008). In addition, as predicted by Wang's model, neurons in LIP are also correlated with the decision during a delay between the stimulus offset and the decision (Roozbeh Kiani, Hanks, and Shadlen 2008). In sum, the standard biophysical model is able to explain different behavioural and electrophysiological results.

Wang's network model has had a great impact on the study of the underlying neural mechanisms of perceptual decision making. In (Wimmer et al. 2015), the authors added a sensory level to the standard attractor network to show that constant choice probabilities in sensory areas can be explained by top down inputs from decision areas. It has also been useful to study the role of different brain areas in cognitive functions such as decision making or working memory. For instance in (Jaramillo, Mejias, and Wang 2019) the authors found that the pulvino-cortical pathway can control the effective connectivity within and across cortical regions and modulate attention, decision making and working memory. The coordination between different cortical areas during the computation of working memory and decision making has been studied in (Murray, Jaramillo, and Wang 2017). The authors found that prefrontal cortex should represent the decision variable more categorically than posterior

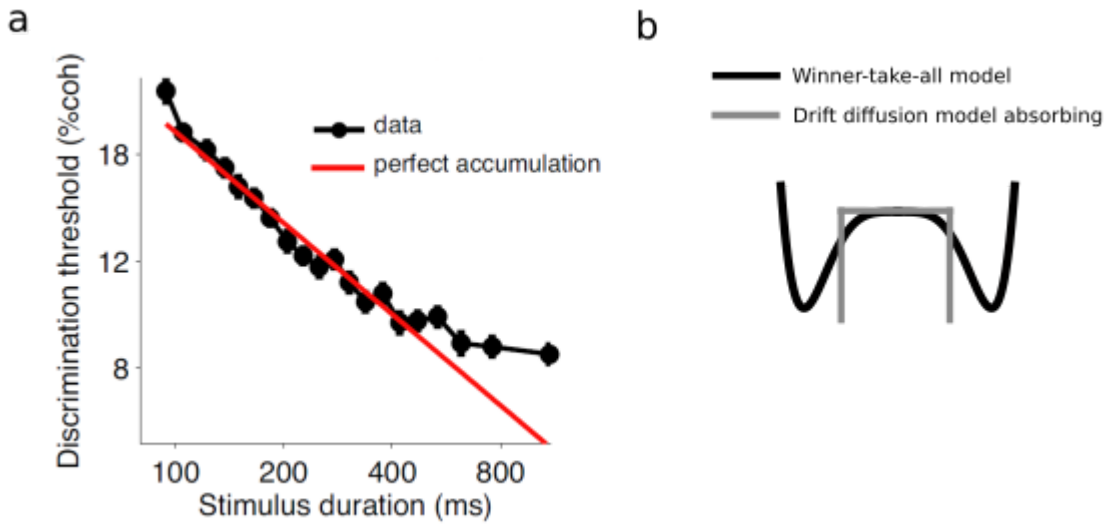

Figure 4 | Monkeys can perfectly integrate evidence for short but not for long trials.
a) Discrimination threshold versus stimulus duration of monkeys performing the dots tasks in a variable stimulus duration paradigm. The accuracy of monkeys increase similar to a perfect integration model for short trials and it tends to plateau at longer trials, figure from (Roozbeh Kiani, Hanks, and Shadlen 2008) b) Shape of the potential $\varphi(X)$ associated with the double well attractor model (black) and the DDM with absorbing bounds (gray). The result in (a) can be explained by both the drift diffusion model with absorbing bounds. Close to the bifurcation where the undecided states become unstable, the potentials of both models are similar.

parietal cortex. In recent years, it has been reported that subjects tend to repeat or alternate choices during a sequence of perceptual decisions (Akaishi et al. 2014; Braun, Urai, and Donner 2018; Fritsche, Mostert, and de Lange 2017). One possible explanation for the tendency to repeat is a slow decay of the decision state during the inter-trial interval. In other words, when the next trial starts the firing rate of the population associated with the previous choice could be still above the other one. Consistent with the model predictions, it was found that repetition bias increases or decreases by depolarizing or hyperpolarizing respectively with transcranial direct current stimulation over the left dorsolateral prefrontal cortex, (Bonaiuto, de Berker, and Bestmann 2016). Different versions of the biophysical attractor model have been able to explain the neural mechanisms underlying many different behaviour and neurophysiological findings.

Line attractors ($w_{rec} = 1$) where first used in tasks that require storing a parametric values in working memory such as spatial positions in a circle (Compte et al. 2000) or frequencies (Machens, Romo, and Brody 2005). But can also be applied in tasks where a stimulus needs to be integrated. We illustrate this using the same simple linear network model from equation 3

$$\tau_{syn}\frac{dr}{dt} = -r(1 - w_{rec}) + I(t) \quad (5)$$

With $w_{rec} = 1$ the mean firing rate of the population is simply the integral of the stimulus

$$r = \tau_{syn}^{-1}\int I(t)dt \quad (6)$$

In that case the model is a neuronal implementation of the perfect integrator model that we described in the previous section. In the context of decision making, similar biophysical line attractors model but with circular symmetry (ring attractor, (Compte et al. 2000)) have been used in tasks with multiple choices. In (Furman and Wang 2008), different bumps of activity compete through common inhibition to model a direction discrimination task with multiple alternatives. In a more recent study (Wei and Wang 2015), the authors use a ring attractor to model a task where the subjects could choose between the standard left and right choices or a choice that gave a small but certain reward (Roozbeh Kiani and Shadlen 2009) . After the stimulus, the authors add another bump between the two possible choices, this bump represents the certain but small reward choice and competes with the other bumps.

A complication of this type of model is the need for fine tuning of the parameters. Because the landscape must be completely flat, small asymmetries (~1%) in the connections can produce a landscape with a few number of attractors (Brody, Romo, and Kepecs 2003; Seung et al. 2000; Renart, Song, and Wang 2003). Possible solutions to this problem have been proposed by adding a fast negative feedback to stabilize the memory (Lim and Goldman 2013) or with bistable neurons (Koulakov et al. 2002) which change the landscape from flat to a series of small attractors. However this mechanism disrupts the perfect integration of evidence because stimuli below a threshold value fail to perturb the small attractor and thus they are not integrated. Another limitation to perfectly integrating the stimulus evidence is the internal noise. In the case of a completely flat potential all the possible states are stable. Consequently any internal noise (e.g. inputs from other brain regions or intrinsic noise of the neurons) would be also integrated by the model. This would produce a degradation of the stored values during the delay in working memory tasks. Actually spatial memories do degrade over time (Funahashi, Bruce, and Goldman-Rakic 1989) and this degradation has been understood as a signature of line attractors (Wimmer et al. 2014). Biophysical line attractors provide a framework to model the perfect accumulation of evidence and to store parametric values in working memory.

In contrast to the canonical models, biophysical attractor network models are high dimensional and rather complicated. Line attractors are basically perfect integrators and can easily be modelled by a one dimensional linear equation. In the next section, we explain how the biophysical attractor network model for decision making can be reduced to a simple one dimensional nonlinear equation.

One dimensional neurobiological models of perceptual decision making

Canonical models for perceptual decision making are simple and can fit several aspects of experimental data, such as performance and mean reaction times. Biophysical models provide a framework to study the neural mechanisms underlying perceptual decisions but they are rather complicated and high dimensional and hence difficult to fit. In what follows, we consider a one dimensional diffusion process for the decision variable (X) which can be formally derived from higher-dimensional neuronal models, and yet which is still described by the diffusion of a particle in a potential (equation 2) (Roxin and Ledberg 2008). In particular, inhibition-mediated winner-take-all attractor dynamics observed in network models of 2AFC contributes to the potential φ, and one finds

$$\varphi(X) = -\mu X - \frac{c_2 X^2}{2} + \frac{c_4 X^4}{4} + \frac{c_6 X^6}{6} \qquad (7)$$

Where μ is proportional to the difference in inputs to the two selective excitatory population in the biophysical network model, thus it represents the strength of the stimulus evidence. The parameter c_2 is proportional to the difference between the mean input to both population and the input at the bifurcation, Finally, the parameters c_4 and c_6 are non-trivial functions of the network. The temporal evolution of the stable states with the stimulus is the same as in the biophysical attractor network model for decision making. The parameter c_2 controls the stable states of the network (figure 5b). Before the stimulus presentation the decision variable remains in the undecided state because it is stable $(c2 < 0)$. With the presentation of the stimulus, the system crosses the bifurcation $(c_2 > 0)$, the undecided state becomes unstable and the decision variable evolves towards one of the two decision states. Finally, after the stimulus the decision states remain stable representing some sort of memory state which can hold on the information of the decision in the absence of any external input. .

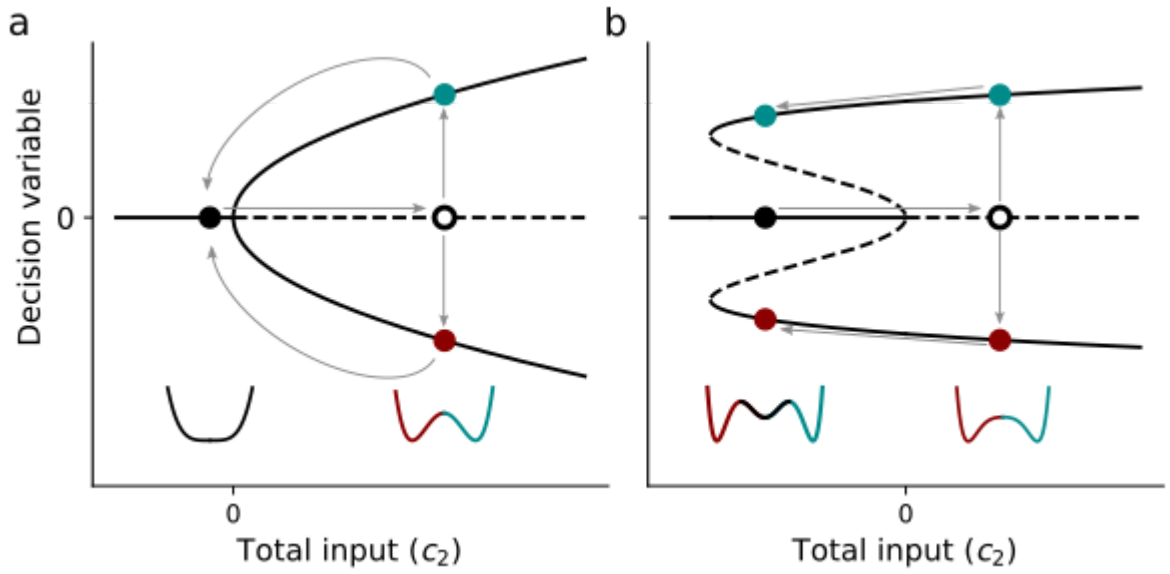

Figure 5 | Bifurcation diagram of the models with winner take all dynamics.
a and **b)** Before the stimulus the system is in the undecided state (black solid dot). When the stimulus is presented , the undecided state becomes unstable (white dot) and the only two possible stable states are the decision states (red and turquoise dots). After stimulus offset, depending on the network parameters, either there still exist decision states (b) or the only attractor of the network is again the undecided state. (a) Insets along the x-axis, illustrate the landscape of the equivalent potential of the system with (right) and without (left) stimulus.

When focusing on the study the dynamics of perceptual decisions without the need of working memory (chapter 1 and 3), we will use the simpler case where the decision states are unstable after the stimulus:

$$\varphi = -\mu X - \frac{c_2 X^2}{2} + \frac{c_4 X^4}{4} \qquad (8)$$

with $c_2, c_4 > 0$ (figure 5a). In chapter 2 we will investigate the case in which the perceptual categorization needs to be maintained in the absence of any input. For this, we will compare the full model given by equation 7. Whether the biophysical network dynamics are correctly described by 7 or 8 depends on the specific choice of network parameters (Roxin and Ledberg 2008). The resulting potential has two local minima corresponding to patterns of neuronal activity which represent the two possible choices. We call this model the double well model (DWM)

The models represented by a potential of the form given in equations 7 and 8 have the advantage that they are simple, can be fitted to data and the relation between the

parameters of the potential $\varphi(X)$ and the neural mechanisms in the corresponding biophysical model is well characterized (Roxin and Ledberg 2008).

Classical view of perceptual decision making

The classical view of perceptual decision making is that decision areas integrate the decision evidence provided by the stimulus represented in sensory areas up to a decision threshold. This view is based on a series of motion discrimination experiments in monkeys (Roitman and Shadlen 2002; Roozbeh Kiani, Hanks, and Shadlen 2008; Nienborg and Cumming 2009; Britten et al. 1992; Shadlen and Newsome 2001). On the one hand, they found that the firing rate of neurons in sensory areas (medial temporal cortex, MT) were proportional to the strength of the stimulus evidence (i.e. the motion direction). On the other hand, they found that the firing rate in decisions areas (Lateral intraparietal cortex) ramped up with the stimulus presentation as if they were integrating the stimulus evidence from the sensory areas. In addition, they found that the slope of the ramping activity depended on the stimulus strength but then it saturated to a value of the firing rate that was independent of the stimulus strength. This feature was indicative of the presence of absorbing bounds.

New experiments in humans, rats and monkeys have however challenged this view. In a landmark study (Brunton, Botvinick, and Brody 2013) used model based behavioral analysis to show that humans and rats can perfectly integrate evidence without bounds. The experimenters used the so-called clicks task where two streams of poisson auditory or visual clicks are played at different rates. The subjects had to choose the stream with a higher rate. Another experiment using the same task has however recently challenged this result (Keung, Hagen, and Wilson 2019). This time the experimenters found different sources of suboptimally including psychophysical kernels across human subjects with different temporal profiles (Keung, Hagen, and Wilson 2019). Consistent with perfect integration of evidence without bounds, a recent study has shown that humans can perfectly integrate the contrast of a sequence of gratings even when the stimulus is interrupted by long delays (up to 8 s) (Waskom and Kiani 2018). Although monotonically increasing psychophysical kernels showing a recency effect can not be explained by a model with absorbing bounds, they have also been reported in direction (Cheadle et al. 2014; Wyart, Myers, and Summerfield 2015) or brightness discrimination tasks (Bronfman, Brezis, and Usher 2016). More recent studies using motion discrimination experiments have also challenged the classical framework by showing that the primacy psychophysical kernels could be more related to

sensory adaption than to a bound mechanism (Yates et al. 2017). Other experiments have shown that the activity of neurons in decision areas is not only related to the integral of the stimulus but also to other mechanisms such as an urgency signal (Park et al. 2014; Thura et al. 2012). In summary, it seems that the classical framework of how the brain makes decisions is too simple to account for all the behaviours and electrophysiological findings in the literature. Thus other mechanisms needs to be studied to complete the classical model for decision making.

Thesis goals

During the 2017 summer, I attended the cognitive computational neuroscience summer school in Shanghai. There, we had a series of lectures about perceptual decision making, and Mike Shadlen and Xiao-Jing Wang, among others, presented their work. Surprisingly, both used the result showing the dependence of the monkeys accuracy on the duration of the dots stimulus (see figure 4a) to support their preferred models, namely the drift diffusion model with absorbing bounds (DDMA) and the double well model (DWM), respectively. As we already explained, the DDMA and the double well model can perfectly integrate evidence for short but not for long stimulus durations. Both models can also fit the mean reaction time for error and correct trials. This is explained by the fact that in a certain parameter regime their dynamics can be similar (figure 4b) (Bogacz et al. 2006). However, the shape of the potentials associated with these two models are in general different: while the DWM has non-linear terms, the DDMA is linear with the only non-linearity represented by the decision bounds. But theoretical predictions that could be used to test this nonlinearities in the potentials have remained elusive.

As already mentioned, the canonical models are widely used because, in contrast to biophysical models, they are simple and easy to fit to data. In a recent review about sequential sampling models (Forstmann, Ratcliff, and -J. Wagenmakers 2016), Forstmann and co-authors wrote "*Unfortunately, the Wang model is relatively complex, and at this point it is not possible to use it to fit data*" (Forstmann, Ratcliff, and -J. Wagenmakers 2016),. The one-dimensional model described by equation 8 has been qualitatively fitted in reaction time tasks (Roxin and Ledberg 2008). But it is unclear how to fit these models using a more rigorous maximum-likelihood approach.

The goals of this thesis are:

- Study the non-linear dynamics of the DWM models and find specific signatures of attractors dynamics that are experimentally testable. Ideally, these predictions should be able to qualitatively distinguish between the DWM and the canonical models.
- Design an experiment to qualitatively and quantitatively test the attractor dynamics in perceptual decision making. We aim to test experimentally test the qualitative signatures of attractor dynamics. In addition, we want to develop a maximum likelihood maximization to fit the DWM. The procedure should be general enough to be able to add extra mechanisms that have been shown that could play a critical role in perceptual decision such as different types of biases, adaptation or an urgency signal. Then using a model-based approach, we aim to quantitatively differentiate between these distinct mechanisms.

2. Flexible categorization in perceptual decision making

Summary

Canonical approaches to model perceptual decision making are based on diffusion processes that assume bounded or unbounded perfect integration of the stimulus. Here we study the integration process in neurobiological models with winner-take-all dynamics that can be reduced to a diffusion process. The key difference between these models and the canonical ones is the shape of the potential landscape along which the decision dynamics evolves. Whereas the models with winner-take-all dynamics have a nonlinear potential, the canonical models have a linear potential, which in principle allows for perfect integration the evidence. To study the implications of the winner-take-all dynamics in the integration of evidence, we use stimuli with different magnitudes of fluctuations. This led us to discover a new integration regime not present in canonical diffusion models, which we call flexible categorization. In this regime, fluctuations late in the trial robustly generate decision reversals by overcoming the internal attractor dynamics when the initial choice is incorrect. One signature of winner-take-all dynamics is a non-monotonic dependence of the accuracy and the response consistency on the stimulus fluctuations. Another is a transition in the temporal weighting of the stimulus impact on the upcoming choice from primacy to recency as a function of the trial duration or the magnitude stimulus fluctuations. We found evidence for such a transition in data from a series of psychophysical experiments where subjects made decisions about the average brightness level of two disks for different stimulus duration T=1,2,3 and 5 s.

Results

Changing the stimulus statistics reveals the dynamics of the decision variable

In typical settings, the stimulus statistics is under the control of the experimenter and can reveal the dynamics of the decision variable. We thus investigated how the psychophysical kernel (PK) for the three DDM models depends on the stimulus fluctuations (σ_S) while keeping the magnitude of the internal noise (σ_i) constant (figure 6). In order to quantify changes in the PK, we calculated both its normalized area, which is a measure of the overall impact of stimulus fluctuations on the upcoming decision (figure 6d; Methods), as well as a primacy-recency index, which ranged from -1 (extreme recency) to 1 (extreme primacy). For very weak stimulus fluctuations all three models are equivalent because the bounds are never reached; in particular the PK is flat, the primacy-recency index is therefore zero (figure 6e) and the normalized area is small because the dynamics is driven by internal noise. As stimulus fluctuations increase, the PK of the DDM with absorbing bounds becomes more markedly primacy-laden, leading to an increasing primacy-recency index. In a similar vein, the primacy-recency index for the DDM with reflecting bounds decreases, indicating enhanced recency. The primacy-recency index for the perfect integrator always remains zero because the PK is always flat. The normalized PK area increases monotonically with the ratio σ_S/σ_i. For the DDM with bounds, the bounds are reached more often as σ_S increases, which complicates the integration of the stimulus and consequently the normalized PK area decreases. In sum, the dynamics of evidence accumulation in the DDMs remains qualitatively the same when changing the strength of stimulus fluctuations.

In contrast, the double well model (DWM) has a much richer dynamical repertoire as a function of stimulus fluctuation strength than the canonical models. Specifically, the presence of two potential wells allows for the possibility of sudden transitions between states. That is, the model can account for “changes of mind” (figure 7a) (Resulaj et al. 2009; Roozbeh Kiani et al. 2014) by virtue of stochastic transitions between distinct attracting states. For a fixed stimulus duration, such transitions become more likely as the strength of stimulus fluctuations is increased. The same effect can be achieved by extending the trial duration. For a fixed strength of stimulus fluctuations the rate of transitions remains constant but because the trials are longer the transitions become more likely. The transition dynamics in the DWM play a major role in shaping the PK (figure 7b,c,d). For weak stimulus fluctuations

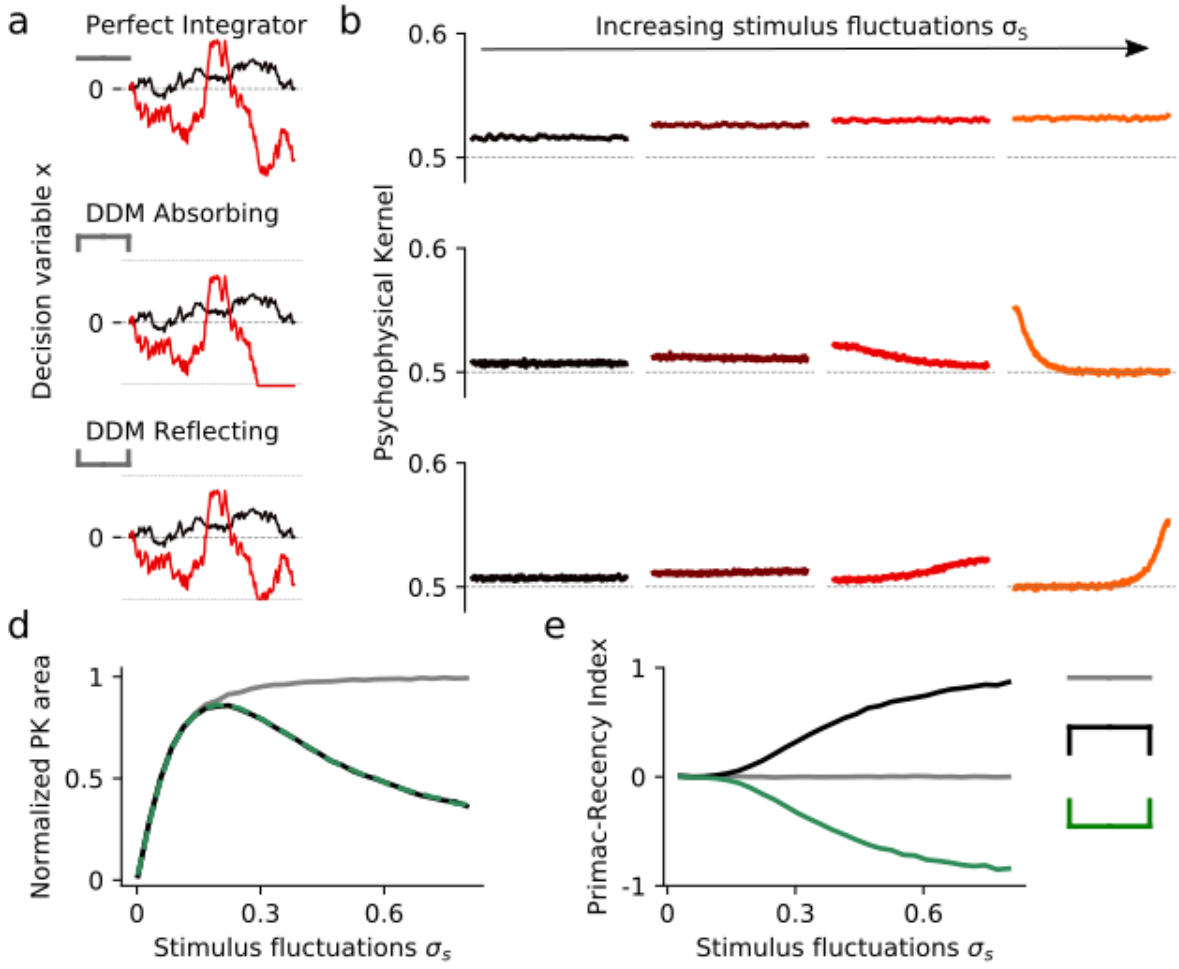

Figure 6 | Dependence of the time course of evidence integration on the magnitude of stimulus fluctuations.

(a) Single-trial traces of the decision variable *x* for low and high stimulus fluctuations with a constant level of internal noise. Top: The perfect integrator integrates the whole stimulus, corresponding to a diffusion process with a flat potential (insets). The slope depends on the signal, in this case μ=0 . Center: The DDM with absorbing bounds integrates the stimulus as the perfect integrator until it reaches the positive or negative bound. These absorbing bounds are represented as infinitely deep wells (inset). Bottom: The DDM with reflecting bounds perfectly integrates the stimulus within the two bounds. If a bound is reached, no more evidence is accumulated in favor of the corresponding choice option (inset). **(b)** Psychophysical Kernels (PK) for the three canonical models with different stimulus fluctuations: $\sigma_S = 0.09,\ 0.15, 0.25,\ 0.53$ and a fixed value of internal noise $\sigma_I = 0.1$. Here we assumed that σ_I is small enough to not reach the bounds by itself. **(c)** Normalized PK area for the Perfect Integrator increases monotonically with the ratio σ_S/σ_i. For DDM models with bounds, it decreases for strong σ_S because the bounds are reached earlier which complicate the integration. **(d)** Primacy-recency index (Methods) for the three canonical models.

transitions do not occur and the choice tends to be determined by fluctuations early in the trial which drive the model to one of the two wells. When transitions occur readily, it is those

fluctuations which come late in the trial which determine the final state of the system; hence the PK shows recency. Therefore, as the strength of stimulus fluctuations increases, and hence as transitions become more likely, the PK switches from primacy to recency, passing through an intermediate regime in which the PK is mixed, but not necessarily flat (figure 7b, red line). This new regime is unique to the DWM, and we call it “flexible categorization” because it allows the sensory input to overcome the internal attractor dynamics. In this regime, stimulus fluctuations impact the choice over the whole trial (the PK does not decay to chance level at any time). The overall impact of the stimulus fluctuations, quantified by the normalized PK area, also changes with the strength of the stimulus fluctuations (figure 7d): For weak stimulus fluctuations the decision is mostly driven by internal fluctuations and the normalized PK area tends to zero. In contrast, for strong stimulus fluctuations the decision is completely driven by the stimulus fluctuations but only for those which come late in the trial. Consequently the normalized PK area decreases. The PK area peaks in the flexible categorization regime where the overall impact of the stimulus fluctuation on choice is maximal. Once again, alternatively, for fixed stimulus fluctuations strength one sees the same progression of the PK as the trial duration is increased (figure 7b,e,f). However, the normalized PK area monotonically decreases with the stimulus duration, because although the ratio between stimulus and internal fluctuations is constant, for longer trials the internal dynamics has the chance to impact the choice more. The DWM model has different integration regimes (primacy, flexible categorization and recency) that are controlled by the transition rates between attractors.

Decision accuracy in models of evidence integration

For the double well model (DWM), changing the strength of stimulus fluctuations σ_S also has a highly non-trivial effect on the probability of a correct choice (figure 8). Strikingly, the accuracy exhibits a non-monotonic dependence on the strength of stimulus fluctuations (figure 8a). That is, although the accuracy tends - as expected - to worsen for increasing stimulus fluctuations, it actually improves over a limited range of σ_S’s. We noted previously that the progression from primacy to recency in the PK as a function of σ_S was due to the occurrence of transitions from one potential well to the other, corresponding to changes-of-mind. This is also the mechanism underlying the observed non-monotonicity in the accuracy. Specifically, on those trials in which the first visited well is in error, sufficiently strong stimulus fluctuations can lead to a correcting transition, thereby improving the accuracy on average over trials. On the other hand, If the first well visited is correct, then a

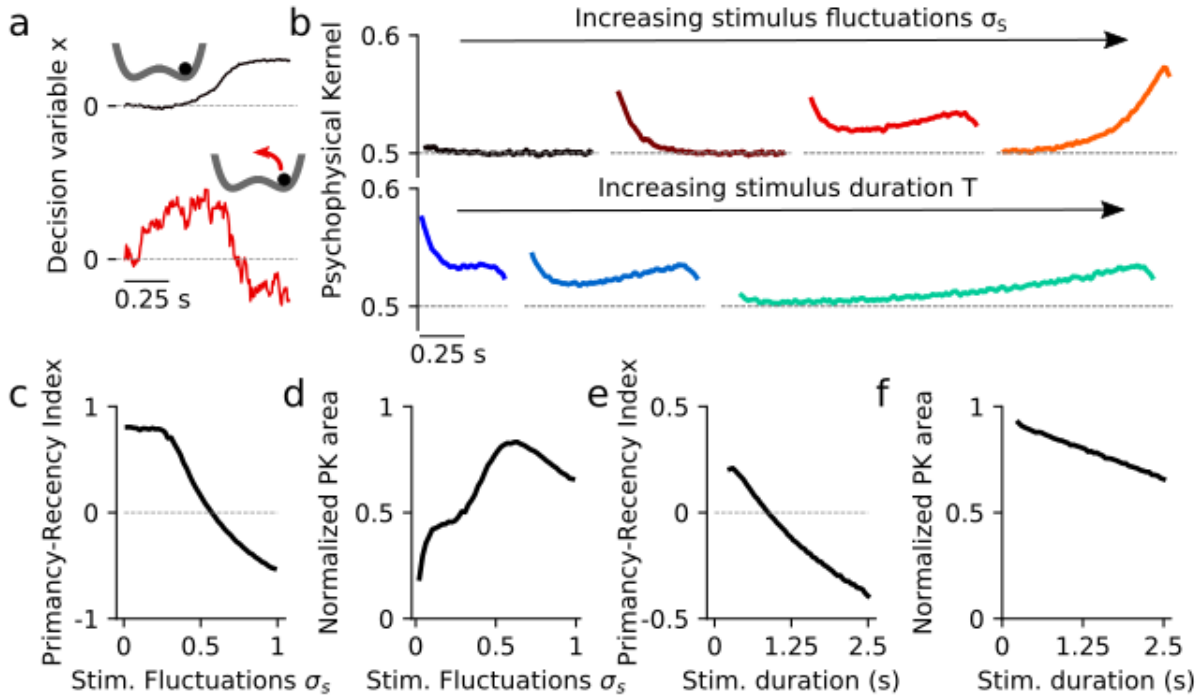

Figure 7 | Time course of evidence accumulation in the double-well model.
(a) Single-trial traces of the decision variable for the DWM. with low (black) and intermediate (red) stimulus fluctuations magnitude σ_S. Reversals (change of mind) are only possible for strong enough σ_S. (**b**) The PK changes form primacy to recency with σ_S (top; $\sigma_S = 0.0025, 0.02, 0.59$ and 1 with $\sigma_i = 0.1$) and stimulus duration T (bottom; $T = 0.5, 1$ and $2.5\,s$ with $\sigma_S = 0.59$ and $\sigma_i = 0.1$). **(c, d)** The Primacy-recency index (PRI) (**c**) and normalized PK area (**d**) quantifies the change from primacy $(PRI > 0)$ to rencency $(PRI < 0)$ as a function of σ_S. **(e, f)** Primacy-recency index (**e**) and normalized PK area (**f**) as a function of stimulus duration T.

transition from the deeper correct well to the error well is much less likely. It is the large difference between the likelihood of correcting- versus error-generating-transitions that leads to the non-monotonic dependence. This difference is maximum in the flexible categorization regime (primacy-recency index=0 figure 8c) where the fluctuations can impact the choice over the whole trial (figure 8a insets). For weaker stimulus fluctuations, in the primacy regime, there are no correcting nor error generating-transitions. For stronger stimulus fluctuations, in the recency regime, both types of transitions are activated (figure 8b).

To be more quantitative, we used Kramers reaction-rate theory (Kramers 1940) to calculate the probability P_{CE} (P_{EC}) of finding the system in the correct (error) well at the end of a trial with any duration T when the first well visited was the error (correct) one (Methods) . We found that the probability of a correcting transition P_{CE} increases steeply as a function of stimulus fluctuations even before P_{EC} reaches non-negligible values (figure 8b) and that correcting transitions are exponentially more likely than error-generating ones (Methods).

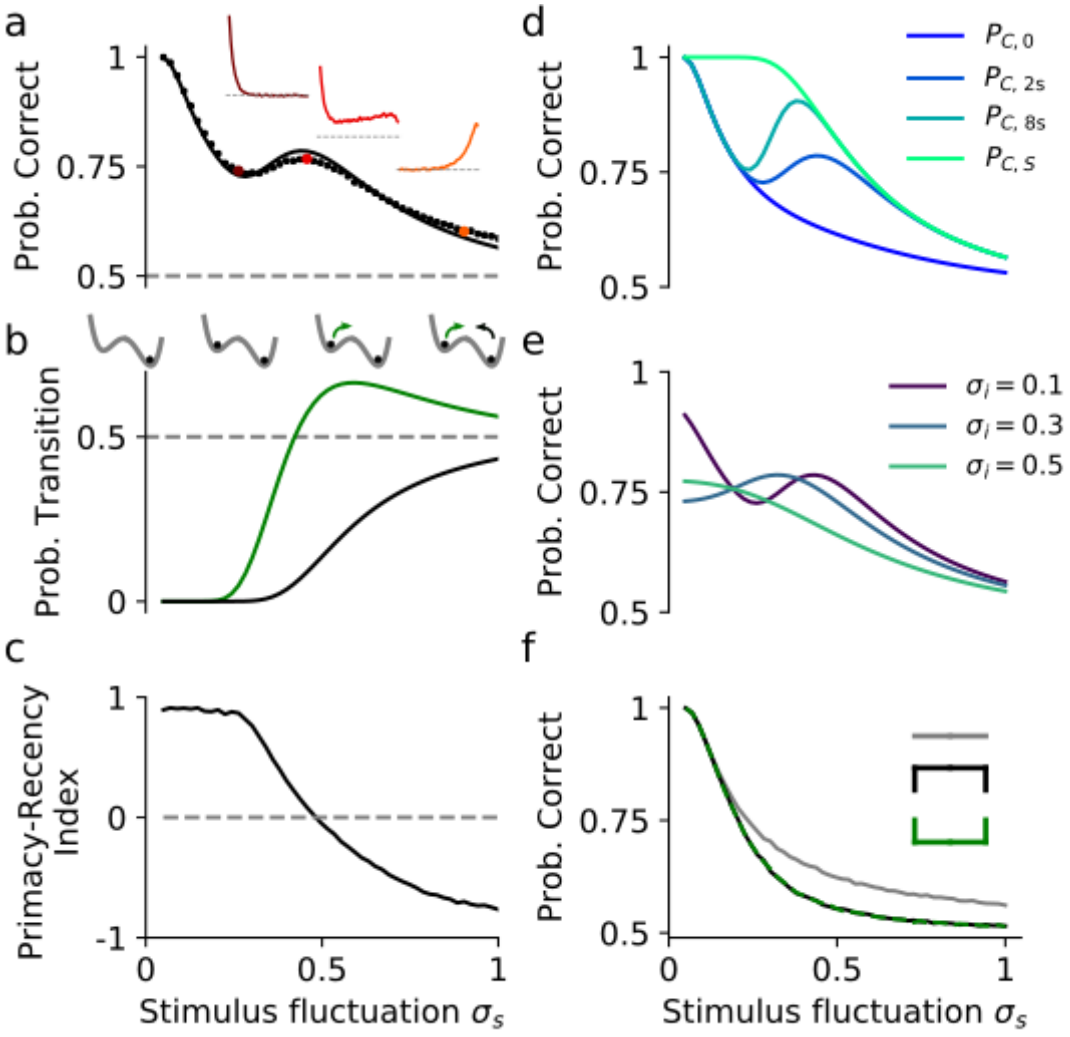

Figure 8 | Impact of stimulus fluctuations on choice accuracy in the DWM.
(a) There is a local maximum of the accuracy with the magnitude of the stimulus fluctuations. For simplicity, we fixed the internal noise to zero $(\sigma_I = 0)$.The mean evidence was $\mu = 0.15$. The solid line is the analytically probability of a correct decision (Methods) and the dots are from numerical simulations. The insets show the PK for three different values of σ_S.**(b)** Probability to finish the trial in the correct (P_{CE}; green) or incorrect (P_{EC}; black) well when the opposite has been visited first. Insets: Sequence of transition activations as σ_S increases. : i) For very low σ_S, the system always evolve towards the correct well, ii) As σ_s increases, it is possible that the systems visits the incorrect well but neither transitions (correcting or error) are activated, ii) For stronger σ_S, the correcting transition (green arrow) are activated iii) Finally for strong σ_S, both transitions are activated.
(c) The PK become monotonically recency as σ_S increases. The flexible categorization regime with PRI close to zero coincides with the local maximum in accuracy.**d)** Decision accuracy as a function of σ_S for different stimulus durations T. The accuracy for any stimulus duration lies between the probability to first visit the correct attractor $(P_{C,0})$ and the stsionat probability of correct $P_{C,S}$. Increasing σ_s drives the system from the initial state to the stationary state enhancing the performance. **(e)**For higher σ_I, the local maximum in the accuracy occurs already for smaller values of σ_S. For very large σ_I (green lines), the internal noise alone is sufficient to generate state transitions and the local maximum in accuracy is not observed. **(f)** Accuracy for the canonical models (perfect integrator, DDM with absorbing and reflecting bounds) always decreases monotonically with σ_S.

The resulting decision accuracy can then be understood in terms of these probabilities and the probability to first visit the correct well by writing

$$P_C = P_{C,0}(1 - P_{EC}) + (1 - P_{C,0})P_{CE} \quad (9)$$

where P_C is the probability of correct at the end of the trial and $P_{C,0}$ is the probability of first visiting the correct well (Methods). This non trivial effect of the accuracy with the stimulus fluctuations is a direct consequence of attractor dynamics. The accuracy of the canonical models decays monotonically with the stimulus fluctuations (figure 8f).

In order to make precise experimental predictions, it is important to understand how this non-monotonic dependence of the accuracy changes with the other stimulus parameter: 1) Above a critical value of $\mu_c = \frac{c_2}{4}\sqrt{\frac{c_2}{c_4}}$, the probability to first visit the error well is too small and the correcting transitions become rare and rare (second term equation 9, methods). 2) To investigate the impact of the stimulus duration (T), we rewrite equation 9 in terms of the stationary probability of correct $(P_{C,\infty})$, the probability to first visit the correct well $(P_{C,0})$ and T:

$$P_C = P_{C,0}exp(-kT) + P_{C,S}(1 - exp(-kT)) \quad (10)$$

Where k is the sum of the transition rate. As expected, the probability of a correct choice tends simply to the probability of first visiting the correct well ($P_C \to P_{C,0}$) in the limit $T \to 0$, and it tends to the stationary probability $P_{C,\infty}$ when $T \to \infty$. Note that $P_{c,0}$ and $P_{c,\infty}$ decrease monotonically with the strength of the stimulus fluctuations. However, for intermediate values, when $kT \sim 1$ the system jumps very quickly from $P_{C,0}$ to $P_{C,\infty}$. As the stimulus duration increases, the strength of the stimulus fluctuations needed to jump from $P_{C,0}$ to $P_{C,\infty}$ decreases and consequently the bump in accuracy is shifted towards weaker stimulus fluctuations values (figure 8d, Methods). Finally, it is also important to understand how the parameters that are not under the control of the experimenter such as the strength of the internal fluctuations affects the accuracy bump. Here, we assumed that the two sources of fluctuations, internal and stimulus-dependent are mathematically equivalent $(\sigma\xi(t) = \sigma_S\xi_S + \sigma_I\xi_I)$. Thus as we increase the strength of internal fluctuations, the region that can be explored with the stimulus fluctuations is cropped from the left and it can be the case that the bump disappears because the internal fluctuations are too strong (figure 8e, see Methods for the computation of the critical value). To summarize, the accuracy bump

will be higher for long trials and intermediate values of the accuracy but it can be the case that we do not see it because the internal fluctuations are too strong.

Consistency in models of evidence integration

In order to better understand how internal noise (controlled by σ_I) and stimulus fluctuations (controlled by σ_S) influence the final choice outcome we studied the self-consistency of the double well model (DWM), that is how consistently an identical stimulus yields the same choice outcome. In the absence of internal noise the decision process is deterministic and consistency is 1. If the final decision does not depend on the stimulus at all, the consistency will be 0.5. Experimentally, consistency can be measured from the behavioral reports to identical repetitions of stimuli, the so-called double-pass method (Nienborg and Cumming 2009; Neri and Levi 2006). We used the same method in the DWM and explored how consistency depends on σ_S and σ_I (figure 9). Note that here we only used stimuli with exactly zero mean signal in order to avoid a trivial increase of consistency with σ_S due to larger deviations from the average, i.e we introduced correlations in the stimuli such that the mean of each stimulus is exactly 0 (methods). As expected, we found that the consistency is close to 0.5 if σ_S is small compared to σ_I, and that it increases with increasing σ_S (figure 8a). However, despite this general increase with σ_S, we find a striking drop in consistency for a range of σ_S values and not too high values of internal noise σ_I. Thus, consistency in the DWM can depend non-monotonically on the strength of stimulus fluctuations, a similar effect as we had observed for choice accuracy but now with a dip instead of a bump shape.

To understand this effect, we studied the time-course of the decision variable X over many repetitions of a single stimulus, i.e. for a single realization of the stimulus fluctuations (figure 8b). By re-scaling the amplitude of the stimulus, we realized different strengths of the stimulus fluctuations σ_S. For fixed σ_I and increasing σ_S, we found four different regimes: For very small σ_S the internal noise is the dominant factor, both choice outcomes were equally likely and consistency was 0.5 (figure 8b,i). In the next regime (ii), stimulus fluctuations determined the first visited well and decision reversals were not activated, yielding a high consistency (figure 8b,ii). Even higher σ_S revealed a regime where transitions can occur but only when internal noise and the stimulus fluctuations together produced a large fluctuation (figure 8b,iii). The necessary contribution of the internal noise, that varies from trial to trial, leads to a lower consistency. Finally, once that σ_S was large enough to activate the reversals on its own, consistency increased again (figure 8b,iv). To

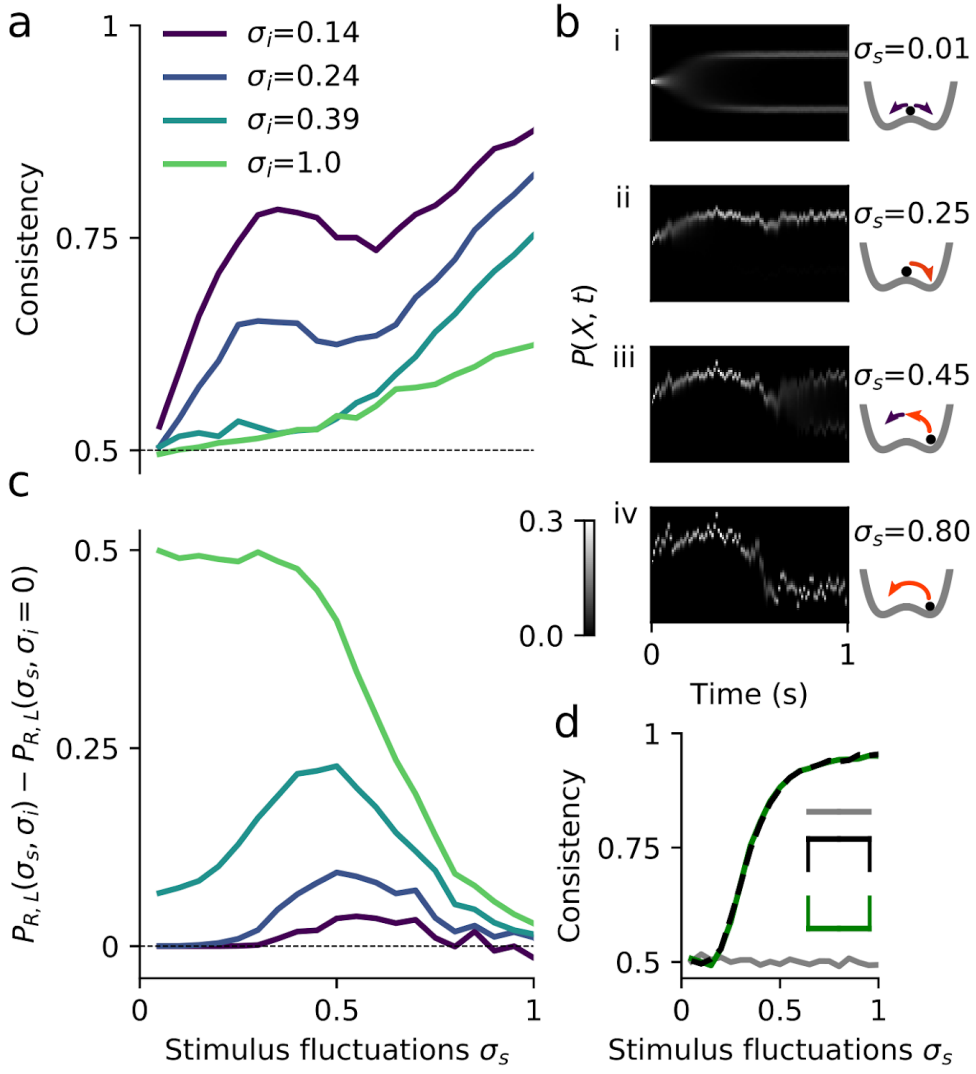

Figure 9 | Dependence of choice consistency on stimulus fluctuations.
(a) In general, the consistency increase with the stimulus fluctuations (σ_S) but for the double well model there is a drop in consistency for a range of σ_S. This occurs when the internal noise by itself is not strong enough to produce transitions. (b) For a fixed stimulus, we computed the temporal evolution of the decision variable probability distribution, $P(X,t)$ for different σ_S and a constant value of the internal noise, $\sigma_i = 0.14$: i) For very weak σ_S, the choice is driven by the internal noise (σ_i) and the consistency is very low $(53.2\,\%)$, ii) In the regime where σ_S determines the first visited well $(\sigma_S >> \sigma_i)$ but it is not strong enough to produce transitions, the consistency is very high (97.8%). iii) When σ_S is almost strong enough to produce transitions by itself, the transitions occur only when σ_i and σ_S together produced a large fluctuation. Because the internal noise have again impact on the choice, the consistency decreases (64.5%). iv) Finally, when σ_S is strong enough to produce transition by itself the accuracy is again very high (100%) (c) $P_{R,L}(\sigma_S, \sigma_i)$ is the probability to finish the trial in the right well when we initialize the trial in the Left well. The difference between $P_{R,L}(\sigma_S, \sigma_i)$ and $P_{R,L}(\sigma_S, \sigma_i = 0)$ indicates how important is the internal noise to produce transitions. Thus if this difference increases, the consistency decreases. (d) The consistency for the canonical models increases monotonically with the stimulus fluctuations. The consistency of the perfect integration is trivially always at chance level because we introduce correlations in the stimuli such that the total evidence is zero.

confirm that this is the underlying mechanism of the observed drop in consistency, we plotted the difference between the reversal probabilities with and without internal noise and found that indeed this difference is maximal for the values of σ_S that showed the drop in consistency (figure 8c). Because it depends on the probability of decision reversals this non-trivial drop in consistency is thus again a direct consequence of the nonlinear evidence accumulation in the DWM and it can therefore not occur in any of the DDMs (figure 8d).

Spiking network

We reproduce the theoretical predictions from the one dimensional version of the attractor model with a biophysical attractor network (methods). The network consists of two populations of excitatory neurons $(N_E = 1000)$ that are selective to one of the two possible choices and an untended inhibitory population $(N_I = 500)$. In addition, we add three untuned external populations that project to each of the populations of the decision circuit. As in Wang's model the two populations of excitatory neurons compete through the inhibitory population. We set the network close to the winner-take-all bifurcation to achieve relatively slow dynamics that allows the network to integrate the stimuli over hundreds of milliseconds. In figure 10, we show two single trials for weak and intermediate magnitudes of the stimulus fluctuations (σ_S). For weak σ_S, the network arrives to one of the attractor and it remains there for the entire trial. For the intermediate σ_S, the network is able to correct an initial error in the categorization. Similarly, to the one dimension version of the model, the transitions between attractor states produce a change from primacy to recency in the psychophysical kernel with the stimulus fluctuations (figure 11a). As we explained, the underlying mechanism of this change is an increase in the number of transitions between attractor states due to an increase of the transition rates. The number of transitions between states also increases with the stimulus duration even when the transition rates are fixed (constant σ_S). Thus the network shows again a change from primacy to recency psychophysical kernels with the stimulus duration (figure 11b). Finally, the biophysical attractor network has also a non-monotonic relation between the accuracy and the stimulus fluctuations (figure 12). The local maximum shifts towards smaller values with the stimulus duration. Thus we are able to reproduce the signatures of attractor dynamics that we found in the one dimensional version of the model using a biophysical attractor network with realistic parameters.

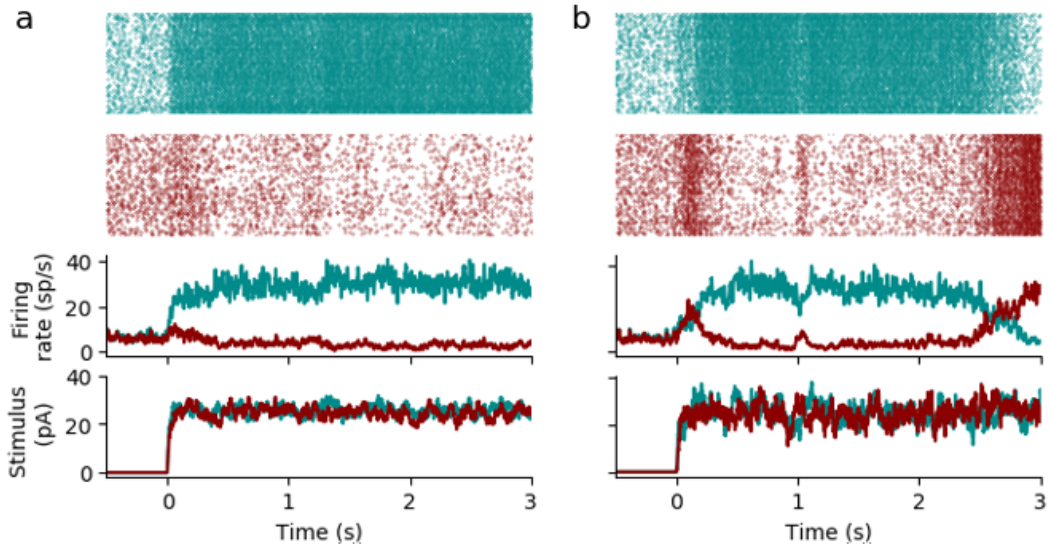

Figure 10 | Single trials of the spiking attractor network with low an intermediate level of stimulus fluctuations

Bottom: Stimulus for right (red) and left (blue) population for weak (a, $\sigma_S = 8$) and intermediate (b, $\sigma_S = 16$) magnitudes of the stimulus fluctuations. Intermediate: Firing rate of the excitatory populations. For strong enough values of stimulus fluctuations. In (b) there is a correcting change of mind. Top: Raster plots for 200 neurons from each of the two populations of excitatory neurons. In each row, we plot the spikes of one neuron with a small dot.

Testing model predictions in a perceptual decision task

We tested a key prediction of the double well model (DWM), namely that the observed dynamics of evidence accumulation depends on the stimulus duration (figure 7b bottom): for short durations the early part of the stimulus should have the highest impact on the final choice and for long durations the late part should have the highest impact. Thus, depending on stimulus duration, PKs in the DWM change from primacy over flexible categorization to recency. To test this prediction, we used data from an experiment in which human subjects performed a brightness discrimination task with variable stimulus duration between 1 s and 5 s (Bronfman, Brezis, and Usher 2016) . Confirming previous analyses (Bronfman, Brezis, and Usher 2016), Psychophysical kernels (PK) of human subjects changed from primacy to recency with increasing stimulus durations (Fig. top). To compare these observations to the predictions of the DWM, we simulated the PKs of the DWM using the same stimuli that were presented to the human subjects (methods). We found that the PKs for different stimulus durations obtained in the DWM were very similar to the experimental data. Note that while the PK changes are qualitatively the same in the experiment and in the DWM, we did not quantitatively fit the model to the experimental data (methods). The important point here is

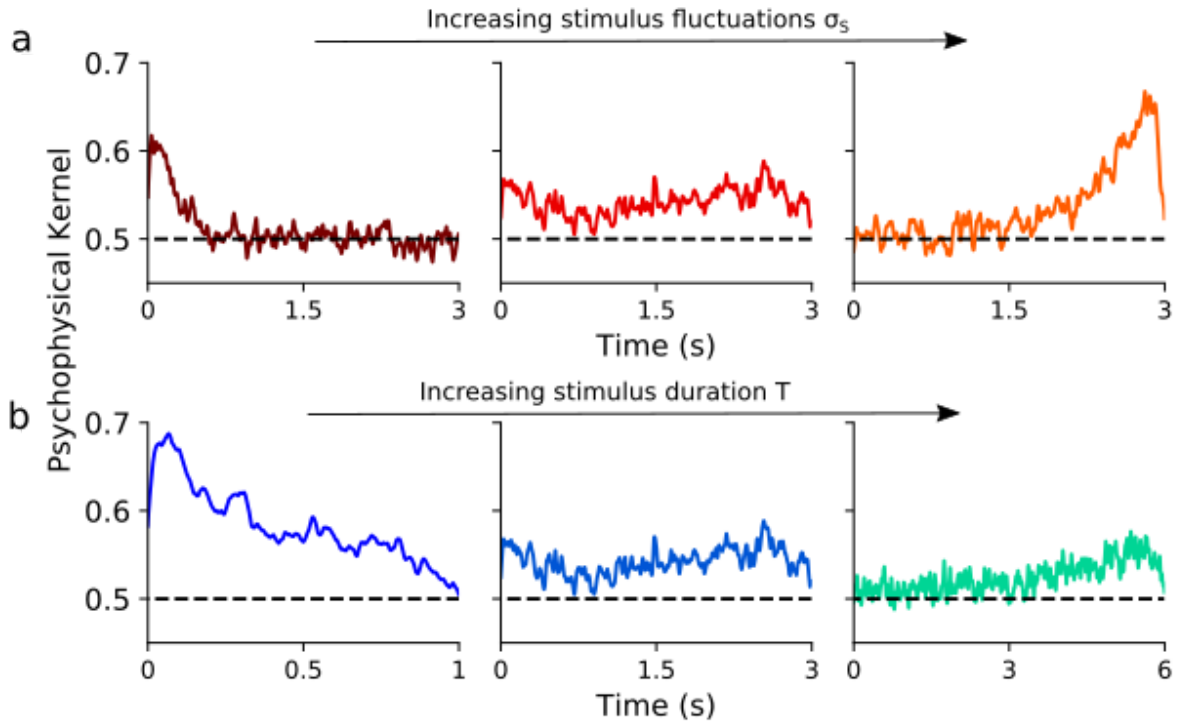

Figure 11 | Flexible evidence accumulation in a spiking neural network model.
a) The psychophysical kernels change from primacy to recency with the magnitude of the stimulus fluctuations, $\sigma_S = 4, 8$ and 40. **b)** For intermediate magnitude of the stimulus fluctuations $(\sigma_S = 8)$, the psychophysical kernel changes from primacy to recency with the stimulus duration $T = 1, 3$ and 6.

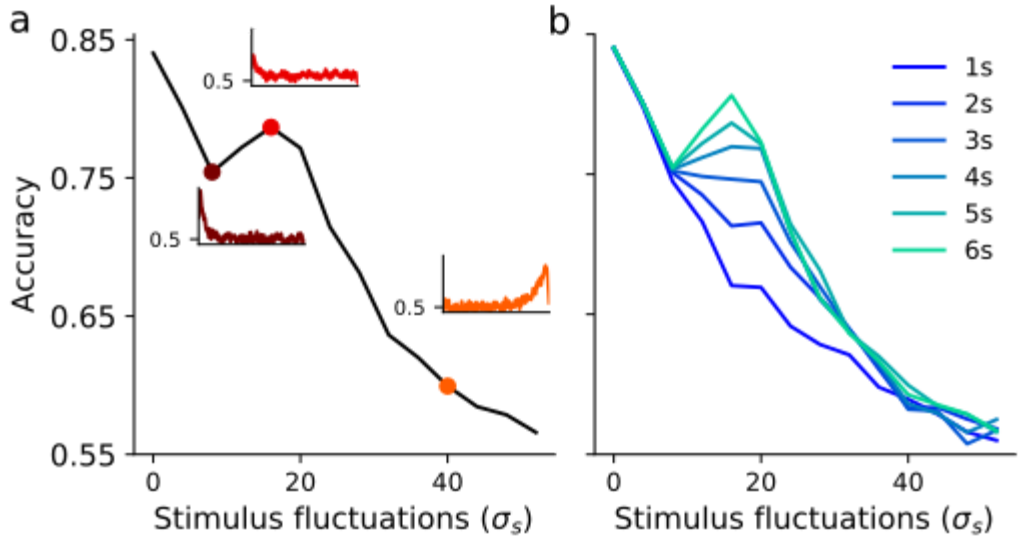

Figure 12 | Non-monotonic relation of the accuracy with the stimulus fluctuations
a) The accuracy increases for a range of stimulus fluctuations. The Insets show the psychophysical kernels for different σ_S. The local maximum in accuracy coincides with the flexible categorization regime where the psychophysical kernels is above chance during the entire trial. **b)** The local maximum in accuracy is shifted towards smaller stimulus fluctuations with the stimulus duration.

that these results were obtained with fixed model parameters for all stimulus durations. Thus, the dependence of the shape of PKs on stimulus duration does not necessarily indicate a change in the dynamics of evidence integration per se. Rather, fixed, but nonlinear internal accumulation dynamics in the DWM parsimoniously account for the observed PK changes without the need for a modulation of internal dynamics.

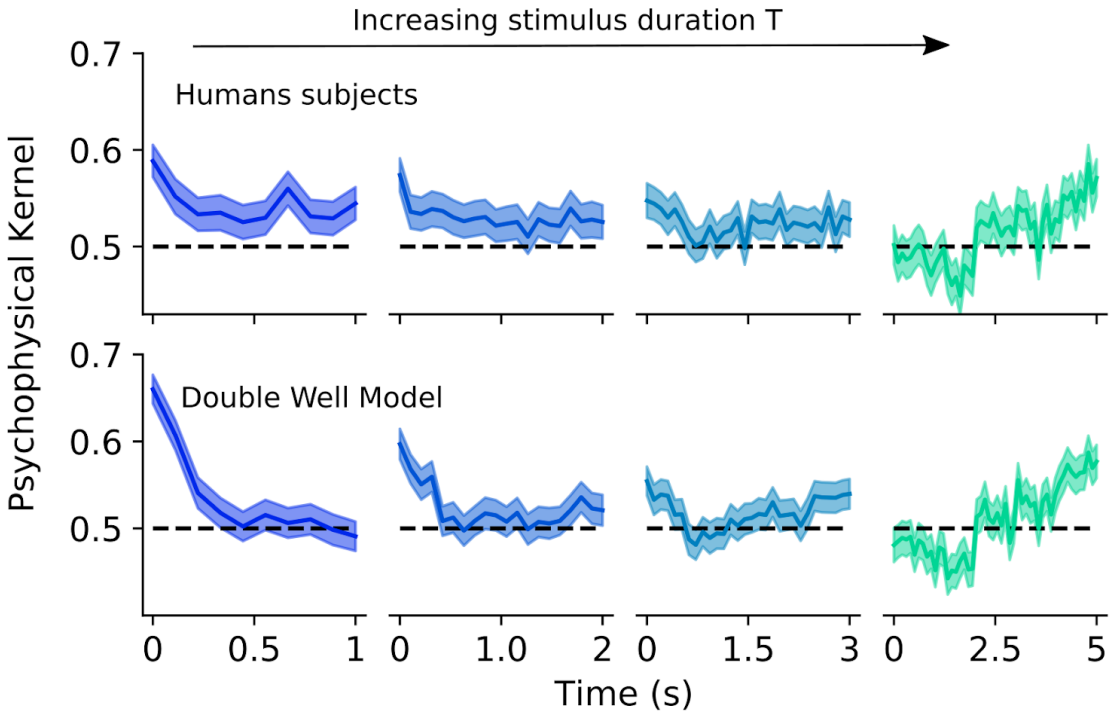

Figure 13 | Decision dynamics of the double well model explains experimentally observed changes from primacy to recency with increasing stimulus duration.
Comparison of psychophysical kernels (PK) for different stimulus durations, obtained from human observers $(N = 21)$ (top) performing a brightness dicrimination task (Bronfman, Brezis, and Usher 2016)and in the DWM (bottom). The PKs of the DWM were computed with the same stimuli presented to the human subjects (methods).

Discussion

In this chapter, we have shown that the winner-take-all models with attractor dynamics can operate in distinct regimes: primacy, flexible categorization and recency. The canonical models with absorbing or reflecting boundaries can reproduce primacy and recency psychophysical kernel (PK). But they can not reproduce the non-monotonic PK which is a signature of attractor dynamics. Here we have explained the dependence of these integration regimes to the stimulus parameters. But similarly analysis can be done with internal parameters that are not under the control of the experimenter. For example, increasing the internal noise has also the effect of changing the PK from primacy to recency. Because the two sources of noise are mathematically identically, we could swap their values and the dynamics will be exactly the same. However, as the internal noise become stronger the psychophysical kernel area would decrease. Another important parameter is the c_2 which controls the height of the barrier. For small barriers the transitions are likely and the PK is recency. As the barrier increases, the transitions become more unlikely and the PK becomes more primacy. Thus the shape of the PK depends on the ratio between the total noise $\sigma = \sqrt{\sigma_S^2 + \sigma_i^2}$ and the height of the barrier c_2. The parameter c_2 is simply the distance of the state of the network to the bifurcation point (Roxin and Ledberg 2008). As the system moves away from the bifurcation (increase c_2), the wells become deeper and the dynamics is more categorical. The height of the barrier could be controlled by an untuned input to the decision network from another brain circuit and it could be a possible mechanism to implement an urgency signal (Cisek, Puskas, and El-Murr 2009; Thura et al. 2012).

Several psychophysical studies have shown different types of psychophysical kernels. In the classic random dot experiment, monkeys and humans have the tendency to give more weight to the early than late evidence (primacy PK) (Roozbeh Kiani, Hanks, and Shadlen 2008; Nienborg and Cumming 2009; Zylberberg, Barttfeld, and Sigman 2012). However, other experiments in similar tasks show recency PK (Cheadle et al. 2014; Wyart, Myers, and Summerfield 2015). Finally, the optimal PK which equally weights the evidence has also been reported in rats and humans (Brunton, Botvinick, and Brody 2013; Wyart et al. 2012), These different behaviours can be explained by different canonical model with absorbing bounds (primacy), reflecting bounds (recency) and without bounds (flat). In contrast, the double well model (DWM) has different integration regime with primacy, recency and almost flat PK. Then the DWM seems difficult to falsify because it is able to explain all possible PK.

However, we test a very specific prediction about how the PK should change with the stimulus duration and we found that subjects tend to be primacy for short trials and recency for long trials (Bronfman, Brezis, and Usher 2016) as predicted by the DWM.

In (Bronfman, Brezis, and Usher 2016), the authors of the paper propose a model that change from inhibition dominated to leaky dominated by changing the parameters during the stimulus. In the framework of the DWM, this is equivalent to an opposite urgency signal for which the height of the barrier decreases during the trial, even to negative values where the two stable states which represent the two possible choices merge into one single state. We proposed the transitions between wells as a possible mechanism to explain the change from primacy to recency without the need to change the parameters during the trial. These transitions represent changes of mind that have been reported in reaction time task (Resulaj et al. 2009; van den Berg et al. 2016) and also in tasks where the stimulus duration was controlled by the experimenters (Roozbeh Kiani et al. 2014). Changes of mind are normally reported in a small fraction of trials, our hypothesis is that with long enough trials or strong enough stimulus fluctuations these transitions should become more likely.

Transitions from wells in bistable systems (double well) have been intensively studied and have many applications in different fields, see (Schneider 1994) for a review. These transitions are also the underlying mechanism for the increase in accuracy when the signal to noise ratio of the stimulus decreases (figure 8). Specifically, the accuracy increases in the range of σ_S where the probability of correcting transitions is much higher than error transitions. The same mechanism drives the classic stochastic resonance (Gammaitoni et al. 1998). Put simply, for a particle moving in a double well potential with a periodic signal that raises and lowers the right and the left wells in an antisymmetric manner, there is a suitable magnitude of noise which allows for the system to follow the signal (i.e. escape from the well when it becomes a local minimum, figure S1). For weak noise, the particle is unable to follow the signal because it can not escape from the local minimum and consequently it remains always in the same well. In the other extreme regime, for strong noise, the particle escapes easily from both wells and the position of the particle is driven by the noise and not by the periodic signal. The difference between our task and the classic stochastic resonance is that in our case the global maximum (the correct well) does not change during the stimulus and the particle starts in the unbiased position. In our task, when the trial starts the particle is in unbiased position $X_0 = 0$ which belongs to the basis of attraction of the correct well. In the deterministic case with $\sigma = 0$, the particle rolls down to the correct attractor (note that

only when the signal is zero $\mu = 0$, the unbiased position coincides with the maximum of the potential). Thus in contrast to classic stochastic resonance, in our case the maximum in accuracy is always at zero noise level and the maximum produced by the correcting transition is only a local maximum. The effect of stochastic resonance has been used to explain many phenomena in physics and also in neuroscience (Gammaitoni et al. 1998). For example it has been used to explain neurophysiological experiments studying interspike intervals under periodic stimulation (Longtin, Bulsara, and Moss 1991; Gammaitoni et al. 1998). More recently has also been applied to evidence accumulation tasks, to enhance the accumulation drift rate for stimuli just below the perceptual threshold with transcranial random noise stimulation (van der Groen et al. 2018). However, to the best of our knowledge it has never been reported that the accuracy in perceptual decision making increases as the signal to noise ratio of the stimulus decreases.

Our results show that the accuracy and the consistency of the DWM changes non-monotonically with the stimulus fluctuations (σ_S). Both predictions could be experimentally tested. In that case, the experimenters should take into account the fact that these non-monotonic effects are limited to a range of σ_S which depend on internal parameters such as the internal noise and the height of the barrier. At the same time these internal parameters can be different for different subjects. Thus one expects to find the non-monotonic relation of consistency and accuracy with σ_S only in a fraction of subjects. Additionally, for the case of consistency, we found a large variability across stimuli, stimuli that presented a large dip in consistency while others almost do not show it. The consistency of the average stimuli is presented in figure 9a, but we also show in figure 9b the consistency of one example stimulus for which the dip in consistency is much deeper, from almost 100 % to less than 65%. One possible strategy would be to first fit the double well model to each subject and then use simulations of the fitted potentials to identify those stimuli with deeper dips.

The relation between the canonical models and the models with attractor dynamics has been studied extensively (Wang 2002; Gold and Shadlen 2007; Bogacz et al. 2006; Ratcliff and Smith 2004). Up until now, most of these studies have been focus to understand under which parameter regimes the models were equivalent. In this first chapter, we emphasized the differences between these models and we make experimentally testable predictions to distinguish between them. We also showed that the new integrations regime of the DWM

can explain psychophysical data that was previously understood as evidence against the attractor models.

Methods

Model simulations

To compute the PK, the accuracy and the consistency of the different models we solved 2 using the Euler method:

$$x(t+1) = x(t) - \Delta t d\varphi/dX + \sqrt{\Delta t}(\sigma_I \xi(t) + \sigma_S \xi(t)) \quad (11)$$

with $\Delta t = \tau/40$.

In the next table, we summarize the parameters used in each figure

	μ	c_2	c_4	τ	σ_I	T	Bound
Figure 6	0	-	-	200 *ms*	0.1	1000 *ms*	0.5
Figure 2	0	2	4	200 *ms*	0.1	1000 *ms*	-
Figure 3 DWM	0.15	2	4	200 *ms*	0.1	2000 *ms*	-
Figure 8 DDMs	0.05	-	-	200 *ms*	0	2000 *ms*	0.5
Figure 9 DWM	0	2	4	200 *ms*	-	1000 *ms*	-
Figure 9 DDMs	0	-	-	200 *ms*	0.08	1000 *ms*	0.5
Figure 13	-	1.6	4	200 *ms*	0.3	-	-
Figure 14	0.15	2	4	10 *ms*	0.3	240 *ms*	-

In figure 9, we only use stimuli with exactly zeros mean evidence, $\int S(t)dt = 0$. For each stimulus i, we first created a stream of normal random variables $y_i(t)$. Then we z-score y and we multiplied by σ_S :

$$S_i(t) = \sigma_S \frac{y_i(t) - \hat{y}}{\sigma_y} \quad (12)$$

After this transformation, the mean and standard deviation of S_i are exactly 0 and σ_S respectively.

Psychophysical kernel

We measure the impact of stimulus fluctuations during the course of the trial on the eventual decision by means of the so-called psychophysical kernel (PK). Put simply, given a fixed mean signal, some stimulus realizations may favor a rightward choice (say a positive decision variable) and others a leftward one. If this is the case, and we sort the stimuli over many trials by decision, we will see a clear separation which can be quantified via a ROC analysis. Mathematically, for each trial i, we subtract the mean evidence (μ_i) of each trial $s_i(t) = \mu_i + \sigma_s \xi_i$ to avoid that the distributions of stimuli that produce a left and right choices are trivially separated by its mean evidence:

$$\widehat{s_i}(t) = s_i(t) - \mu_i \tag{13}$$

With $\widehat{s_i}(t) = \sigma_s \xi_i$ are simply the stimulus fluctuations. Then, for each time t, we compute the probability distribution function of the stimuli that produce a right ($f((\widehat{s_R}(t))$) or left ($f((\widehat{s_L}(t))$) choice. The PK is the temporal evolution of the area under the ROC curve between these two distributions

$$PK(t) = auc\left(f(\widehat{s_R}(t)), f(\widehat{s_L}(t)) \right) \tag{14}$$

Normalized psychophysical kernel area and primacy-recency index

In order to quantify changes in the PK, we characterized the PK with two measures:

1) The Normalized PK area is a measure of the overall impact of stimulus fluctuations on the upcoming decision, it ranges from 0 (No impact) to 1 (the stimulus fluctuations are perfectly integrated to make a choice).

$$NPKA = \frac{\int_o^T PK(t)\, dt - 0.5T}{\int_0^T PK_{PI}(t, \sigma_i = 0)\, dt - 0.5T} \tag{15}$$

Where T is the stimulus duration. $NPKA$ is the PK area normalized by the PK area of a Perfect Integrator in the absence of internal noise $(\sigma_i = 0)$. $NPKA$ is a measure of the overall impact of stimulus fluctuations on the upcoming decision and it ranges from 0 (No impact) to 1 (the stimulus fluctuations are perfectly integrated to make a choice).

2) Primacy-recency index:

$$PRI = \int_0^T \omega(t) NPK(t)\, dt \tag{16}$$

with

$$NPK(t) = \frac{PK(t) - 0.5T}{\int_0^T PK(t)dt - 0.5T} \tag{17}$$

$$\omega(t) = 1 - \frac{2}{T}t \tag{18}$$

Where $NPK(t)$ is the PK with normalized area to 1 and $\omega(t)$ is the weighting function that linearly decrease with time from 1 to -1. First we normalized the PK area to factor out the effect of the PK area because we want to measure the PK shape without taking into account the total area. The role of the linear weighting function is to weigh the early (late) regions with positive (negative) values. The PRI ranges from -1 (extreme recency) to 1 (extreme primacy).

In figure 15 , we define the Primacy-Recency Index

$$PRI = \frac{\beta_1 - \beta_2}{\beta_1 + \beta_2} \tag{19}$$

Where β_1 and β_2 are the coefficients of a logistic regression with the coherence of the first and second pulse as predictors:

$$logit(P_C) = \beta_0 + \beta_1 coh_1 + \beta_2 coh_2 \tag{20}$$

Accuracy for the DWM

To compute the accuracy for the DWM, we assume that the time spent in the unstable region is much shorter than the time spent in one of the attractors. This assumption allows us to treat the system as a Continuous Markov Chain (CMC) with only two possible states correct and error. The first step is to compute the probability of first visiting the correct attractor which will be used as the initial state of the CMC (Gardiner 1985)

$$P_{C,0} = \frac{\int_{x_E}^{x_0} exp(\frac{2\varphi(x)}{\sigma_I^2+\sigma_S^2})\,dx}{\int_{x_E}^{x_C} exp(\frac{2\varphi(x)}{\sigma_I^2+\sigma_S^2})\,dx} \quad (21)$$

where φ is the potential in Eq. 3, x_C and x_E are the x values of the correct and incorrect attractors whereas $x_0 = 0$ is the initial position of x.

The integrals of $P_{C,0}$ can be computed assuming that the term x^4 is very small for values of $x_0 \simeq 0$

$$P_{C,0} = \frac{erf\left(\frac{\sqrt{c_2}}{\sigma}\left(x_0+\frac{\mu}{c_2}\right)\right)-erf\left(\frac{\sqrt{c_2}}{\sigma}\left(x_E+\frac{\mu}{c_2}\right)\right)}{erf\left(\frac{\sqrt{c_2}}{\sigma}\left(x_E+\frac{\mu}{c_2}\right)\right)-erf\left(\frac{\sqrt{c_2}}{\sigma}\left(x_C+\frac{\mu}{c_2}\right)\right)} \quad (22)$$

The second step is to compute the correcting and error transition rates (Gardiner 1985, Kramer 1949)

$$k_{CE} = \frac{\sqrt{|\varphi''(x_E)\varphi''(x_U)|}}{2\pi} exp(\frac{-2(\varphi(x_U)-\varphi(x_E))}{\sigma_I^2+\sigma_S^2}) \quad (23)$$

$$k_{EC} = \frac{\sqrt{|\varphi''(x_C)\varphi''(x_U)|}}{2\pi} exp(\frac{-2(\varphi(x_U)-\varphi(x_C))}{\sigma_I^2+\sigma_S^2}) \quad (24)$$

With the transitions rates we can compute the probability of making a correcting transition and the probability to remain in the correct attractor at the end of the trial (Durrett 2016):

$$P_{CC}(T) = P_{C,S}(1 - exp(-kT) + exp(-kT) \quad (25)$$

$$P_{CE}(T) = P_{C,S}(1 - exp(-kT)) \quad (26)$$

where $k = k_{CE} + k_{EC}$, T is the stimulus duration and $P_{C,S} = \frac{k_{CE}}{k_{CE}+k_{EC}}$ is the probability of correct at the stationary state ($T \to \infty$). Finally, the probability of correct given the model and stimulus parameters ($c_2, c_4, \sigma_I \mu, \sigma_S$ and T)

$$P_C = P_{C,0}P_{CC} + (1 - P_{C,0})P_{CE} \quad (27)$$

Thus the probability of correct is the probability to first visit the correct attractor and remain in it ($P_{C,0}P_{CC}$) plus the probability to first visit the error attractor and correct the initial decision ($(1-P_{C,0})P_{CE}$).

To be more quantitative, if the first well visited is not the correct one, then the probability of finding the state in the correct well at time T is given by Eq. X (2 equations above). The probability of finding the state of the system in the error well if the initial well is correct is given by

$$P_{EC} = k_{EC}(1-exp(-kT))/k \quad (28)$$

The ratio of these probabilities is

$$P_{CE}/P_{EC} \propto exp(2(\varphi(X_E)-\varphi(X_C))/\sigma^2) \quad (29)$$

which shows that correcting transitions are exponentially more likely than error-generating ones, as long as stimulus fluctuations are not too large. In particular, for weak stimulus strength μ, this ratio is

$$P_{CE}/P_{EC} = exp(4\mu\sqrt{c_2/c_4}/\sigma^2) \quad (30)$$

These probabilities are illustrated in Fig.4B; P_{CE} (green) increases steeply as a function of stimulus fluctuations even before P_{EC} reaches non-negligible values.

Asymptotic analysis

Here we investigate the range of parameters where the accuracy is non-monotonic with the stimulus fluctuations. Concretely, we compute the critical values of μ_C and σ_I beyond which the performance decays monotonically with σ_S. First, we compute the positions of the attractors when $\mu << 1$ by finding the potential roots of order $\vartheta(\varepsilon^2)$ using $\bar{\mu} = \varepsilon\mu$ and $x = x_0 + \varepsilon x_1$

$$x_C = \sqrt{\frac{c_2}{c_4}} + \frac{\bar{\mu}}{2c_2} + \vartheta(\varepsilon^2) \quad (31)$$

$$x_E = \sqrt{\frac{c_2}{c_4}} - \frac{\bar{\mu}}{2c_2} + \vartheta(\varepsilon^2) \quad (32)$$

$$x_U = -\frac{\bar{\mu}}{2c_2} + \theta(\varepsilon^2) \quad (33)$$

Where x_U is the x position of the unstable state (x_U =0 when $\mu = 0$) and x_C (x_E) are the positions of the correct (error) attractor. Plugging these attractor positions into equations 23 and 24, the transitions rate for small values of μ are

$$k_{CE} = \frac{c_2}{\sqrt{2\pi}} e^{-\frac{1}{2\sigma^2}\frac{c_2^2}{c_4}} e^{\frac{2\bar{\mu}}{\sigma^2}\sqrt{\frac{c_2}{c_4}}} \quad (34)$$

$$k_{EC} = \frac{c_2}{\sqrt{2\pi}} e^{-\frac{1}{2\sigma^2}\frac{c_2^2}{c_4}} e^{-\frac{2\bar{\mu}}{\sigma^2}\sqrt{\frac{c_2}{c_4}}} \quad (35)$$

If there is a non monotonicity of the accuracy with σ^2 ($\sigma^2 = \sigma_I^2 + \sigma_S^2$), we should find a maximum of the probability of correct when the error attractor was first visited (equation 26).

$$P_{CE} = \frac{exp(a\beta)}{2cosh(a\beta)}(1 - e^{-kT}) \quad (36)$$

$$k = k_{CE} + k_{EC} = \frac{\sqrt{2}c_2}{\pi} e^{-\frac{\beta c_2}{2c_4}} cosh(a\beta) \quad (37)$$

Where $a = 2\mu\sqrt{\frac{c_2}{c_4}}$ and $\beta = \frac{1}{\sigma^2}$. To check the existence of a local maximum we derive P_{CE} respect to σ

$$\frac{dP_{CE}}{d\sigma} = -\frac{2}{\sigma^3}\frac{dP_{CE}}{d\beta} = a(1 - tanh(a\beta))\,(1 - e^{-kT}) + \frac{dk}{d\beta} T e^{-kT} = 0 \quad (38)$$

$$\frac{dk}{d\beta} = \frac{\sqrt{2}c_2}{\pi}(asinh(a\beta) - \frac{c_2^2}{2c_4}cosh(a\beta))e^{-\frac{\beta c_2}{2c_4}} \quad (39)$$

For small values of μ both equations can be approximated by

$$\frac{dP_{CE}}{d\sigma} = a\,(1 - e^{-kT}) + \frac{dk}{d\beta} T e^{-kT} \quad (40)$$

$$\frac{dk}{d\beta} = -\frac{\sqrt{2}}{\pi}\frac{c_2^3}{2c_4} e^{-\frac{\beta c_2}{2c_4}} \quad (41)$$

For small values of σ, $1 - e^{-kT} \simeq 0$. However there is always a large enough T so that $1 - e^{-kT} \simeq 1$. The local maximum of the accuracy must be in the region where these two effects are of the same order $kT \sim \theta(1)$. Thus we defined $T = \frac{\tau}{\varepsilon}$ and $e^{-\frac{\beta}{2}\frac{c_2^2}{c_4}} = \varepsilon y$. Plugging these into equation 40

$$\frac{dP_{CE}}{d\sigma} = a\left(1 - e^{-\frac{\sqrt{2}c_2}{\pi}y\tau}\right) + \frac{y\tau}{\sqrt{2}\pi}\frac{c_2^3}{c_4}e^{-\frac{\sqrt{2}c_2}{\pi}y\tau} = 0 \quad (42)$$

To have a maximum of P_{CE}, there must be a solution to the following implicit equation

$$z = \frac{1}{\sqrt{2}}log(1 + \frac{c2}{\sqrt{2}}\sqrt{\frac{c_2}{c_4}}\frac{z}{\mu}) \quad (43)$$

Where $z = \frac{y\tau c_2}{\pi}$, using the definitions of τ and y, there is a maximum of P_{CE} at

$$\sigma_{MAX}{}^2 = \frac{c_2^2}{2c_4}\frac{1}{log\left(\frac{Tc_2}{\pi z_0}\right)} \quad (44)$$

Where z_0 is the solution of the implicit equation 43.
Similarly, to find the maximum of the accuracy we derive equation 27 respect to σ

$$\frac{dP_C}{d\sigma} = -\frac{2}{\sigma^3}\frac{d}{d\beta}\left[P_{C,0}exp(-kT) + P_{C,E}\right] \quad (45)$$

Where we rewrite equation 27 as a function of $P_{C,E}$ and $P_{C,0}$ is the probability to first visit the correct attractor . As long as $\frac{\sqrt{c_2}x_R}{\sigma} >> 1$ (and similarly for x_L), equation 22 is well approximated by

$$P_{C,0} = \frac{1}{2}\left(1 + erf\left(\frac{\sqrt{c_2}}{\sigma}\left(x_0 + \frac{\mu}{c_2}\right)\right)\right) \quad (46)$$

In the range of parameters where μ is small and β is large we can assume that $\beta\mu^2 << 1$, $\sqrt{\beta}\mu << 1$ and $\mu\beta >> 1$. Using these inequalities, equation 45 can be simplified to

$$\frac{dP_C}{d\sigma} = a(1 - tanh(a\beta))(1 - e^{-kT}) + \frac{1}{2}\frac{dk}{d\beta}Te^{-kT} = 0 \quad (47)$$

With these simplifications the derivative $\frac{dP_C}{d\sigma}$ is equivalent to the derivative $\frac{dP_{CE}}{d\sigma}$ (equation 40) with a $\frac{1}{2}$ factor in the second term. This factor modifies the implicit equation 43 to

$$z = \frac{1}{\sqrt{2}}log\left(1 + \frac{c2}{2\sqrt{2}}\sqrt{\frac{c_2}{c_4}}\frac{z}{\mu}\right) \quad (48)$$

Then the critical value of the internal noise for which accuracy decreases monotonically with the stimulus fluctuations is

$$\sigma_{IC}{}^2 = \frac{c_2^2}{2c_4}\frac{1}{log\left(\frac{Tc_2}{\pi z_0}\right)} \tag{49}$$

By expanding in Taylor series equation 48, $log(1+x) = x - \frac{x^2}{2} + \theta(x^3)$ we found an approximate solution of the implicit equation

$$z_0 = \frac{16\sqrt{2}\mu^2 c_4}{c_2^3}\sqrt{\frac{c_4}{c_2}}\mu\left(1 - 4c_2\sqrt{\frac{c_2}{c_4}}\mu\right) \tag{50}$$

Because z_0 must be positive there is a critical value of μ for which the accuracy also decreases monotonically with the stimulus fluctuations

$$\mu_C = \frac{c_2}{4}\sqrt{\frac{c_2}{c_4}} \tag{51}$$

Psychophysical data and model fitting

In figure 13, we used data from experiments 1 and 4 from (Bronfman, Brezis, and Usher 2016) with a total of $N = 21$ humans subjects. The data can be accessed here: https://doi.org/10.1371/journal.pcbi.1004667.

The stimuli consisted of two brightness-fluctuating round disks. At each time frame (100 ms). the brightness level of each disk was updated from a generative gaussian distribution. The generative distributions for both the disks had the same variance but different mean (high or low). At the end of the stimulus, the subjects had to report the disk with an overall higher brightness (higher mean of the generative gaussian distribution). Trials were separated into 5 equal length segments, in 80 % of the trials, a congruent or incongruent pulse of evidence was presented at a random segment. This increase or decrease of evidence was corrected in the rest of the segments and as a consequence the stimuli were anticorrelated. In experiment 1 trials with 1,2 or 3 seconds duration were presented in blocks of 60 trials whereas in experiment 4, the trial duration was 5 seconds. We computed the PK using the usual procedure but first we subtract the brightness of the two disks and their means to have a 1-dimensional stimuli with zero mean. Namely

$$S^i(t) = S_R^i(t) - S_L^i(t) - (\mu_R^i - \mu_L^i), \quad (52)$$

where $S_L^i(t)$ is the brightness of the Left disk during the i-th stimuli and μ_L^i is the mean of the generative gaussian distribution for the Left i-th stimuli. We computed the confidence interval using bootstrap with 1000 repetitions.

To compute the PK of the DWM we simulated Eq 2 with the exact same stimuli presented to the subjects. We modeled it by updating $\mu^i(t)$ from Eq. 3 with the difference in brightness at each time between the Right and Left disk:

$$\mu^i(t) = S_R^i(t) - S_L^i(t) \quad (53)$$

Note that in this framework the stimulus fluctuations were set to zero $\sigma_S = 0$ because σ_S was captured inside $\mu^i(t)$. The DWM parameters ($c_2 = -1.6, c_4 = 4, \sigma_I = 0.3$ and $\tau = 200\ ms$) were tuned to qualitatively explain the change from primacy to recency with the stimulus duration.

Network of integrate-and-fire neurons

We consider a network of recurrently coupled integrate-and-fire neurons, similar to Roxin&Ledberg 2008. The network consists of two populations of excitatory neurons (A and B), both of which are coupled to a population of inhibitory interneurons. We will study the case in which the system is near a steady bifurcation to a winner-take-all state. It is in the vicinity of the bifurcation that the dynamics can be captured in a one-dimensional amplitude equation which describes the slow evolution along the critical manifold (see chapter blabla of this thesis and Roxin&Ledberg 2008). The evolution equations for the neuronal membrane potentials are

$$\tau_{me}\frac{dV_{A,i}}{dt} = -\left(V_{A,i} - E_l\right) + I_{AA.i} - I_{AI.i} + I_{Aext.i}/g_L,$$

$$\tau_{me}\frac{dV_{B,i}}{dt} = -\left(V_{B,i} - E_l\right) + I_{BB.i} - I_{BI.i} + I_{Bext.i}/g_L,$$

$$\tau_{mi}\frac{dV_{I,i}}{dt} = -\left(V_{I,i} - E_l\right) + I_{IA.i} - I_{IB.i} + I_{Iext.i}/g_L,$$

where the synaptic inputs of the form I_{XY} indicate interactions from neurons in population Y to neurons in population X, while external synaptic inputs are given by I_{Xext}. The synaptic inputs are sums over all postsynaptic potentials (PSPs), modeled as exponential functions

with a delay (note that this different from (Roxin and Ledberg 2008) which used Dirac-delta functions with a delay) The synaptic inputs take the form

$$I_{XY,i} = \sum_j J_{ij}^{XY} g_{ij}^{XY} \ .$$

The dynamics of excitatory and inhibitory synapses are described by

$$\tau_{se} \frac{dg_{ij}^{XY}}{dt} = - g_{ij}^{XY} \ ,$$

$$\tau_{si} \frac{dg_{ij}^{XY}}{dt} = - g_{ij}^{XY} \ .$$

After each presynaptic spike at time t_{XY}^k , the corresponding dynamic variable is incremented by one at $t_{XY}^k + \delta_{X,ij}$, that is after a delay $\delta_{X,ij}$.

External synapses have instantaneous dynamics

$$I_{Xext,i} = \sum_j J_{ij}^{ext} \sum_k \delta(t - t_{Xext,j}^k),$$

i.e. a presynaptic action potential from neuron j of the external population at time $t_{Xext,j}^k$ results in an instantaneous jump of the external synaptic input variable. A spike is emitted whenever the voltage of a cell from an excitatory (inhibitory) population crosses a value Θ, after which it is reset to a reset potential V_r .

We consider the case of sparse connectivity for which, on average, each neuron from population X receives a total of C_{XY} synapses from population Y. The pairwise probability of connection is thus $\varepsilon_{XY} = C_{XY}/N_Y$, where $N_A = N_B = N_E$ and N_I are the number of neurons in the respective populations. For nonzero synapses we choose $J_{ij}^{AA} = J_{ij}^{BB} = J_{ee}$, $J_{ij}^{IA} = J_{ij}^{IB} = J_{ie}$ and $J_{ij}^{AI} = J_{ij}^{BI} = J_{ei}$.

The stimulus input is modeled similar to Wimmer et al 2015, but with the exact same stimulus input to each neuron in the two excitatory populations A and B (rather than with a common and private contribution as in Wimmer et al 2015). The stimulus input to two excitatory populations A and B is given by

$$I_{stim}^A(t) = I_0(1 + \mu) + \sigma_{stim} z^A(t)$$
$$I_{stim}^B(t) = I_0(1 - \mu) + \sigma_{stim} z^B(t),$$

where the first term describes the average stimulus input and the second term the temporal modulations of the stimulus with standard deviation σ_{stim}. Finally, $z^A(t)$ und $z^B(t)$ are

independent realizations of an Ornstein-Uhlenbeck process, defined by $\tau_{stim}\frac{dz}{dt} = -z + \sqrt{2\tau_{stim}}\xi(t)$, where $\xi(t)$ is Gaussian white noise (mean 0, variance dt).

Table 1: Simulation parameters for the spiking neural network model.

Populations		
N_E	1000	Size of excitatory populations A and B
N_I	500	Size of inhibitory population
Recurrent connectivity		
J_{ee}	0.16 mV	Weight of excitatory to excitatory connection
J_{ie}	0.08 mV	Weight of excitatory to inhibitory connection
J_{ei}	-4 mV	Weight of inhibitory to excitatory connection
C_{ee}	100	Average number of synapses for excitatory to excitatory populations
C_{ie}	50	Average number of synapses for excitatory to inhibitory populations
C_{ei}	50	Average number of synapses for inhibitory to excitatory populations
Neuron model		
τ_{me}	20 ms	Membrane time constant of excitatory neurons
τ_{mi}	10 ms	Membrane time constant of inhibitory neurons
g_{Le}	12.5 nS	Leak conductance of excitatory neurons
g_{Li}	25 nS	Leak conductance of inhibitory neurons
E_l	-70 mV	Resting potential
Θ	-50 mV	Spiking threshold
E_r	-60 mV	Reset potential
Synapse model		
τ_{se}	12.5 ms	Time constant of excitatory synapses
τ_{si}	1 ms	Time constant of inhibitory synapses

δ_e	5 ms	synaptic delays for excitatory synapses (uniform distribution with mean 5 ms)
δ_i	1 ms	synaptic delays for excitatory synapses (uniform distribution with mean 1 ms)
External Poisson inputs		
J_{ext}	0.2 mV	Weight of external inputs
$\nu_{e,ext}$	5000 Hz	Firing rate of external Poisson inputs to excitatory neurons
$\nu_{e,ext}$	9000 Hz	Firing rate of external Poisson inputs to inhibitory neurons
Stimulus inputs		
I_0	25 pA	Mean input for zero-coherence stimulus
μ	0.03	Additional input for non-zero coherence stimulus
σ_S	varied	Amplitude of temporal modulations of the stimulus
σ_{stim}	0.25 pA $\cdot \sigma$	S. d. of temporal modulations of the stimulus
τ_{stim}	20 ms	Correlation time of Ornstein-Uhlenbeck process

3. The double well model in tasks involving working memory and decision making

Summary

Many studies have addressed the question whether the brain can make optimal decisions. In principle, if the stimulus duration is controlled by the subject, the optimal strategy is to maximize the reward rate by trading accuracy for speed. In fixed duration tasks, the optimal strategy is simply to linearly sum all the stimulus evidence. Defining the optimal strategy, however, depends on the constraints of the system. But little is known about the biological constraints under which brain circuits operate. Here, we study this problem by considering a couple of fundamental constraints derived from general arguments about neural physiology. First we assume that the range for accumulating evidence in a neural circuit is bounded because of the limits in the physiological range of neural firing rates. In that case, the double well model became optimal because the categorization introduced by the winner-take-all dynamics compensates the loss of accumulated evidence caused by the integration with reflecting bounds. The double well model is also suitable to store a decision during a period without stimulus. Actually, in tasks where the stimulus is interrupted by a temporal gap during which the accumulated evidence must be maintained by the circuit, the optimal strategy is to strengthen the winner-take-all dynamics. We furthermore show that, for such a task combining evidence integration and working memory, the double well model can actually fit data from an already published psychophysical experiment. Strikingly, in this task, the accuracy does not decrease with the length of the temporal delay which suggests that information about the first part of the stimulus is categorical stored. Overall, these results complement the analysis shown in the previous chapter by explaining how neural circuits could be implementing the integration.

Results

Impact of the winner take all dynamics in the accumulation of evidence

In the previous chapter we have shown that the Double Well Model (DWM) has different integration regimes and how the performance depends on these regimes. Here, we show that the DWM can be computationally advantageous over other models when basic biophysical constraints are considered. In principle, optimal performance in a categorization tasks with ambiguous fluctuating stimuli would be achieved by linearly summing each sample of evidence without leak nor absorbing bounds, that is by a temporally uniform integration of all the evidence. The dynamics of the DWM, in contrast, introduce transient integration (i.e. primacy or recency effects) which can *a priori* decreased performance because some parts of the stimulus stream are barely weighted into the final choice. A perfect integrator however is not the optimal model when one imposes reflecting bounds in the integration (Zhang and Bogacz 2010). This is a plausible constraint given that, among other factors, individual neurons show spiking refractoriness, an effect that limits the range of output firing rate. To compare the categorization accuracy across models respecting bounded integration, we used the DWM with different barrier heights (c_2) (figure 14a). When the barrier height was set to zero, the model was equivalent to a perfect integrator with reflecting bounds: increasing the magnitude of stimulus fluctuations, increased the probability to hit the bounds during stimulus integration, causing that some stimulus evidence was lost (figure 6a, bottom traces). Specifically, as early evidence made the system approach the bound, the integration of further evidence was biased towards reverting the impact of the early evidence, because any confirmatory evidence would be essentially lost by trying to *push* the system against the bound. As a consequence, the larger stimulus fluctuations, the smaller was the categorization accuracy (figure 8f). In these circumstances in which the combination of bounded integration and large stimulus fluctuations caused recency, introducing a barrier compensated the bias introduced by the bounds and increased the accuracy (figure 14a). The categorization improvement occurred because, once the system approached the side bounds, the central barrier introduced a confirmation bias that compensated the reverting bias caused by the bounds. The optimal barrier height was achieved when these two effects balanced in the flexible categorization regime (primacy-recency index ≈ 0), and correspondingly it increased with stimulus fluctuations (figure 14a). Thus, when the biophysical constraints of integration bounds were introduced, a

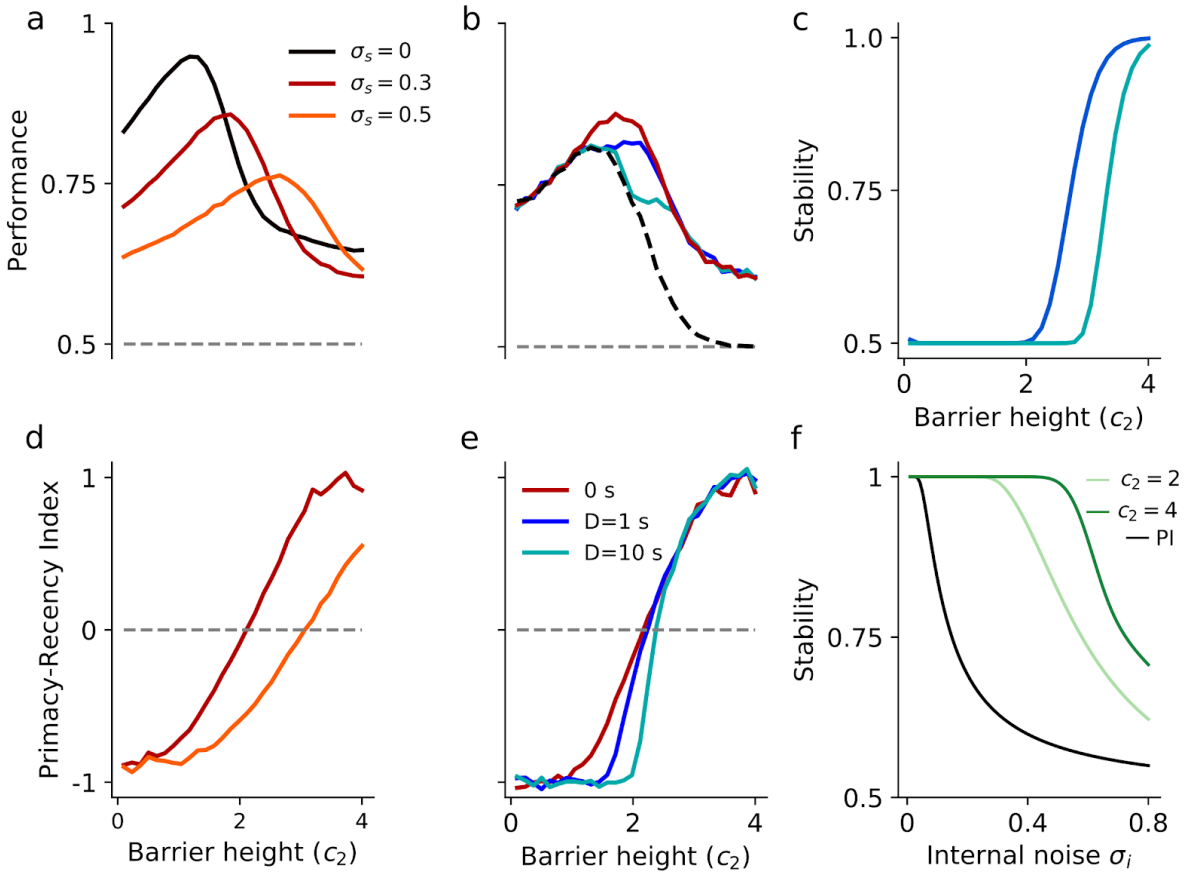

Figure 14 | Effect of the barrier height in the categorization accuracy of the DWM and the impact of temporal integration gaps .
(a) Categorization accuracy versus the barrier height for different levels of stimulus fluctuations (see inset) obtained from numerical simulations of a model with integration bounds. The non-zero optimal barrier height increases with the magnitude of stimulus fluctuations. For all the panels $\sigma_i = 0.3$ and $T = 240\ ms$ **(b)** Categorization accuracy when the stimulus is divided in two input short streams $(T = 120\ ms)$ separated by a temporal gap of duration D. Longer gaps shift the optimal barrier towards higher values. Red line shows the case $D = 0$ (same as in panel a) . Dashed black line shows the accuracy with only one frame of evidence and random initial condition, extreme case for which the information of the first pulse is completely lost. **(c)** The probability to maintain the initial categorization (stability) monotonically increases with the height of the barrier. **(d)** The optimal barrier coincides with the Flexible categorization with a primacy-recency index close to zero. **(e)** The change from recency to primacy is affected by the stimulus fluctuations and the length of the delay. To better show the difference between the impact of the first and second pulse, we compute the primacy-recency index as $PRI = (a_2 - a_2)/(a_2 + a_1)$ where a_1 and a_2 are psychophysical kernel area in the first and second pulse. **(f)** For non zero level of internal noise, the models without stable fixed points are unable to maintain the initial categorization during the temporal integration gap.

DWM with a non-zero barrier height outperformed an equivalent model with no barrier.

Impact of temporal gaps in models with winner take all dynamics

Introducing a barrier also had the consequence of making the system more fitted to maintain information during delay periods without stimulus evidence. For instance, in some tasks the decision evidence is presented in two or more stimuli that subjects must combine in order to perform the task. In these circumstances, the evidence after the first pulse of stimulus evidence needs to be maintained by the circuit in the absence of any external input (R. Kiani, Churchland, and Shadlen 2013a) . This is simply because the attractors in the double well model (DWM) are stable fixed points of the system that can support short-term memory (Amit and Brunel 1997; Wang 2002)(Amit and Brunel 1997; Wang 2002). On the one hand, the stability (i.e. the probability to remain in the same attractor during the temporal gap between pulses) improve monotonically with the height of the barrier (figure 14c). On the other hand, although stimuli without temporal gaps the optimal barrier height is not zero, the accuracy is very poor for high barriers for which the integration process becomes extremely primacy (figure 14a). The interaction of these two effects, namely the need for stability (high barrier) and integration accuracy (small barrier), cause a shift of the optimal barrier height towards higher barriers (figure 14b). However, for very long delays, it is not worth it to maintain the categorization after the first pulse of evidence because this would require a very high barrier which would produced a very poor initial categorization. Thus, for long delays it is better to only use the second pulse after the temporal gap assuming that the state of the system after the delay will be one or the other category with the same probability because of the random transitions during the delay. This would be an extreme case in which, because the barrier is small and the delay is long, the information about the first pulse is completely erased. To illustrate this, we plot the accuracy as a function of the barrier height for different delays (figure 14b) . We also compare these curves with the performance to a stimulus of one single pulse with the initial condition being randomly distributed between the two categories (dashed black line figure 14b). For short barriers, the information of the first pulse is completely lost for all the delays and the accuracy curves collapse with the dashed black. As we increase the barrier height, the system is able to maintain in memory the initial categorization for longer delays (the system become more primacy, figure 14e). When the barrier height is high enough to guarantee the stability during the delay, the accuracy and the primacy-recency index curves collapse with the no-delay curve (red line figure 14b and e). Note that it is easier to maintain a decision during the delay than during the stimulus

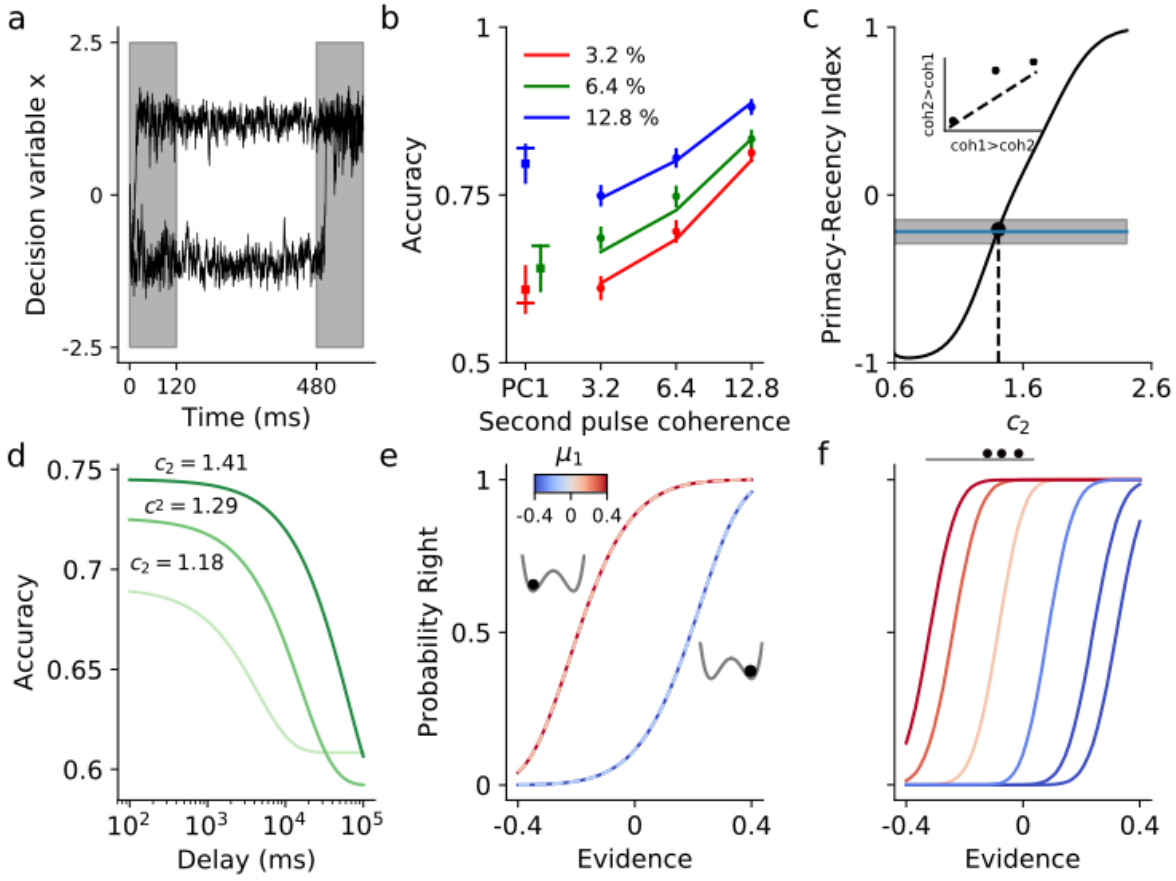

Figure 15 |Flexible categorization regime explains combination of two pulses of evidence. **a)** Single trial traces for a double pulse trial of the DWM model. Using the fitted parameters with the data from (R. Kiani, Churchland, and Shadlen 2013a; Tohidi-Moghaddam et al. 2019) . **b)** Probability of correct for single (squares) and double (dots) pulse trials for the three possible first pulse coherence (3.2% red, 6.4% green, 12.8 % blue) (dots). Solid lines show the accuracy of the fitted DWM.**c)** Primacy-Recency Index as a function of the barrier height (c_2) The black circle mark the PRI for the fitted parameters. The blue line is the PRI computed from the psychophysical data (grey area 95% confidence interval). Inset show that the accuracy is slightly better when the second pulse has higher coherence (slightly Recency). **d)** For any barrier, there is a long enough delay for which the accuracy decrease due to the transitions during the delay. For the fitted parameters, the accuracy is independent of the delay (up to 1 s) even if we consider that the internal noise and stimulus fluctuations have a similar magnitude $\sigma_S/\sigma_i = 1.25$ (methods). **e)** For the DWM, the probability of right only depends on the state of the system before the second pulse and the second pulse itself, but it is independent of the first pulse mean evidence (μ_1). Inset shows the possible states before the second pulse. **f)** For the perfect integrator, the decision variable before the second pulse is a parametric value proportional to μ_1 (see inset). Consequently, the decision depends on both pulses. For clarity purposes, we only show correct categorization after the first pulse.

because the internal noise is the only source of noise during the delay ($\sigma_s = 0$). For a zero level of internal noise, any model would trivially maintain the decision. However, for non-zero values of internal noise, the initial categorization degrades much quicker for models

that assume perfect integration of the evidence, figure 14f . In total, the existence of integration bounds in conjunction with the need to maintain the categorization during stimulus gaps, favored the winner-take-all dynamics provided by the DWM.

Double well model combines stimulus evidence from two pulses

We have shown that the double well model (DWM) is able to combine information from two pulses of evidence separated by a temporal gap. To test if in fact the DWM could explain psychophysics data from a task in which subjects must combine information from two pulses to make a decision, we used data from two experiments (Tohidi-Moghaddam et al. 2019; R. Kiani, Churchland, and Shadlen 2013a) . In both experiments, the task design interleaved trials with single pulses of random dot kinematograms with trials having two pulses separated by a temporal delay. In the two pulses trials, subjects had to combine information of both pulses in order to identify the average motion direction. Subjects were able to combine the evidence from the two pulses without a dependence of the accuracy on the delay between pulses (up to 1s). Moreover, they tend to slightly give more weight to the second that the first pulse (Primacy-Recency Index=-0.22; methods). As we explained, the DWM can naturally solve this task, with the first pulse of 120 ms the decision variable evolve towards one of the attractors. During the delay the system maintains the initial categorization because transitions are very unlikely (there are not stimulus fluctuations, σ_S=0). Finally, if there is enough evidence during the second pulse, the initial categorization can be reversed (figure 15a). To combine both pulses close to the flexible categorization regime, we hypothesize that subjects can adapt the height of the barrier between the two attractors, with common input to the two excitatory population (represented by the parameter, c_2 ; figure 15c). We fitted the DWM (solid lines, figure 15b; methods) with the data extracted from (Tohidi-Moghaddam et al. 2019; R. Kiani, Churchland, and Shadlen 2013a) (square and circular dots (figure 15b). Because the accuracy do not decrease with the temporal gap, we assumed there are no transitions between wells thus during the delay the $\sigma = 0$ (methods). We found that the DWM was able to fit the data for one and two pulses trials indicating the transitions between attractors as a possible explanation for the difference in accuracy between trials with one and two pulses.

One of the intriguing results of (R. Kiani, Churchland, and Shadlen 2013a; Tohidi-Moghaddam et al. 2019) is that the accuracy was independent of the delay between pulses up to 1 second. To explain this behaviour the models that assume perfect integration

of evidence must fix the internal noise to zero (figure 14f). In contrast, the DWM can maintain the initial categorization even when the stimulus fluctuations and the internal noise have similar magnitudes (figure 14d). However, the DWM also predicts that for long enough delays the accuracy would eventually decrease (figure 14d) as suggested by data from a similar experiment in which longer delays were explored (Melcher et al. 2004).

The major difference between the DWM and the canonical models that assume perfect integration is that after the first pulse the state of the DWM is categorical, either left or right whereas the state of the canonical models is a parametric value proportional to the first pulse coherence. For the single pulse trials, it seems reasonable that the state of the system is the same for all the right and left choices independently of the first pulse coherence because a decision needs to be made. However, for the two-pulse trials the DWM is unable to hold in working memory a parametric value of the first pulse coherence. Consequently, the decision depends only on the state of the network just before the second pulse and the second pulse itself but it is independent of the first pulse coherence . In contrast, the state of the canonical models just before the second pulse is a degraded (due to the internal noise during the delay) parametric value that depends on the first pulse coherence. Thus the final decision is also influenced by the first pulse coherence (figure 15 e,f). This experimental prediction illustrates the consequences of a model with categorical choices.

Alternative model with urgency and undecided state

We also try to use the model in the full model with a multistable region and a winner-take-all region. In the multistable region there are three stable states representing the left and the right decision and an undecided state. If the decision variable end in the undecided the decision is taken randomly. As we explained in the introduction, the system can move from the multistable region to the winner-take-all region with the parameter c_2 Additionally, because the trials had different durations (one pulse vs two pulses + delay), we introduce a mechanism that mimics an urgency signal and that change the value of c_2. Finally, the potential is:

$$\varphi = -\mu X - \frac{c_2(t)X^2}{2} + \frac{c_4 X^4}{4} + \frac{c_6 X^6}{6} \qquad (54)$$

When $c_2 < 0$ (with $c_4 < 0$ and $c_6 > 0$) the system is in the region where the undecided state is stable and when $c_2 > 0$ the undecided become unstable. Because c_2 can change during the trial, the unstable state can appear or disappear. We fit the model using the method described in the method section of chapter 3. With this method, we compute the time

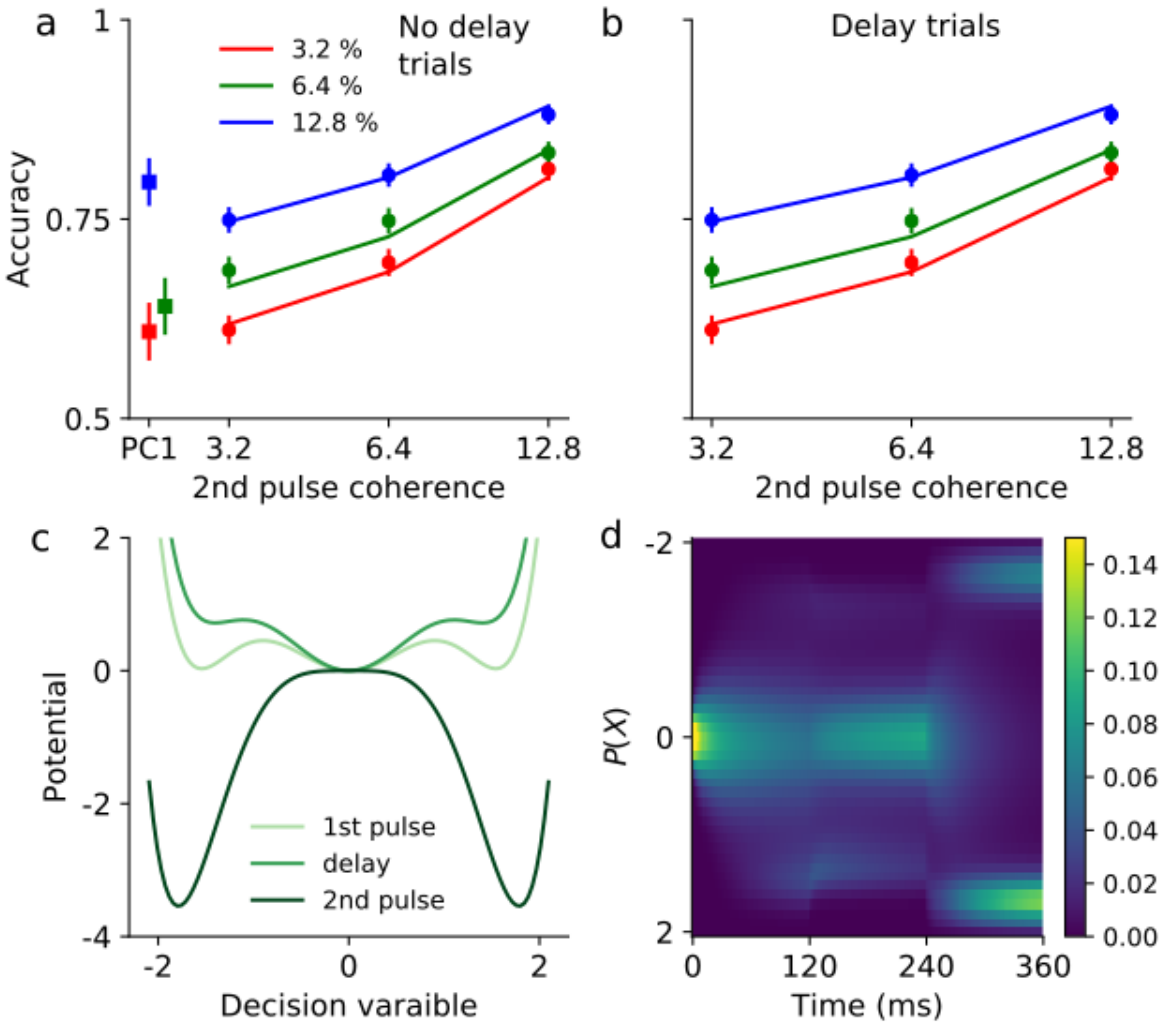

Figure 16 | Alternative model with urgency signal and undecided state.
a) Probability of correct for single (squares) and double (dots) pulse trials without delay for the three possible first pulse coherence (3.2% red, 6.4% green, 12.8 % blue) (dots). Solid lines show the accuracy of the model with urgency signal and undecided state. **b)** Same as a witht trials with a temporal gap of 120 ms. **c)** During the first pulse and the delay there are three stable states (left, undecided and right) whereas during the second pulse, there are only two stable states (left and right) **d)** Temporal evolution of the decision variable probability density function for a trial with 3.2% coherence in both pulses of evidence. During the delay, there are three possible stable states: left, right and undecided.

evolution of the decision variable probability distribution function. There are two main advantages, we do not need to assume that the time spent in the unstable region is small compared to the pulse duration and we can easily introduce the undecided state (if the particle finishes in the undecided state the decision is taken randomly). In order to introduce more constraints to the model, we also model the dynamics during the temporal gap. Because the accuracy do not change with the delay, we can not fit two separate source of noise (internal and stimulus fluctuations) and we impose that during the delay the noise is

reduced by a factor of $\sqrt{2}$ which implies that $\sigma_S = \sigma_i$ (methods).

The parameters that maximize the likelihood of the model yield to a potential with undecided state during the first pulse and the delay but without undecided state during the second pulse (figure 16c). In this case, the temporal change of c_2 mimics an urgency signal. In most of the trials there are two pulses, thus after the first one there is no rush to make a choice and it is possible to remain in the undecided state when there is not enough evidence to commit to a choice. During the delay the three states remain stable and the information of the first pulse is not lost. Finally, during the second pulse when a decision must be taken the undecided state disappears and the particle evolves towards one of the wells (figure 16d). Note that as expected the accuracy for the trials with and without delay is very similar (figure 16a and b). This model can also fit the psychophysics data and under the assumption that stimulus fluctuation and the internal noise are equally strong $(\sigma_S = \sigma_i)$ it is more likely than the double well model $(\Delta AIC = 22.4,$ see methods).

Discussion

The optimal way to solve a two alternative forced choice task with fixed duration is by linearly summing each sample of evidence. Under certain assumptions this can change, for example assuming that there is a cost associated with accumulating evidence, the optimal strategy is to perfectly accumulate evidence with collapsing absorbing bounds (Drugowitsch et al. 2012). The Bayesian approach to solve this task is equivalent to the optimal strategy but if we considered that the mean signal is unknown to the subjects the Bayesian strategy will lead to an overweighting of the early information (Deneve 2012). In this chapter we have studied the optimal strategy under neurobiological constraints. The common belief is that the decision variable is encoded in the firing rate of neurons in cortical regions (Roozbeh Kiani, Hanks, and Shadlen 2008; Britten et al. 1992; Roitman and Shadlen 2002) but neurons have spiking refractory periods which could limit the range of their firing rates. In a model with perfect integration of evidence this would be equivalent to impose reflecting boundaries. In (Zhang and Bogacz 2010), the authors show that a winner-take-all mechanism $(c_2 > 0)$ improves the accuracy when reflecting boundaries are imposed. They also show that the optimal value of this barrier increases with the stimulus duration. In the neurobiological models with winner take all dynamics the reflecting barriers appear naturally from the neuron properties and the network structure. We also found that there is an optimal barrier different from zero which increases with the stimulus fluctuations.

By introducing a barrier we created two stable states that can also be used to maintain information in the absence of stimulus. Thus the models with winner-take-all dynamics are also suitable to perform tasks that combine perceptual decision making with working memory (Wang 2002; Murray, Jaramillo, and Wang 2017). In (R. Kiani, Churchland, and Shadlen 2013a), the authors designed a task involving perceptual decision making and working memory to test the attractor network model presented in the seminal paper (Wang 2002). In this paper, the author presented a network of leaky-integrate and fire neurons with a subcritical bifurcation, the network had two stable states, one for each possible choice and an extra undecided state which became unstable during the stimulus presentation. This network was designed to allow almost perfect integration of evidence over hundreds of milliseconds and to be robust to fluctuations (Wimmer et al. 2015; Wang 2002). Consequently the transitions between states were unlikely. In this primacy regime, if the stimulus is short enough the evidence would be integrated almost perfectly. Then if we divided the stimulus in two pulses separated by a temporal gap, the accuracy would

decrease because during the temporal gap the network would continue evolving towards one of the decision states or will return to the undecided. In the first case, the accuracy would decrease because the second pulse would not be integrated and in the second case, the information about the first pulse would be completely erased by the network dynamics. In (R. Kiani, Churchland, and Shadlen 2013a), the authors found that contrary to the attractor network model prediction, the accuracy was independent of the delay. However, they also noted that in the regime where the network "jumps" from the initial state to one of the decisions states based on momentary evidence, the accuracy would not depend on the delay because the network would evolve much faster to the stable points. But they discard this model because it would lose information. We have shown that although the network can "jump" this does not mean that is losing information because the asymmetry between correcting and error transitions allow the network to combine evidence from the two pulses. The parameter regime described in (Wang 2002) was chosen to explain data from psychophysics experiments with long stimulus duration (around 2 s). Our hypothesis is that subjects can adapt the dynamics of the network to the stimulus properties. For example, with short stimuli (120 ms) like the one used in (R. Kiani, Churchland, and Shadlen 2013a), the urgency to choose between one of the two alternatives could produce that the effective dynamics of the network is faster than when longer stimuli are used. This can be simply achieved by an untuned input to the decision circuit. One possibility to test this prediction would be to train the subjects with long stimuli and introduce catch trials with short stimuli.

It has been shown that when the tasks requires storing a parametric value in working memory, this value undergoes diffusion over time (Funahashi, Bruce, and Goldman-Rakic 1989; Wimmer et al. 2014). This diffusion has been understood as a signature of line attractors (models that assume perfect integration of evidence). However, in (R. Kiani, Churchland, and Shadlen 2013a) the accuracy of the subjects does not decrease with the temporal gap (at least up to 1s) suggesting that in this task the subjects might be storing a categorical value of the first pulse (either left, right or undecided) instead of a parametric value proportional to the coherence (Fleming, Maloney, and Daw 2013). The double well model naturally implements this categorical categorization of the stimuli. It could also be the case that a line attractor could somehow reduce the internal noise to zero. This scenario seems unlikely because the internal noise is key to explaining the diffusion of parametric values during working memory tasks and it would produce a consistency of 100% when the consistency in random dot tasks is much lower (Ratcliff, Voskuilen, and McKoon 2018) .

One possible experiment to test if the information of the first pulse is categorical or a parametric value could be to read out the decision variable before the second pulse from simultaneously recorded neurons (Roozbeh Kiani et al. 2014). By splitting the trials in left or right initial categorization, the accuracy should be independent of the first frame (figure 15 e and f). It could be the case that the categorization is categorical but with three stable states (left, undecided and right, figure 16). Figure 16 Similarly to the DWM, this model could also be tested by splitting the trials in left, right or undecided using the read out of the decision variable (Roozbeh Kiani et al. 2014) or by undecided and decided using the pupil size as a proxy for uncertainty (Kawaguchi et al. 2018; Urai, Braun, and Donner 2017) . Then the trials that end up in the undecided state after the first pulse should only be influenced by the second one.

We found that under the assumption that $\sigma_i = \sigma_S$, the model with an undecided state and urgency signal is more likely than the standard double well model. However, in order to better compare both alternative, we should design an experiment where the two sources of noise were distinguishable. For example we could use a stimulus that change by frames of 100 ms (Bronfman, Brezis, and Usher 2016) to include the stimulus fluctuations in a potential that changes in every frame according to the stimulus (see, methods chapter 4).

In (R. Kiani, Churchland, and Shadlen 2013a; Tohidi-Moghaddam et al. 2019) subjects tend to slightly overweight the second pulse, as we explained the DWM and the drift diffusion model with reflecting boundaries are compatible with a slightly recency psychophysical kernel. Another alternative suggested by (Tohidi-Moghaddam et al. 2019) is a drift diffusion model with absorbing boundaries where the sensitivity of the second pulse is larger. However, it remains unclear why the subjects do not use their maximum sensitivity during the whole trial.

In summary, we have found that winner-take-all models with attractor dynamics can be optimal under certain biological constraints and are suitable to solve tasks involving perceptual decision making and working memory. We have shown that during the temporal gap, the information about the first pulse could be stored in stable fixed points rather than in a line attractor and we finally propose an experiment to distinguish between these two alternatives.

Methods

Double well model fitting

In figure 15 we use data from two equal experiments (Kiani et al 2013 and Tohidi-Moghaddam 2018), we extract the accuracy of the subjects directly from the paper figures (with GraphClick, a software to extract data from graphs) and the number of trials from the methods of the papers. In these experiments, the human subjects had to discriminate between left and right motion direction of a random dots stimulus, the experimenters interleaved trials with one and two pulses of 120 ms. For single pulse trials the possible coherences levels were 0%, 3.2%, 6.4%, 12.8%, 25.6% and 51.2%. For double pulse trials, the pulses were separated by a delay of 0,120,360 or 1080 ms and the coherences were randomly chosen from 3.2%, 6.4% and 12.8% (nine different coherence sequences). In both papers they reported that the accuracy of the subjects in double pulses trials was independent of the delay. Thus we assume that the internal noise was too small to drive transitions during the delay and we pull the data across delays to compute the accuracy for each coherence sequence. We fit the model by maximizing the log-likelihood (Nelder-Mead algorithm):

$$LL = \sum_{i}^{N_i} N_{C,i} P_{C,i} + N_{E,i}(1 - P_{C,i}) \tag{55}$$

Where $N_{C,i}$ and $N_{E,i}$ are the number of correct and error trials for each coherence sequence i whereas $P_{C,i}$ is the accuracy for sequence i.

For single pulse trials, we computed $P_{C,i}$ as

$$P^1_{C,i} = P_{C,0}\ P_{CC}\,(1 - P_{C,0}\ )P^1_{C,E} \tag{56}$$

Where $P_{C,0}, P_{CC},$ and $P_{C,E}$ were computed using equations 22, 25 and 26 whereas the super index indicates the pulse number. Note that we are assuming that the time spent for the particle in the unstable state is short compared with the pulse duration. In this model, the particle starts in the correct well with probability $P_{C,0}$. Similarly for double pulse trials:

$$P^2_{C,i} = P^1_C\ P^2_{CC}\,(1 - P^1_C\ )P^2_{C,E} \tag{57}$$

In order to avoid that the model was degenerated, we fixed one of the parameters, in this case we fixed $c_4 = 1$. Then the potential and the diffusion equation can be written as

$$\varphi(X) = k\mu X - \tfrac{1}{2}c_2 X^2 + \tfrac{1}{4}X^4 \quad (58)$$

$$\tau \frac{dX}{dt} = -\frac{d\varphi}{dX} + \sigma\xi(t) \quad (59)$$

Where k is a linear scaling of the coherence to X units. We found that the parameters that maximize equation 55 and their 95% confidence interval were $k = 0.012 \pm 0.0011$, $c_2 = 1.41 \pm 0.1$, $\sigma = 0.52 \pm 0.05$ and $\tau = 3.3 \pm 0.5$.

To compute the confidence intervals we assume that the likelihood function around the best-fit parameters is a multi-dimensional Gaussian. Then the confidence intervals are two times the diagonal of the inverse of the Hessian matrix (MacKay and Mac 2003; Brunton, Botvinick, and Brody 2013) . The Hessian matrix is the matrix of second derivative and we compute it numerically using the finite difference method.

Limitations of the double well model fitting

The fitting procedure described above has two important assumptions: 1) The wells are deep compared with the noise. The computation of the probability of a correct choice is based on the transition rates between wells which are only true when the noise is small compared with the barrier height (Kramers 1940). 2) The trial starts in the correct well with probability $P_{C,0}$. We assume that the time spent in the unstable state is small compared with the trial duration.

The first assumption becomes important when the stimulus evidence is strong and the barrier of the incorrect well is small or even disappears. In that case, there is a divergence between the theory and the simulations. In the limit when the incorrect fixed point disappears because the evidence is too strong, we impose that the probability to make a transition to the correct well is 1 (figure S2 a).

The second assumption is not that problematic because the time spent in the unstable state is normally short. However, in the parameter regime where the unstable fixed point $(X = 0)$ becomes almost flat, the particle can take some time to reach one of the wells. One possible extension of this model could be to compute the mean passage time to the well (t) and then subtract this time from the stimulus duration $T' = T - t$.

To ensure that these assumptions are not affecting the fitting with maximum likelihood, we compared the probability of right of the simulations and the theory for a set of stimuli. We

found that for the data set in figure 15 the assumptions were correct (figure S2b). However, when we tried to fit the data from (Bronfman, Brezis, and Usher 2016), that was not the case (figure S2b). Thus the theory based on the transition rates between wells it is only correct for a reduced region of the parameter space.

Alternative model and comparison with the double well

We fit a model with three stable states and urgency signal (figure 16) and the standard double well model (figure S3) using the method described in chapter 4. The model with urgency signal and undecided state has a set of 7 parameters $\theta_u = \{c_2^1, c_2^2, c_2^3, \sigma, c_4, c_6, k\}$. We introduce the urgency signal by allowing the parameter c_2 to change during the 3 phases of the trial: during the first pulse (c_2^1), the delay (c_2^2) and the second pulse (c_2^3). In the network version of the model, this would correspond to move the system between the multistable region $(c_2 < 0)$ and the winner-take-all region $(c_2 > 0)$ with an external untuned input. We also fit the double well model with 4 parameters $\theta_{dw} = \{c_2, \sigma, c_4, c_6, k\}$. Because the internal noise does not have any impact during the delay and it is indistinguishable of the stimulus fluctuations during the first and second pulses, we can not dissociate the internal noise (σ_i) and the stimulus fluctuations (σ_S). Because we want to study models that are stable during the delay, we impose that $\sigma^2 = \sigma_i^2 + \sigma_S^2$ and we only fit σ. To speed up the process, we set the temporal gap between the two pulses to 120 ms for all the trials with temporal gap. We compared the likelihood of the models using the Akaike information criterion (AIK).

$$AIC_i = 2m - 2log(ll) \tag{60}$$

Where m is the number of parameters, ll is the likelihood of the models and the AIC_i is the akaike number for each model. We found that $\Delta AIC = AIC_{dw} - AIC_u = 22.4$ indicating that the double well model have essentially no support compared to the model with urgency and undecided state (Burnham and Anderson 2004).

4. Modifying the magnitude of stimulus fluctuations to identify different neural mechanisms

Summary

Here we tested in a psychophysical experiment two of the key signatures of attractor dynamics explained in the first chapter: the non-monotonic relation of the accuracy with the stimulus fluctuations and the change from primacy to recency psychophysical kernels as the stimulus fluctuations are increased. For this purpose, we used a new stimulus where the mean and the standard deviation were completely independent. Specifically, we used the single dot task where subjects had to discriminate if the mean position of a sequence of ten dots fell in the right or the left side of the screen. The x-coordinates of the dots were drawn from a Gaussian distribution with mean $\bar{\mu}$ and standard deviation $\overline{\sigma_S}$. We fixed $\bar{\mu}$ for each subject while we varied $\overline{\sigma_S}$ in a trial by trial basis. We did not find evidence for a non-monotonic relation between the accuracy and the stimulus fluctuations nor a change from primacy to recency in the psychophysical kernels. We found a large variability across subjects in the psychophysical measurements such as psychophysical kernels or bias. None of the simple models explained in this thesis is able to explain the idiosyncratic psychophysical results. To further analyze them, we are developing a model-based analysis. This approach allows us to add new mechanisms to the one-dimensional model with attractor dynamics and test whether they are important to explain the data or not. Preliminary results show that at least for a fraction of subjects, a model with attractor dynamics can fit the psychophysical kernels and the biases for different stimulus fluctuations. In sum, we did not find the qualitatively behaviour of the attractor model described in chapter 1 in our data set. This does not mean that the attractor dynamics is not important to explain the data, other mechanisms could be masking the qualitatively signatures of attractor dynamics or we did not test the predictions for the correct stimulus parameters. Actually, quantitatively model-based analysis suggests that attractor dynamics mechanisms, among others, are important to explain the behavioural results.

Results

The “ single dot“ task

In the dot task, the stimulus consists of a sequence of ten white dots presented in frames of $200ms$. While the y coordinate is constant in the middle point between the center and the bottom of the screen, the x coordinate is drawn from a Gaussian distribution with mean $\overline{\mu}$ or $-\overline{\mu}$ and standard deviation σ_S (figure 17). During the trial, the subjects have to maintain fixation on a black dot presented at the center of the screen. After the stimulus, they have to report if the mean position x of the dots falls to the right or to the left region of the black dot. While $\overline{\mu}$ is fixed for each subject, $\overline{\sigma}_S$ changes in a trial by trial basis and it can take on six different values. The smallest $\overline{\sigma}_S$ is exactly zero and the other five are logarithmically spaced between 0.02 and 1 degrees of visual angle. In this task, the standard deviation and the mean of the stimulus can be modified independently. Actually, we fixed the sample mean and the standard deviation of each stimulus to the mean ($\overline{\mu}$ or $-\overline{\mu}$) and the standard deviation ($\overline{\sigma}_S$) of the generative distribution (see methods). Theoretical simulations of the double well model show that in this case the bump in accuracy is higher (figure S4). However, by fixing the mean and the standard deviation of each individual stimulus, we effectively introduce correlations in the stimulus. These correlations cause the psychophysical kernel to be significantly below chance (see methods).

The accuracy of subjects does not show a systematic non-monotonic relation with the strength of stimulus fluctuations

We used the dot task to test the non-monotonic relation of the accuracy with the stimulus fluctuations (figure 8). We found that the accuracy of the subjects does not show a systematic bump in accuracy (figure 18). In general, the accuracy of the subjects was constant for weak stimulus fluctuations but it decayed when the stimulus fluctuations become stronger. This result is inconsistent with a perfect integration of evidence without bounds because it

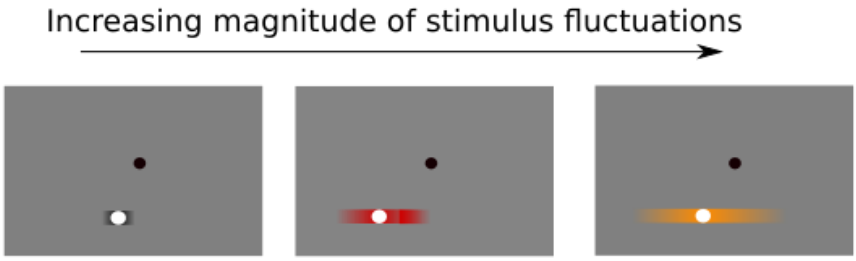

Figure 17 | Cartoon of the dot task with different magnitudes of stimulus fluctuations
The dot task consists of a sequence of ten white dots where the positions of the x-coordinate is drawn from a Gaussian distribution with mean $\overline{\mu}$ and standard deviation $\overline{\sigma_S}$. The mean remains constant for each subject whereas the standard deviations change in a trial by trial basis with six possible values. The shaded colors show the extent of the possible x-coordinates values as the standard deviation increases. The y-coordinate remains constant during the trial.

predicts that the accuracy does not change with the stimulus fluctuations (σ_S) when the mean of each stimulus is fixed to the mean of the generative distribution. The effect of the stimulus fluctuations on the accuracy could be explained by a flat potential for small decision variables with a mechanism to commit for a decision such as absorbing bounds or attractors. Thus the results are compatible with the drift diffusion model with absorbing bounds or with an attractor model close to the bifurcation.

Idiosyncratic behaviour in the dot tasks

We found that different subjects have completely different psychophysical results in at least three different measures, the psychophysical kernels, the spatial kernels and the bias. In this section, we explain why this heterogeneity of results across subjects can not be explained by the simple models we described in the first chapter.

As expected, the psychophysical kernels with weak stimulus fluctuations have a small impact on the choice. Because of this reason, we do not have enough data to assess the shape of the psychophysical kernels for small stimulus fluctuations (figure S5). For strong stimulus fluctuations, we found idiosyncratic psychophysical kernels, namely the subjects can exhibit primacy, recency or non-monotonic psychophysical kernels (figure 19). The heterogeneity of psychophysical kernels can not be explained by any of the canonical models. As we have

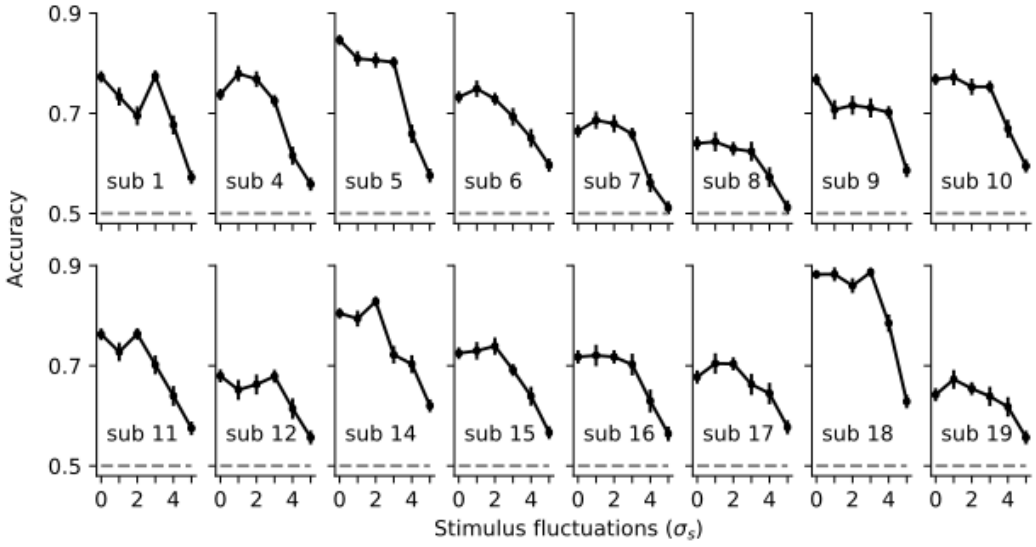

Figure 18 | Accuracy as a function of the stimulus fluctuations
Although some subjects have different modulation of the accuracy with the stimulus fluctuations, in general the accuracy is constant for weak stimulus fluctuations and it decays when the fluctuations are stronger

shown in figure 7, the double well model has different regimes of integration that could explain the heterogeneity of the psychophysical kernels. However, it also predicts a change from primacy to recency psychophysical kernels with the stimulus fluctuations (figure 7), but we did not find evidence for such a modulation (figure 20).

To further characterize the impact of frames with different stimulus strength on the choice, we compute the spatial kernel (figure 21): first we discretize the stimulus space in $N_{bins} = 11$ bins. Then we transform each stimulus to a N_{bins} dimensional vector where each component n_i is the number of frames in each bin i. To compute the impact of the frames in each bin, we fit a logistic regression model where the regressors are the n_i:

$$log\left(\frac{P_R}{1-P_R}\right) = \sum_{i=1}^{N_b} w_i n_i \qquad (61)$$

Where P_R is the probability of a right choice and w_i is the impact (weight) associated to the stimulus strength in bin i. As expected, the frames with stronger evidence (e.g. large distance to the center of the screen) have a higher impact on the choice. The subjects show

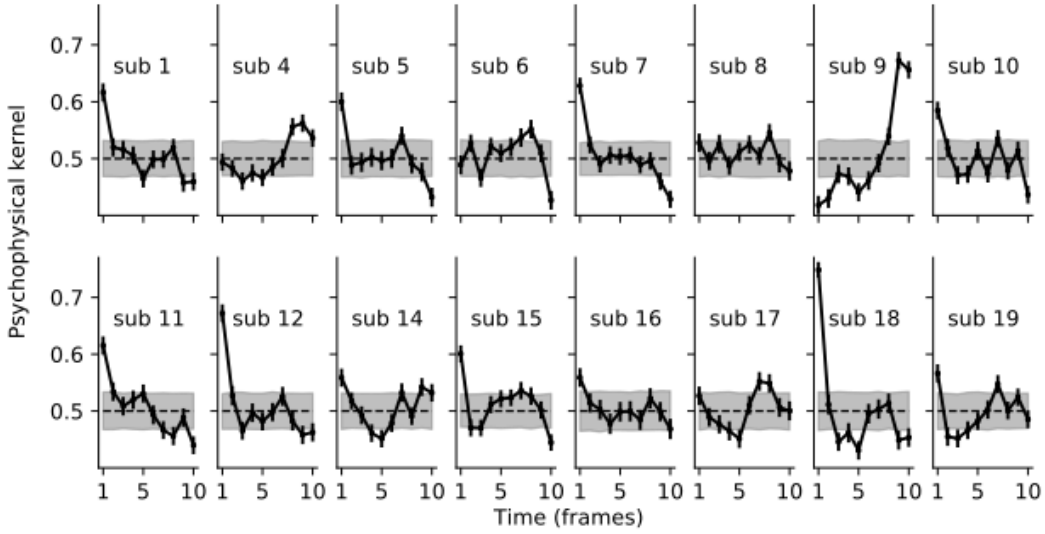

Figure 19 | Idiosyncratic psychophysical kernel for strong stimulus fluctuations
The subjects show primacy, recency and non-monotonic psychophysical kernels for strong stimulus fluctuations. The error bars correspond to the standard errors (bootstrap, $N = 500$). The grey regions show two standard deviations of the distribution of psychophysical kernels computed by shuffling the decisions. Psychophysical kernels can be significantly below chance because of the correlation that we introduce in the stimulus (methods).

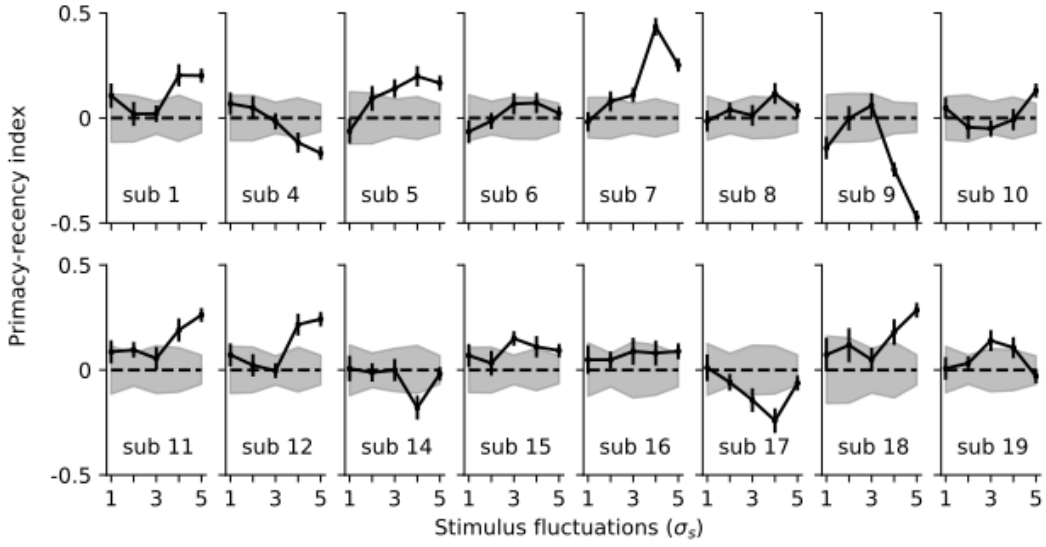

Figure 20 | Idiosyncratic primacy-recency index.
We do not find evidence for a systematic change from primacy to recency psychophysical kernels. Error bars correspond to standard errors ($N = 500$). The grey regions are two standard deviations of the distribution of primacy-recency index computed by shuffling the decisions. Only outside this region the primacy-recency is significantly different from the null hypothesis of flat psychophysical kernel (methods).

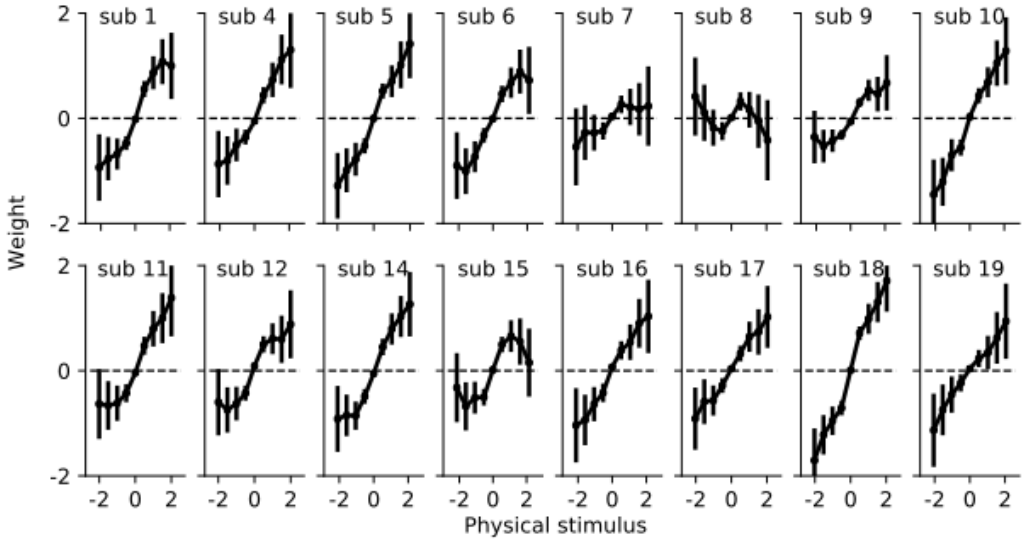

Figure 21 | Spatial kernels
The spatial kernel is the less idiosyncratic psychophysical measurement. All the subjects, show a monotonic increase of the weight with the physical stimulus. For a fraction of the subject this weight saturates for strong physical stimulus values.

a linear relation between the physical evidence and the impact on the choice for weak physical evidence. For frames with strong evidence, the impact on choice plateaus only for some subjects. This transformation removes the temporal structure of the stimulus and allows us to investigate the impact of each stimulus strength on the decision. Note that this analysis can not distinguish between sensory mechanisms and decision related mechanisms. In all perceptual decision tasks, the subjects need to perform two computations in each frame. First, they need to transform the physical stimulus into evidence to discriminate between the two possible choices. Then they need to update the decision variable with the evidence of that frame. The spatial kernel is not the transformation of the physical stimulus into evidence. It also reflects any decision-related mechanism that could have an impact on how the decision variable is updated. For instance, in the double well model the maximum impact of a frame is to produce a change of mind. There is a critical value of the stimulus strength for which the incorrect well disappears and the decision variable evolves towards the correct well. Above this critical value, the impact of the stimulus saturates. Thus, the spatial kernel is informative of how the subjects weight the stimulus as a function of the stimulus strength but it is not directly the transformation of the physical stimulus into evidence.

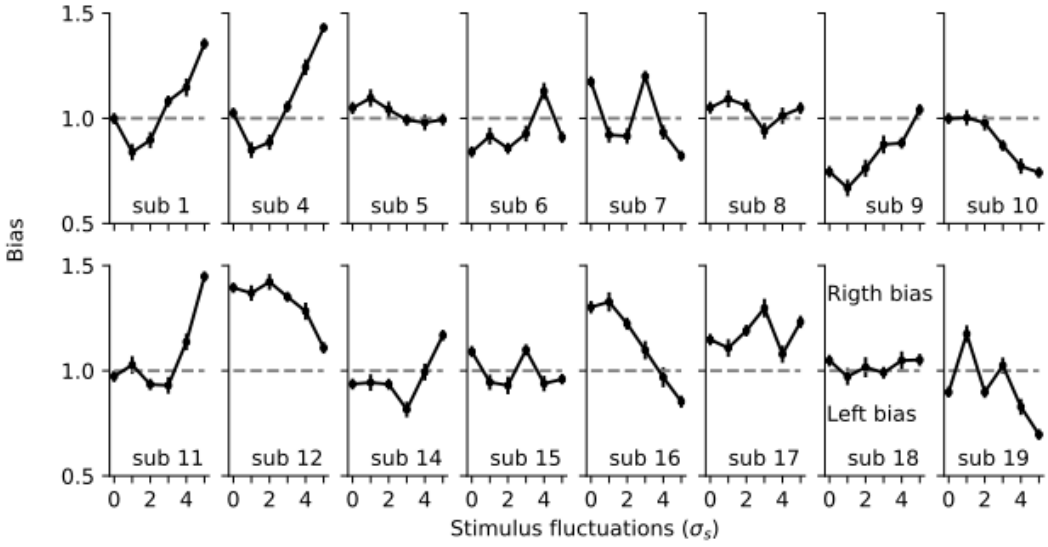

Figure 22 | The stimulus fluctuations idiosyncratically modulate the bias
The modulation of the bias with the stimulus fluctuations is idiosyncratic. We compute the bias as the ratio between the number of right choices and the number of right stimuli in each condition. Values larger than 1 indicate a right choice bias. Error bars correspond to the standard error.

Finally, the bias of the subjects is also idiosyncratically modulated by the stimulus fluctuations. Some subjects show strong bias for weak stimulus fluctuations and almost no bias for strong stimulus fluctuations. Other subjects show the opposite modulation. We even found biases in opposite directions for weak and strong stimulus fluctuations (figure 22). This suggests that different bias mechanisms could be affecting the choices. For instance, in a double well model a bias in the initial decision variable can have a critical impact on the choice in the primacy regime where the transitions are not activated but in the recency regime where transitions are likely, it does not have any impact. In contrast, a bias generated by an extra input to one of the population produces a bias in all the regimes.

The behavioural results in the dot task are idiosyncratic, the subjects show different psychophysical and spatial kernels and biases. None of the simple models described in this thesis can explain this variety of behavioural results. For instance, the double well model can explain the strong non-monotonic relation with the stimulus fluctuations of subject 1. The underlying mechanism that produces this effect in the double well model is the asymmetric transitions between correcting and error transitions (figure 8). In that case, the psychophysical kernel of subject 1 should be recency however, it is completely primacy. The drift diffusion model with absorbing bounds can not explain neither the non-monotonic

psychophysical kernels (subjects 14, 15, 17 and 19) nor the recency psychophysical kernels (subjects 4 and 9). To further characterize the idiosyncratic psychophysical results, we are developing a model based analysis to find the necessary mechanisms to explain the behaviour of each individual subject.

Testing the model based analysis with synthetic data

In order to test the potential of the fitting algorithm, we use different synthetic data sets to test if the model can distinguish between mechanisms such as variability at the initial condition or an urgency signal. The advantage of using synthetic data sets is that we know the ground truth of the models that generated the data. The procedure is the following: first we create a data set with a new mechanism. We call the model with the parameters that we used to generate the data the original model. Then, we use this data to fit the parameters of the same original model. We call this model the original fitted model. Note that if the fitting algorithm works properly, the parameters of the fitted original model should be the same as the parameters that we use to create the data (original model). Finally we use the same data to fit the standard double well model. To compare the fitted models, we use the Akaike information criterion (methods). Additionally we create a test data set and we compare the probability of right of each trial from the original model with the original fitted model and the fitted double well model.

First, we verified that we can recover the original parameters for the standard double well model from equation 8 (figure 23). To test if the fitting procedure can distinguish between models with different mechanisms we tested two examples mechanisms variability at the initial condition and an urgency signal. For the variability at the initial condition (figure 24 a and b), we created a data set where the initial decision variable was generated from a Gaussian distribution with zero mean and σ_{x0} standard deviation. As expected, the fitted model without variability at the initial condition can not fit a test data set. For the original model, the fitting procedure is able to recover the parameters that we used to create the data. For the urgency signal(figure 24 c and d), we created a data set where the parameter c_2 linearly increases with time

$$c_2(t) = c_{2u}(n_f(t) - 1) \tag{62}$$

where c_{2u} is a parameter and n_f is the frame number. In the standard biophysical model for decision making, this is simply an untuned ramp of input to the excitatory populations.

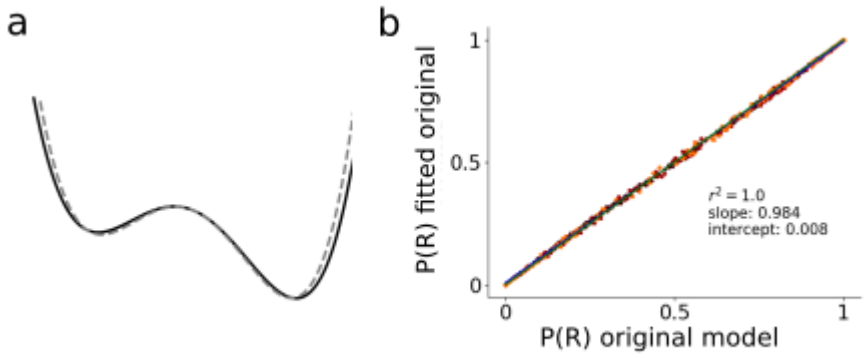

Figure 23 | The fitting algorithm recovers the original parameters for the Double well model
a) The dash grey line is the potential that we used to generate the training data set $N = 1000$. The solid black line is the potential with the fitted parameters. **b)** Probability of right for the original model and the fitted original model. Each point is a trial of a test data set. Different colors are stimuli with different magnitudes of stimulus fluctuations increasing from black to yellow $(\sigma_S = 0.05, 0.11, 0.24, 0.52 \; and \; 1.14)$. The original model and the fitted model have the same probability of right for a test data set.

Effectively the urgency signal moves the network towards stronger winner-take-all regions (figure 3c) and the dynamics become more categorical. Again, the fitting procedure is able to recover the parameters of the original model whereas the model without urgency signal can not fit the test data set. Finally, we tested whether the fitting procedure can distinguish between two different bias mechanisms. These two mechanisms are: 1) A bias in the initial decision variable, the initial decision variable was generated from a Gaussian distribution with mean b and standard deviation σ_b. In the network, this can be implemented with a small input to one of the population before the stimulus onset. 2) An extra input to one of the excitatory populations during the stimulus. In the potential, this affects the parameter μ that represents the difference between the inputs that each network is receiving $(\mu = \mu_{stim} - \mu_b)$. Where μ_{stim} is proportional to the strength of the stimulus and μ_b the bias parameter. This time we created a synthetic data set with each of the mechanisms and we fitted both data sets with both mechanisms. As expected, The fitting procedure can distinguish the mechanism that we used to create the original data (figure 25) . In sum, the fitting procedure is able to distinguish between different mechanisms that we could potentially test in our data psychophysical data set.

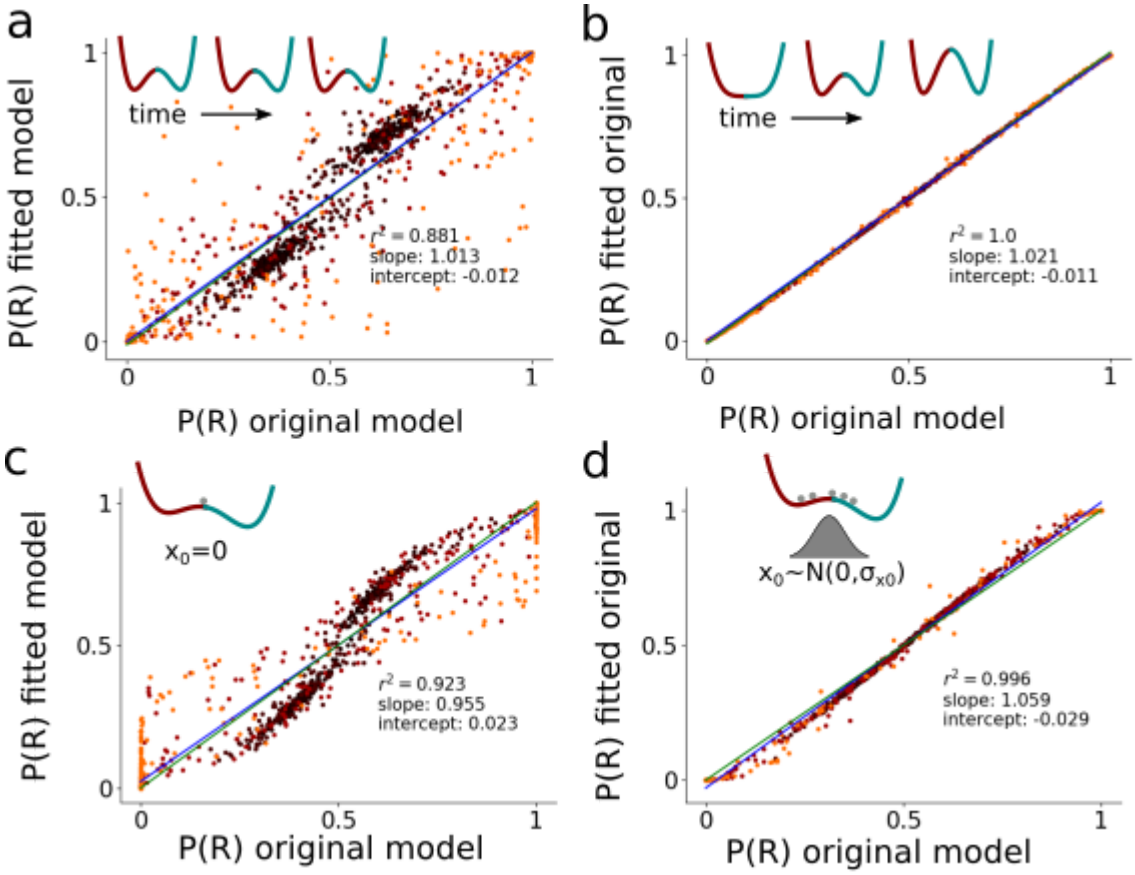

Figure 24 | The fitting algorithm is able to distinguish between different mechanisms.
Each point is a trial of a test data set. Different colors correspond to stimuli with different magnitudes of stimulus fluctuations increasing from black to yellow $(\sigma_S = 0.05, 0.11, 0.24, 0.52 \; and \; 1.14)$. The correlation of the probability of right for trials in a test data set between the fitted original model and the original model is almost perfect. Thus the fitting algorithm recovers the original parameters with a data set of $N = 1000$ trials. Blue lines indicate perfect correlation while the green line is a linear regression fit. **a)** The standard double well model can not fit the data generated with an urgency signal. The relative likelihood of the fitted model compared to the original fitted model is $RL < 10^{-6}$ **b)** When we introduce the urgency we recover the original parameters. **c , d)** Only the fitted original is able to fit the test data set, $RL < 10^{-14}$.

Extended neurobiological model to explain idiosyncratic behaviour

As we explained, the idiosyncratic behaviour in the single dot task can not be explained by any of the simple models that we described in this thesis. Thus a more general model to fit the data is needed. Using synthetic data, we showed that a model based analysis can identify the true underlying mechanisms. We aim to build a model as general as possible and use a model-based analysis to identify the mechanisms that are important to explain the

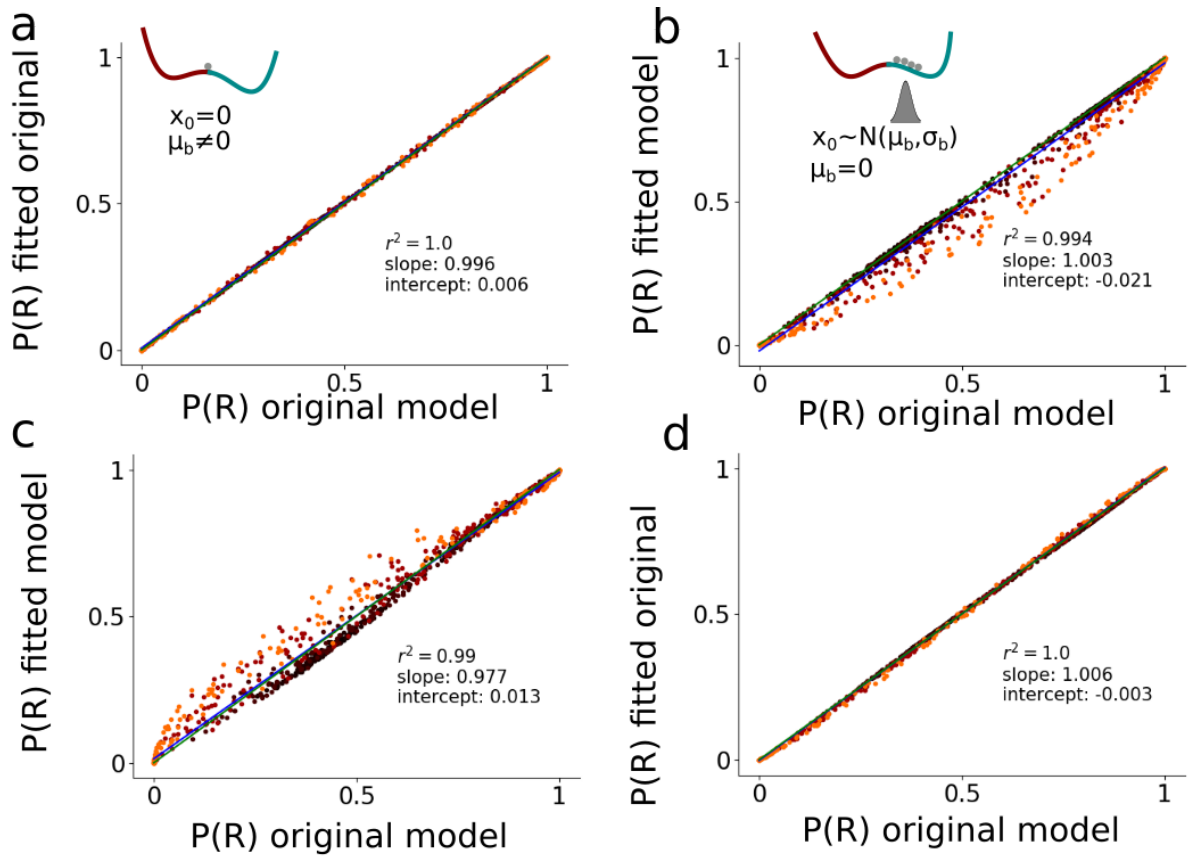

Figure 25 | The fitting algorithm is able to distinguish between different bias mechanisms. **a,b)** Fitting of the data created with constant bias of the input $N = 10000$. The model can distinguish the original mechanism. The relative likelihood of the fitted model compared to the original fitted model is $RL < 10^{-22}$ **c,d)** Same as in a and b but with a data set generated by a bias in the initial condition with $N = 10000$. $RL < 10^{-39}$

data. In this section, we present the extended model that we are currently using to fit the data. The results are still preliminary and this model can be further extended in the future.

The extended model has two modules, the first one is a nonlinear transformation of the physical stimulus into evidence. We call this module the sensory module. The second one is a diffusion process that accumulates the evidence, we call this module the decision module. The focus of this thesis is the decision module and we know the relation of their mechanisms with the biophysical models. However, the neural mechanisms underlying the transformation of the physical stimulus into evidence are beyond the scope of this thesis.

The sensory module is a simple logistic function (figure 26 a):

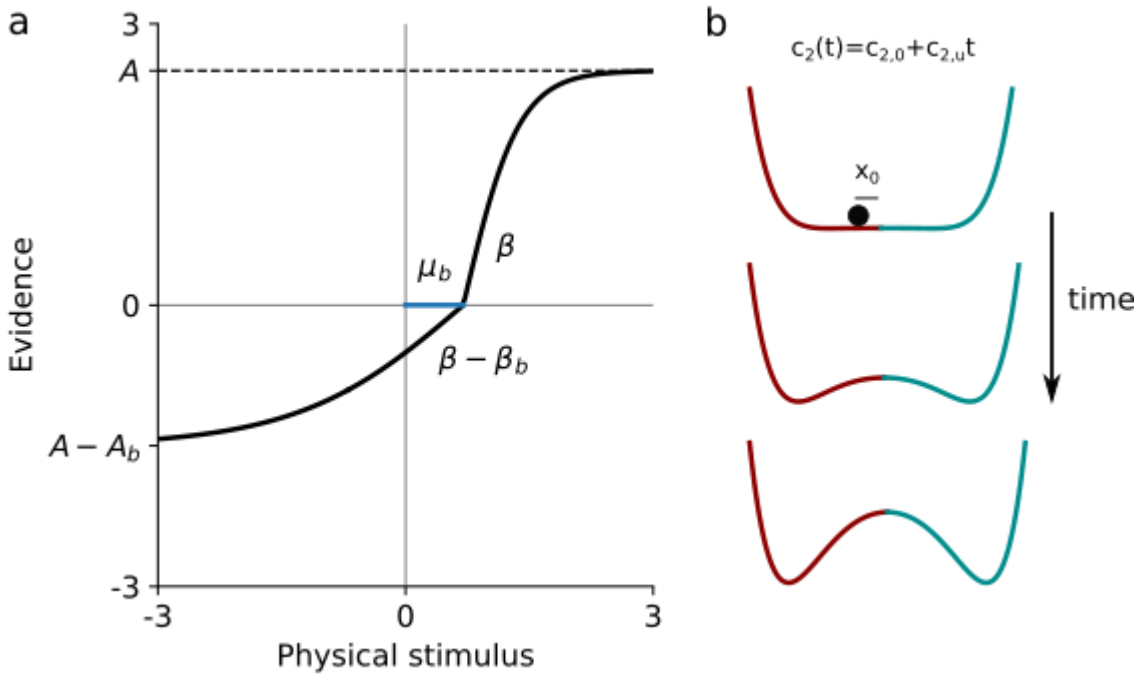

Figure 26 | Extended model with bias mechanisms.
a) Sensory module. The sensory module is a logistic function where we introduce different biases mechanism. β_b is a bias in the steepness of the curve, A_b is a bias in the maximum value of the curve and μ_b shifts the curve (blue line). **b)** The decision module is a diffusion process of a particle in the potential derived from the biophysical network. We add an urgency mechanism that for positive values of $c_{2,u}$ makes the dynamics more categorical during the trial. We also add a mechanism to bias the initial condition of the decision variable (x_0).

$$\mu(n) = A\,(1 + exp(-\beta d(n))^{-1} \tag{63}$$

Where A is the value at which the logistic function saturates, β is the slope around zero physical stimulus, $d(n)$ is the physical distance from the center of the screen to the dot position in frame n and $\mu(n)$ is the evidence that we use in the decision module. In order to model the idiosyncratic bias in the dot task, we include three bias mechanisms: 1) β_b represents a bias in the steepness of the logistic functions 2) A_b is a bias in the saturation value of the logistic function and 3) μ_b is a shift of the logistic function. With these biases mechanisms the sensory module is

$$\mu(n) = (A - A_b)\,(1 + exp(-(\beta - \beta_b)(d(n) - \mu_b))^{-1} \quad for\ d(n) < \mu_b \tag{64}$$

$$\mu(n) = A\,(1 + exp(-\beta(d(n) - \mu_b))^{-1} \quad for\ d(n) > \mu_b \tag{65}$$

Note that the bias in the saturation values (A_b) controls the sensory transformation only for the strong physical evidence. The shift of the logistic function (μ_b) and the bias in the slope (β_b) control the transformation of the weak physical stimulus. In the parameter regime where the logistic function becomes linear, μ_b and β_b can also affect the strong physical evidence.

The decision module (figure 26b) is the one dimensional version of the attractor model. It is a diffusion process (equation 2) of a particle in the following potential:

$$\varphi(X) = -\mu(n)X - \tfrac{1}{2}c_2(n)X^2 + \tfrac{1}{4}c_4X^4 + \tfrac{1}{6}c_6X^6 \qquad (66)$$

where we add two new mechanisms: 1) An urgency signal can change the parameter c_2, $c_2(n) = c_{2,0} + c_{2.u}n$, where n is the frame number. 2) A bias mechanism in the initial decision variable $X(t = 0) = x_0$. In the biophysical models, this mechanism can be implemented by a weak input to only one of the excitatory population. Note that a bias in the initial condition of the decision variable only impacts the choice when the integration of the evidence is primacy.

The bias mechanisms that we add to the sensory and the decision modules can impact the decision in different phases of the stimulus and also for different magnitudes of the physical stimulus. A combination of these mechanisms can produce a modulation of the bias with the stimulus fluctuations. We also add an urgency signal that can shape the potential during the trial, this makes the model more flexible to produces different types of psychophysical kernels.

Preliminary results of the extended neurobiological model

As proof of concept, we fit the extended neurobiological model to 4 different subjects (1,9,11 and 14). We choose these subjects because they have different psychophysical kernels and different modulation of the bias with the stimulus fluctuations. In general, we found that the extended model is able to explain the psychophysical kernels, the spatial kernel, the modulation of the bias with the stimulus fluctuations and the accuracy of the four subjects (figure 28 to figure 31).

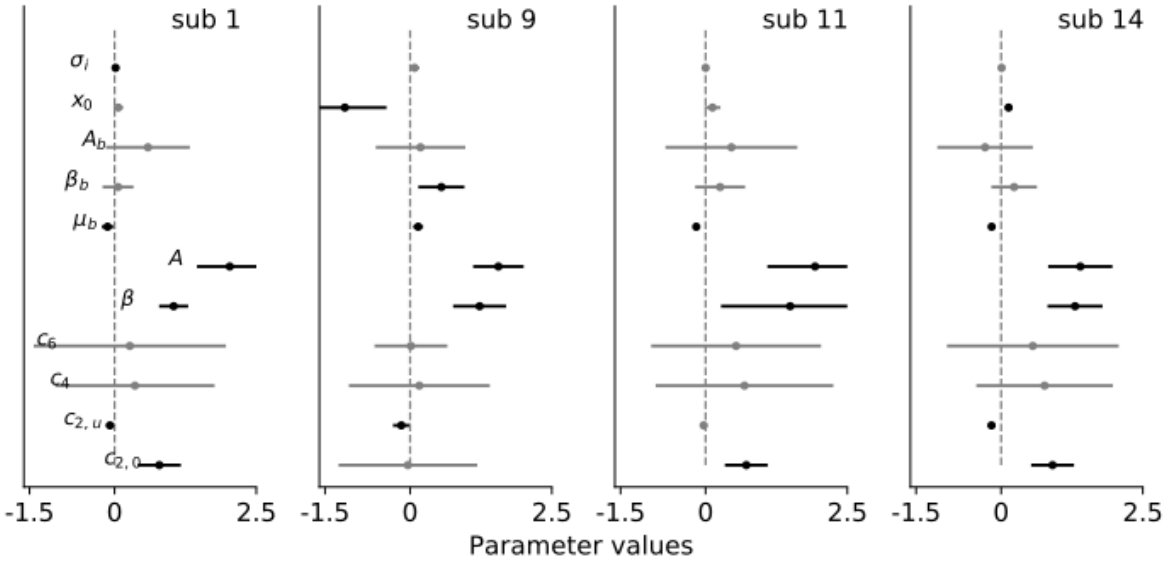

Figure 27 | Parameters of the extended model fitted to four subjects
Fitted parameters for each subject. Error bars indicate the 95 % confidence interval. Black and grey colors indicate significant and not significant parameters.

The subjects number 1 and 11 have primacy psychophysical kernel. This is captured by the model with an initial barrier at the beginning of the trial $(c_{2,0} > 0)$ (figure 27). Both of them have negative $c_{2,u}$ which indicates that the height of the barrier decreases linearly during the trial but it does not disappear (see potentials shape in figure 28g and figure 30. This is the opposite effect of an urgency signal. In contrast, the subject number 9 has a recency psychophysical kernel. The fitted potential is almost flat at the beginning of the trial ($c_{2,0}, c_4$ and c_6 not significantly different from 0, figure 27) and it evolves towards a leaky potential $(c_{2,u} < 0)$. Finally, subject number 14 has a non-monotonic psychophysical kernel which is captured by a barrier at the beginning of the trial $c_{2,0} > 0$ and a leaky potential at the end $c_{2,u} < 0$. The extend neurobiological model captures the shape of the psychophysical kernel by modulating the parameter c_2.

The extended neurobiological model has four different bias mechanisms. Combinations of them can produce different modulation of the bias with the stimulus fluctuations. For instance, the model fitted to the data from subject 1 has a right bias in the saturation value of the sensory module $(A_b > 0)$, a right bias in the initial condition of the decision variable $(x_0 > 0)$ and a left bias introduced by a shift in sensory module $(\mu_b < 0)$. The combination of

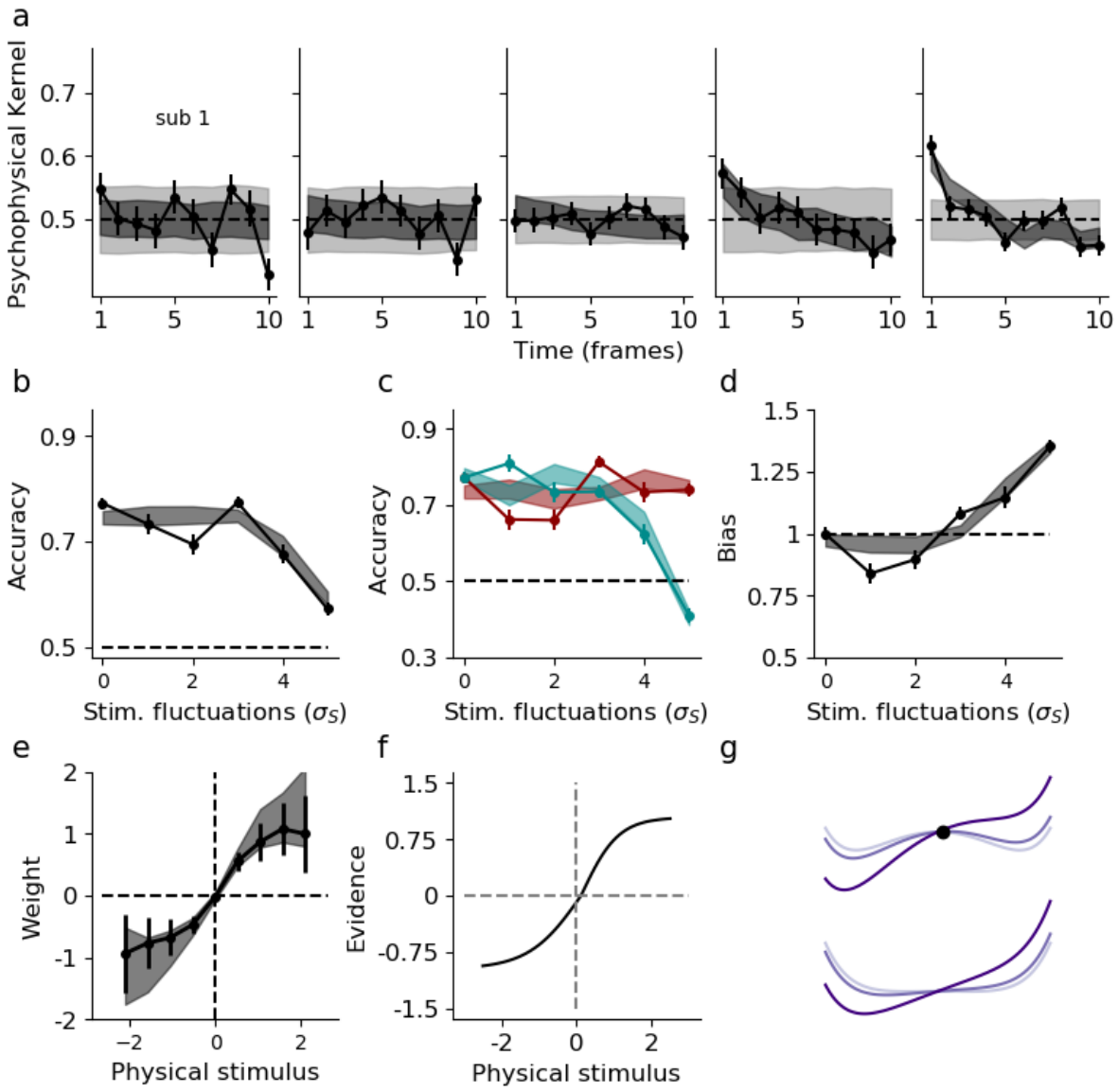

Figure 28 | Subject 1. Comparison between psychophysical results and model fit.
a) From left to right, psychophysical kernels for increasing values of stimulus fluctuations. The black solid lines with dots are the psychophysical kernels of the subject, black transparent areas are the standard error of the psychophysical kernels computed for the extended fitted model using the same stimuli. The grey areas areas are the 95% confidence interval i **b)** Accuracy as a function of the stimulus fluctuations. The extended model can not explain the **c)** Accuracy for left (red) and right (blue) trails. **d)** Modulation of the bias with the stimulus fluctuations **e)**Spatial kernels **f)** Sensory module of subject, **g)** Shape of the potential for different evidence $\mu = 0, [0, \overline{\mu}, 0.5]$ where $\overline{\mu}$ is the evidence associated with the mean of the generative distribution.The colors indicate the strength of the evidence from light to dark purple). Top and bottom panels show the potential for the first and last frame of the trial respectively.

these biases produces a small left bias for weak stimulus fluctuations and a strong right bias for strong stimulus fluctuations. Another interesting example is subject 11 that has no bias for weak stimulus fluctuations, left bias for intermediate stimulus fluctuations and right bias

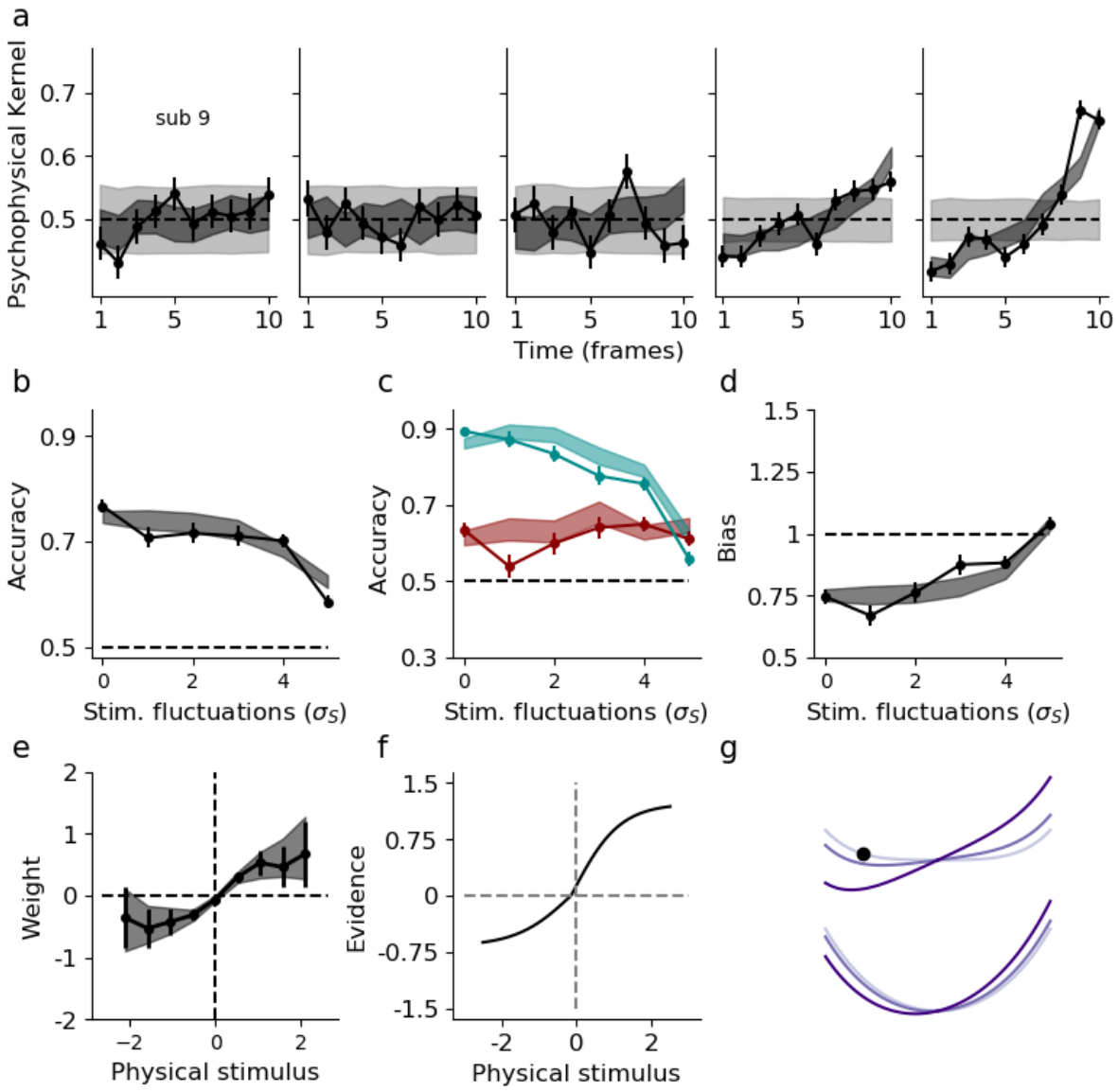

Figure 29 | Subject 9. Comparison between psychophysical results and model fit.
Same as figure 28 for subject 9. **a)** The psychophysical kernels are recency produced by a leaky potential **(g) c,d)** The left bias decreases with the stimulus fluctuations.

for strong stimulus fluctuations. In the model, this is captured by a left bias in the shift of the sensory module $\mu_b < 0$, a right bias in the initial condition $x_0 > 0$ and a right bias in the steepness of the sensory module (β_b). For small stimulus fluctuations, the μ_b and the left and right sources of biases compensate each other and there is no bias. For intermediate stimulus fluctuations, the left bias in μ_b dominates over β_b and x_0. In contrast, for strong stimulus fluctuations, the right sources of noise (β_b and x_0) dominate over μ_b. The preliminary results of the model based analysis suggests that combinations of different

sources of bias can explain non trivial modulations of the bias produced by the stimulus fluctuations.

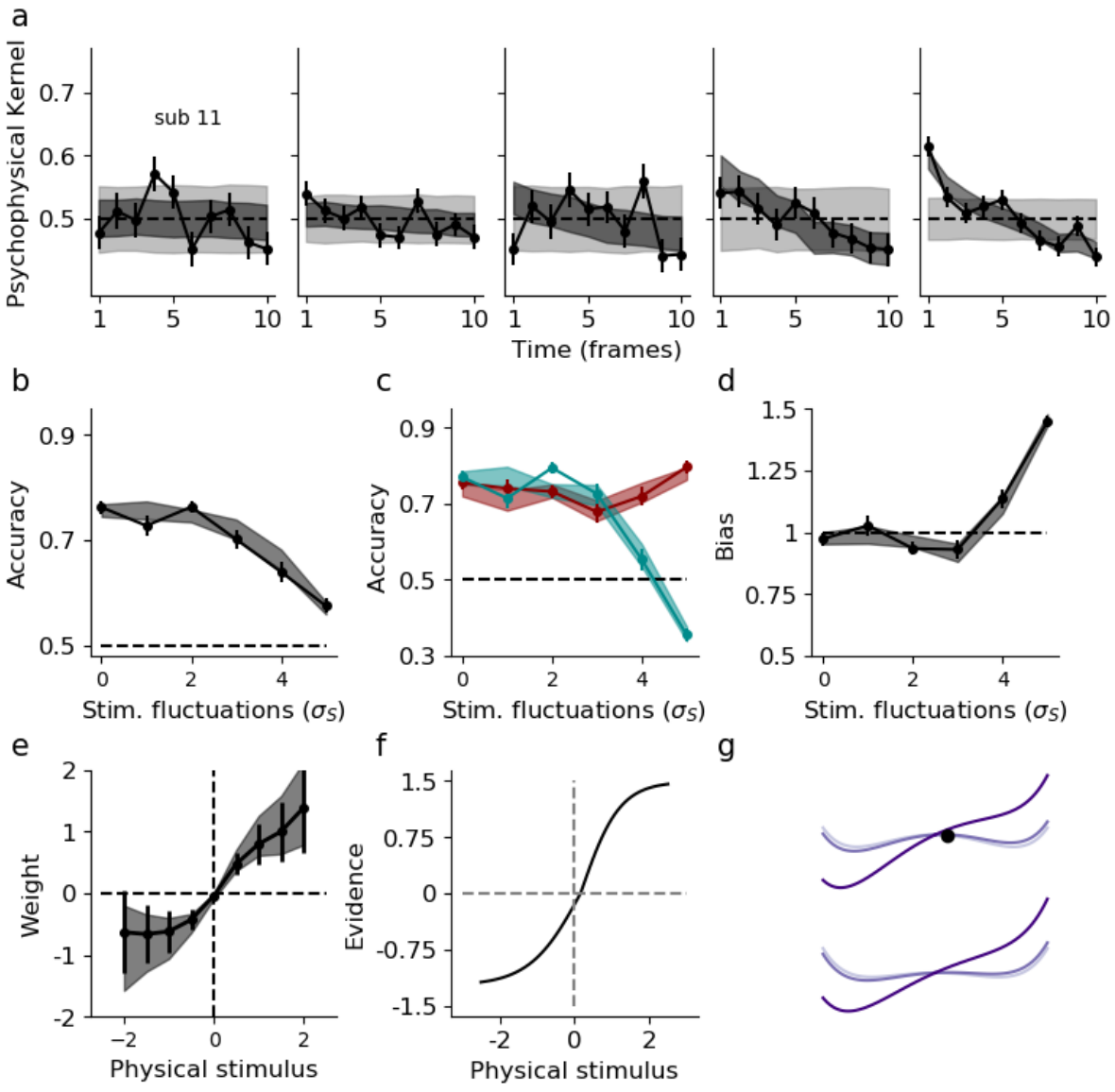

Figure 30 | Subject 11. Comparison between psychophysical results and model fit.
Same as figure 28 for subject 11. **a)** The psychophysical kernels are primacy produced by a double-well potential **(g) c,d)** The bias increases with the stimulus fluctuations.

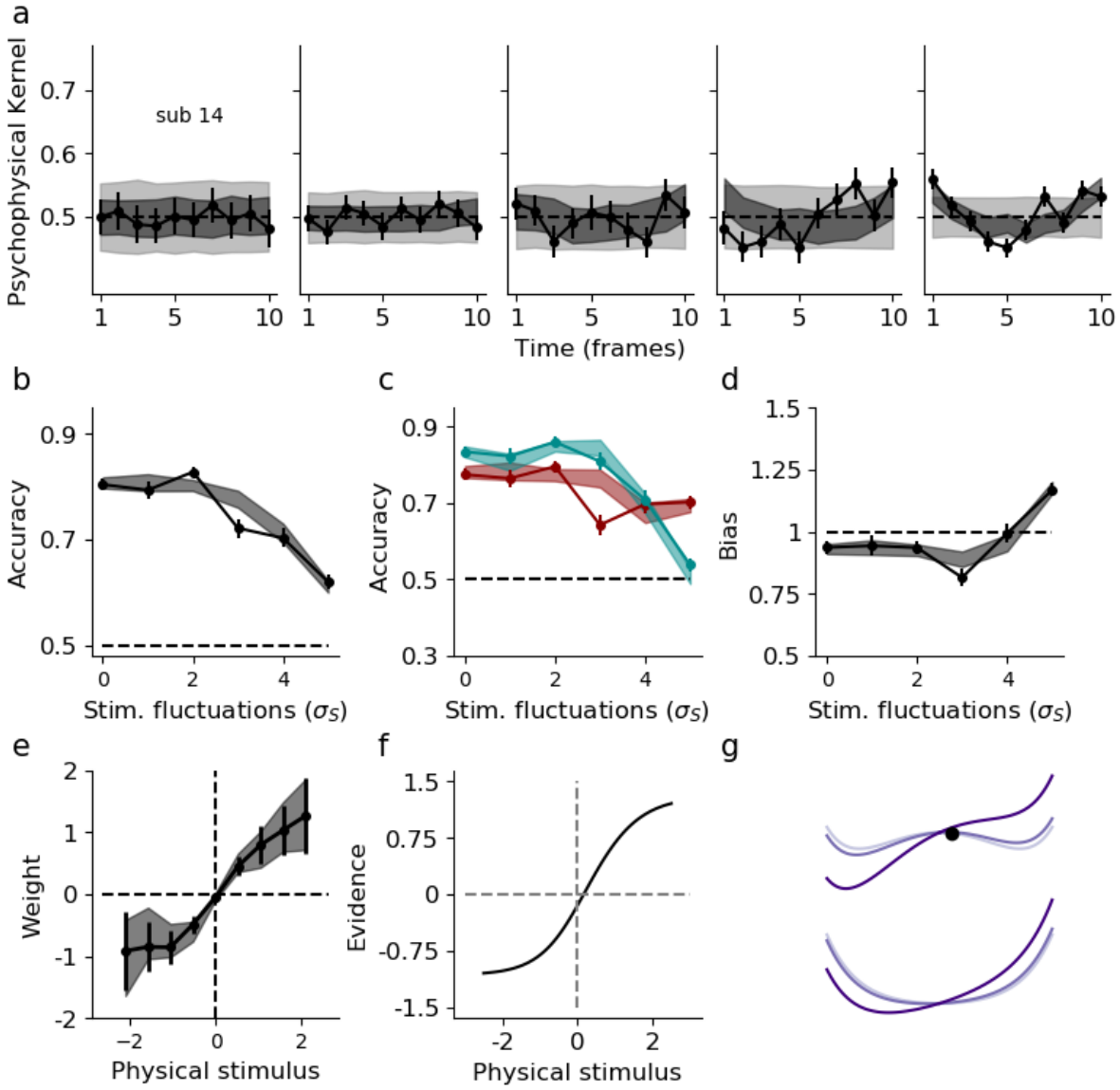

Figure 31 | Subject 14. Comparison between psychophysical results and model fit
Same as figure 28 for subject 14 **a)** The psychophysical kernels are non-monotonic produced by a double well potential at the beginning of the trial and a leaky potential at the end **(g) c,d)** Left bias for weak stimulus fluctuations and right bias for strong stimulus fluctuations.

Discussion

The aim of the psychophysical experiment was to find the signatures of attractor dynamics that we described in the first chapter. Specifically, we tested the non-monotonic relation between the accuracy and the stimulus fluctuations and the change in the psychophysical kernels from primacy to recency with the stimulus fluctuations. We find no evidence for a non-monotonic relation between the accuracy and the stimulus fluctuations and no evidence for a change from primacy to recency psychophysical kernel with the stimulus fluctuations. Despite the fact that we find no qualitatively signatures of attractor dynamics, this does not discard the attractor models. Other mechanisms that we did not consider when we made the theoretical predictions could be masking these signature. For instance, we find that the bias can play an important role to explain the behavioral results. Thus the qualitative analysis of the psychophysical kernels and the accuracy with the stimulus fluctuations might be too simple to test the existence of attractor mechanisms. In addition, we find idiosyncratic results in different psychophysical measurements such as psychophysical kernels, spatial kernels, and bias which discard the simple canonical models.

To further analyze the idiosyncratic psychophysical results in the single dot taks, we are developing a model-based analysis. The advantage of this approach is that we can introduce different mechanisms to the model and quantitatively test if they are important to explain the data. By fitting the model to each subject, we can study the mechanisms that produce the observed idiosyncratic behavior. To this day, we extended the one-dimensional version of the attractor model with different bias mechanisms, a non-linear transformation of the physical stimulus into evidence and an urgency signal. Preliminary results show that we can fit the model to each subject and we can study which mechanisms are important to explain the data. Although the model can already explain some characteristics of the behavior, the model could be completed with other mechanisms. For instance we could add bias mechanisms that depend on previous trials, e.g. a bias to repeat or alternate the previous choice. Other examples could be a constant bias in the potential or an adaptation mechanism that effectively decrease the steepness of the sensory transformation function during the trial. In sum, the model-based analysis described in this chapter seems a powerful tool to study the mechanisms underlying the decision process and the idiosyncratic behavioral results. Preliminary results show that the attractor dynamics $(c_2 > 0)$ is important to explain the behaviour of at least in 3 out of 4 of the subjects that we fitted.

This model-based analysis can be used not only to study variability across subjects but also to variability across tasks. Many studies have reported different primacy, flat and recency psychophysical kernels in different tasks, (R. Kiani, Churchland, and Shadlen 2013a; Nienborg and Cumming 2009; Brunton, Botvinick, and Brody 2013; Wyart et al. 2012; Wyart, Myers, and Summerfield 2015). With the model-based analysis, we could study if the variability in the psychophysical kernels arises because of the transformation of the physical stimulus into evidence is different across tasks or because the decision dynamics are different.

To summarize, the idiosyncratic behaviour of the subjects has prompted us to use a more sophisticated model-based analysis to investigate the mechanisms that explain the idiosyncratic results. Preliminary results with a model-based analysis show evidence for: 1) attractor dynamics in at least 3 of the subjects and 2) combination of different bias mechanism to explain the modulation of the bias with the stimulus fluctuations.

Methods

Psychophysical Experiment

Participants: Sixteen participants (9 female, 7 male) participated in the experiment. All had normal or corrected to normal vision and no history or indications of psychological or neurological disorders. The experiment was approved by the ethics committee of the Hamburg Medical Association and conducted in accordance with the declaration of Helsinki. Each participant completed one training session, three sessions in the psychophysics lab and three recording sessions in the MEG. Sessions were spread out over several days and were typically completed within 10 days.

Task and procedure: Each session consisted of 6 to 9 blocks of 100 trials, lasting approximately 60 minutes. The first session was a training session used for exposing participants to the task and completed QUEST staircase to determine their mean stimulus evidence $\bar{\mu}$ (Watson and Pelli 1983). The stimulus consists of a sequence of ten white dots. To avoid the appearance of motion between consecutive dots, each dot was presented in the following sequence: 50 ms with contrast 75%, 50 ms with 100% contrast and 50 ms with 75% contrast. We add an extra 50 ms frame between dots. The total stimulus duration was 2s. Each trial started with a random delay between 0.5 and 1 s. During the stimulus presentation we controlled fixation with an eye-tracker (Eyelink 1000). After the stimulus, the subjects respond with the keyboard and received feedback for 200 ms. The subjects started a new trial by pressing the spacebar.

Stimuli: The Stimuli were generated using Psychtoolbox 3 for Matlab. In the sessions performed in the psychophysics lab, they were presented on a 782 VIEWPixx monitor with 1920x1080 at 60Hz. In the MEG sessions, they were back-projected on a transparent screen using a Sanyo PCL-XP51 projector with the same resolution and frame rate. The mean stimulus strength was fixed for each subject and we interleave trials with different stimulus fluctuations $\bar{\sigma} = [0, 0.02, 0.05, 0.14, 0.37, 1]$ degrees of visual angle. For each stimulus we fixed the sample mean and the sample standard deviation, First, we draw 10 random variable from a Gaussian distribution with mean $\bar{\mu}$ and standard deviation $\bar{\sigma}_S$, $x_i \sim N(\bar{\mu}, \sigma_S)$ for $i = 1, 2..., 10$. The final stimulus is

$$s_i = \bar{\mu} + \frac{x_i - \bar{x}}{\sigma_x} \quad (67)$$

Where $\bar{x}$ is the sample mean of x_i and σ_x is the standard deviation of x_i. This introduces correlations in each stimulus that can affect the psychophysical kernel. For instance, if we consider a toy model that only takes into account the first frame to make the decision, then the psychophysical kernel is significantly positive for the first frame and significantly negative for the rest of the frames. This is because we impose that $x_{pos,1} = -\left(\bar{\mu} - \sum_{i=2}^{10} x_{pos,i}\right)$.

Primacy-recency index

In chapter 1, we compute the primacy-recency index in two steps. First, we normalize the area of the psychophysical kernel. Second, we compute a weighted sum of the stimulus. In the psychophysical data set, the area of the psychophysical kernel is very small for weak stimulus fluctuations. This produces numerical problems when we try to normalize the area. For the psychophysical data, we compute the primacy-recency index using only the second step

$$PRI(n) = PK(n)\omega(n) \quad (68)$$

with $\omega(n) = 1 - 2\frac{n}{T}$ where n is the frame number and T is the total number of frames, $T = 10$ in our experiment. This affects the interpretation of the results because a primacy-recency index which is not significantly different from 0 can be produced for a flat psychophysical kernel or for a psychophysical kernel that is not flat but with a very small magnitude.

Model fitting to the psychophysical data

Maximum likelihood estimation**:** We fit the best potential for each subject by maximum likelihood estimation. Given a set of stimuli s_i for $i = 1...N$ and a set of subject's decisions d_i for $i = 1...N$ where N is the number of stimuli of each subject. Assuming that the trials are independent, the likelihood of the observed data given the model is

$$l = \prod_{i=0}^{N} p(d_i|\theta, S_i) \quad (69)$$

Because the logarithm is a monotonic function, the set of parameters that maximize the likelihood, also maximize the function $log(l)$. Thus to avoid numerical problems, we will use

$$log(l) = \sum_{i=0}^{N} log\left(p\left(d_i|\theta, S_i\right)\right) \tag{70}$$

We also add a regularization parameter. The final function that we are going to maximize is

$$f = log(l) - \lambda \sum_{i=0}^{N_p} \theta_i^2 \tag{71}$$

Where N_p is the number of parameters, we used cross validation with the standard double well model to choose the hyperparameter $\lambda = 0.63$. To maximize the log-likelihood, we adapted the software from (Yartsev et al. 2018) where the authors used the L-BGFS algorithm to minimize the negative log-likelihood. This algorithm requires the gradient of the target function that was computed using automatic differentiation (Revels, Lubin, and Papamarkou 2016)**.**

Probability of right for each trial: In order to compute the probability of Right and Left choice, we need the distribution of the decision variable at the end of the trial $p(X, T)$ where T is the stimulus duration. Then the probability of right is simply the positive area of $p(X, T)$. We adapt the computation of the time evolution of $p(X, t)$ from (Yartsev et al. 2018; Brunton, Botvinick, and Brody 2013) to our model.

In each frame n the potential is

$$\varphi(X) = \mu(n)X - \tfrac{1}{2}c_2(n)X^2 + \tfrac{1}{4}c_4X^4 + \tfrac{1}{6}c_6X^6 \tag{72}$$

Where μ is the evidence from the sensory module (equation 64 and 65) and $c_2(n) = c_{2,0} + c_{2,u}$. The dynamics of the decision variable (X) follows the diffusion equation

$$\frac{dX}{dt} = -\frac{d\varphi}{dX} + \sigma_i\xi(t) \tag{73}$$

Note that we fixed the time scale $\tau = 1$ because the model has a free parameter. In order to compute the probability of right, we need the distribution of the decision variable at the end of the trial $p(X, T)$ where T is the stimulus duration. If we discretize the time, we can solve equation 73 by the euler method

$$X(t+1) = X(t) - \frac{d\varphi}{dX}\Delta t + \sqrt{\Delta t}\sigma_i\xi(t) \tag{74}$$

Where $\xi(t)$ are independent and identically distributed random variables from a Normal distribution $N(0,1)$. It is clear that the distribution of the decision variable at time $X(t+1)$ is

$$p(X,t+1) = N\left(X(t) - \frac{d\varphi}{dX}\Delta t, \sqrt{\Delta t}\sigma_i\right) \quad (75)$$

From $p(X,t+1)$ we see that the diffusion process obeys the Markov property: the distribution of $X(t+1)$ only depends on the previous position $X(t)$. Now, we discretize the decision variable space in $2N_b$ bins of width ΔX. The bin centers are $\nu_i = (i - N_b)\Delta X \quad for\ i = 0,...,2N_b$ and the bounds of these bins are $\alpha_i = i\Delta x - N_b\Delta X - \frac{\Delta X}{2} \quad for\ i = 0,...2N_b + 1$ (figure 32b). The probability to make a transition from bin i to bin j in one frame is simply the area of $N\left(\nu_i - \frac{d\varphi}{dX}\Delta t, \sqrt{\Delta t}\sigma_i\right)$ inside bin j. Similarly we can build a transition matrix F for all bins and compute the temporal evolution of the decision variable as

$$p(\nu, t+1) = F\,p(\nu, t) \quad (76)$$

Where $p(v_i,t)$ is the probability of finding the decision variable in bin i at time t. For illustration purposes, we show the temporal evolution of $p(v,t)$ for a single trial of the double well model (figure 32a)

Initial distribution and transition matrix: To compute the initial distribution and the transition matrix we use a method that preserves the mean of the distribution when we discrete space (Brunton, Botvinick, and Brody 2013). In the extended neurobiological model the initial distribution is a delta function at x_0. Imaging that x_0 falls in the bin i, one possibility is to set $p(\nu_i,0) = 1$. In this case the mean of the distribution of the decision variable is ν_i instead of x_0. A better approximation is to distribute the probability between the two closest bins to x_0. If $\nu_i < x_0 < \nu_{i+1}$ where ν_i is the center of bin i then

$$p(v_i,0) = \frac{\nu_{i+1} - x_0}{\nu_{i+1} - \nu_i} \quad (77)$$

$$p(v_{i+1},0) = \frac{x_0 - \nu_i}{\nu_{i+1} - \nu_i} \quad (78)$$

With this approach the mean of $p(\nu,0)$ is exactly x_0. We apply the same technique to compute the transition matrix. The distribution of the decision variable at time $t+1$ given that

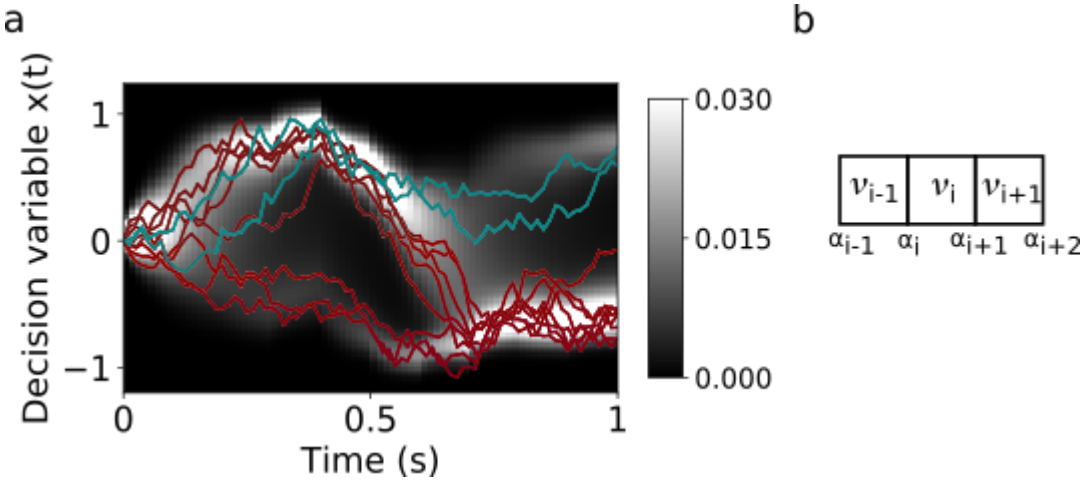

Figure 32 | Temporal evolution of the decision variable distribution
a) Temporal evolution of the decision variable distribution for one trial of the double well model. The model captures the transitions between states. Color lines are single trial simulations of the double well model using the euler method (equation 11). **b)** Discretization of the space to compute the temporal evolution of the decision variable distribution. ν_i are the center of the bounds and α_i are the bounds.

the decision variable was at ν_j in time t is $p = N\left(\nu_j - \frac{d\varphi}{dX}\Delta t, \sqrt{\Delta t}\sigma_i\right)$. Now we use bins much smaller than $\sqrt{\Delta}\sigma_i$ to discretize p, we define the center of these bins as s_k. Finally we distribute the probability of $p(s_k)$ between the two closest bin ν_i and ν_{i+1}. Then the elements $F_{i,j}$ of the transition matrix are computed as the sum over all the bins $p(s_k)$ whose positions fall between ν_i and ν_{i+1} weighted by the relative distance between ν_i and s_k

$$F_{i,j} = \sum_{\nu_i < s_k < \nu_{i+1}} p(s_k)\frac{\nu_{i+1} - s_k}{\nu_{i+1} - \nu_i} + \sum_{\nu_{i-1} < s_k < \nu_i} p(s_k)\frac{s_k - \nu_{i-1}}{\nu_{i+1} - \nu_i} \tag{79}$$

Model fitting to synthetic data

To fit the synthetic data, we used the same method as the psychophysical data but we used a gradient free algorithm to find the best parameters (Nelder-mead). To speed up the likelihood maximization, we fixed two of the parameters to the true value. Note that there is only one free parameter in the model, $\tau = 1$. We fit the parameters $\theta = [c_2, c_4, \sigma_i]$. and we fixed the transformation of stimulus into evidence and the time scale to 1.

To compare the likelihoods of the original fitted models and the fitted model in figure 24 and figure 25, we compute the relative likelihood of the fitted model compared to the original fitted model as

$$RL = exp(-\Delta AIC/2) \quad (80)$$

Where ΔAIC is the difference between the AIC values of the original fitted model and the fitted model. The AIC values are computed with equation 60.

5. Conclusions

Chapter 2. Flexible categorization in perceptual decision making

1. In the second chapter, we showed that the attractor model for perceptual decision making has different integration regimes controlled by the transitions between attractor states. These integration regimes are characterized by the shape of the psychophysical kernel: primacy when the transitions are very unlikely, recency when the transitions are very likely and non-monotonic in between these two extreme regimes. We modified the probability of transitions with the stimulus parameters and we made three experimentally testable predictions.
2. The attractor model predicts a change from primacy to recency psychophysical kernel as we increase the magnitude of the stimulus fluctuations or the stimulus duration.
3. The attractor model predicts an increase of accuracy for a range of stimulus fluctuations. This is explained by an asymmetric transition rates between correcting and error transitions.
4. A similar mechanism causes a non-monotonic change in the consistency with the stimulus fluctuations.
5. We found evidence for a change from primacy to recency psychophysical kernels with the stimulus duration in a psychophysical experiment.

Chapter 3. The double well model in tasks involving working memory and decision making

1. We found that under the biological constraint that the accumulated evidence towards one of the choices is bounded, increasing the winner-take-all dynamics produces an increase in the accuracy.
2. The double well model in a regime close to the flexible categorization is able to combine information from two pulses of evidence separated by variable duration temporal gap.

3. The double well model and an alternative attractor model with an undecided state are able to fit psychophysics data from an experiment where the stimulus was interrupted by a variable delay.

Chapter 4. Modifying the magnitude of stimulus fluctuations to identify different neural mechanisms

1. We found no evidence for the qualitative signatures of attractor dynamics described in chapter 1.
2. Preliminary results with model-based analysis showed that an extended attractor model is able to explain the richness behavior of the subjects.
3. Preliminary model-based analysis showed: 1) evidence for winner-take-all dynamics at least in a fraction of subjects and 2) evidence for different bias mechanisms.

Supplementary figures

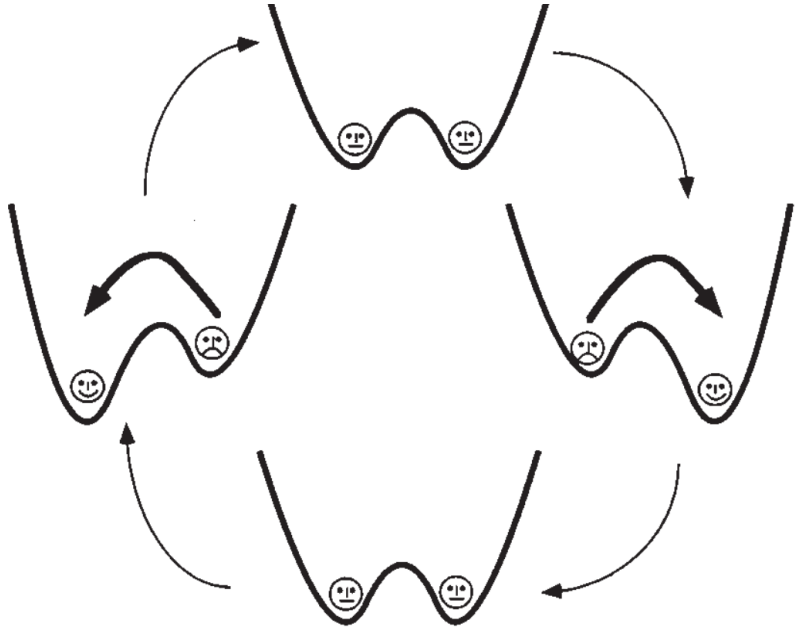

Figure S1 | Stochastic resonance cartoon

In classic stochastic resonance, the task is to follow the periodic signal that make the potential antisymmetric. To follow the signal, the particle moving in this potential has to escape from the well when it becomes a local minimum (sad face) and remain in the global minimum. There is an optimal magnitude of noise that allows the particle to escape from the local minimum but not from the global minimum. Figure from (Gammaitoni et al. 1998)

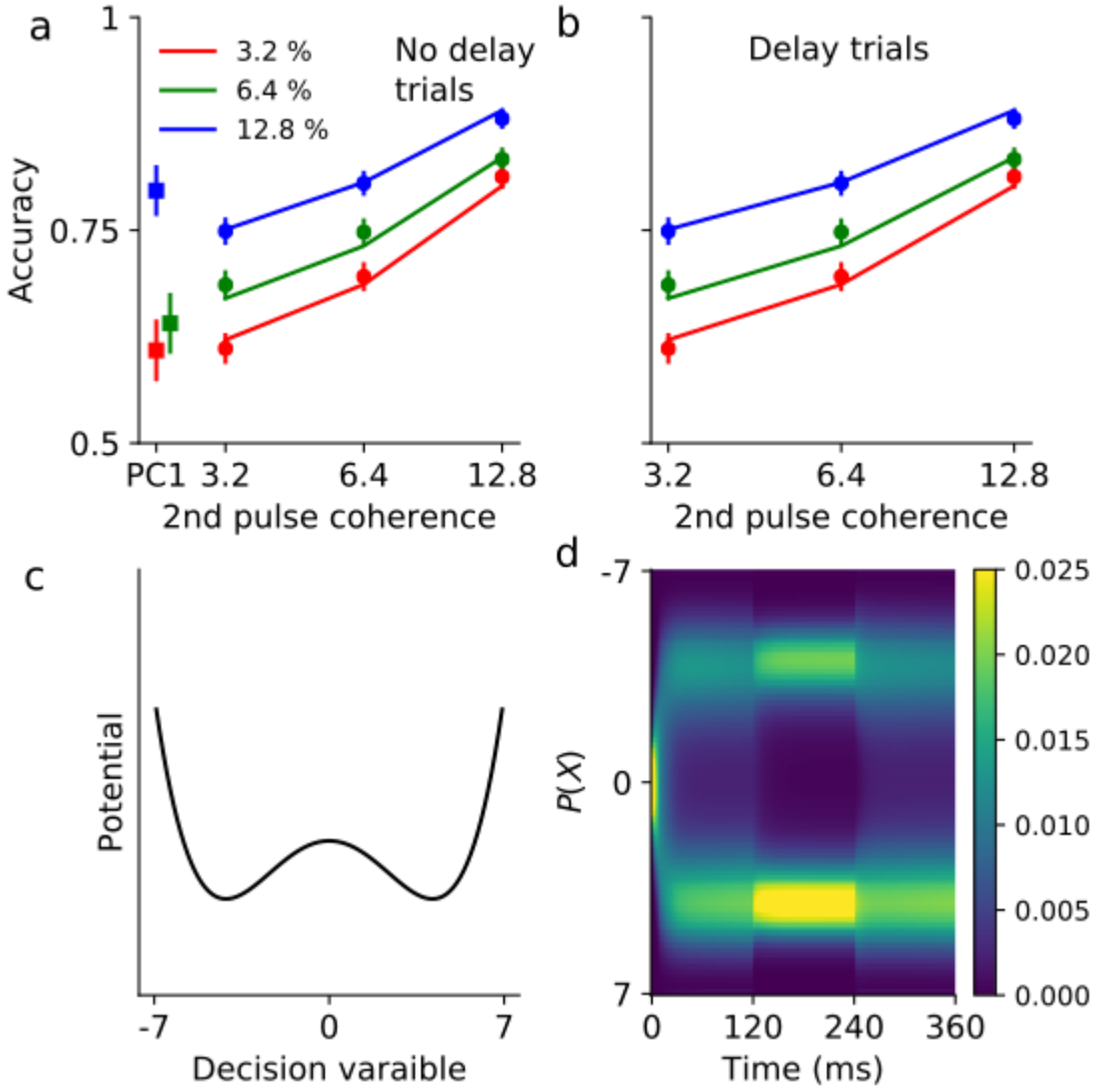

Figure S2 | Double well model fitted to the data from (R. Kiani, Churchland, and Shadlen 2013a; Tohidi-Moghaddam et al. 2019)

a) Probability of correct for single (squares) and double (dots) pulse trials without delay for the three possible first pulse coherence (3.2% red, 6.4% green, 12.8 % blue) (dots). Solid lines show the accuracy of the fitted double well model. **b)** Same as a with trials with a delay of 120 ms. **c)** Double well potential with the fitted parameters **d)** Temporal evolution of the decision variable probability density function for a trial with 3.2% coherence in both pulses of evidence.

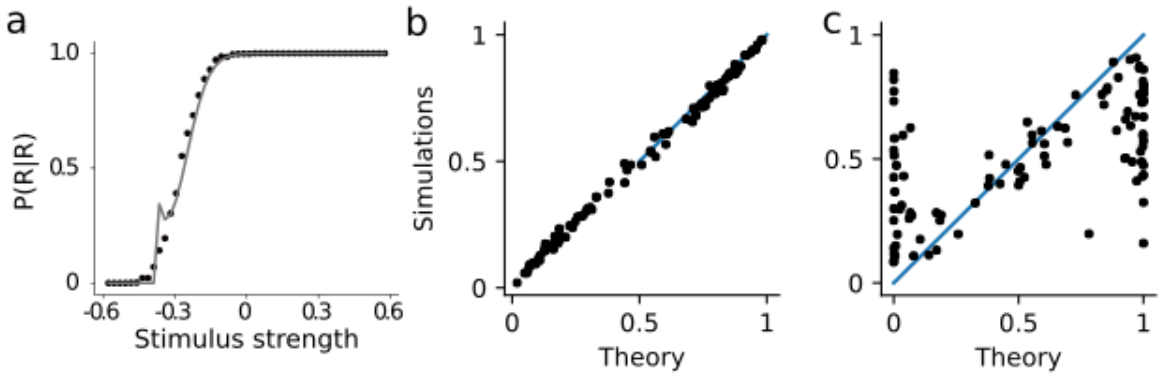

Figure S3 | Limitations of fitting the double well model using the transitions between wells.

a) Probability of right when the trial started on the right well as a function of the stimulus strength. The black dots are simulations and the grey line is computed with the transitions rates (equation 25). For very strong stimulus, the theory fails because the barrier become very small. For a critical value of the stimulus strength, the right well disappears and the theory predictions a deterministic transition to the left well. **b)** Probability of right for a set of 100 stimuli, computed with the transitions rates theory (equation 27) and simulations using the parameters that best describe the data set from (R. Kiani, Churchland, and Shadlen 2013a; Tohidi-Moghaddam et al. 2019). The theory based on the transitions rates capture the dynamics of the model ($r^2 = 0.99$. **c)** Same as in b but using the parameters that best describe the data from (Bronfman, Brezis, and Usher 2016). For these parameters, the dynamics of the model is not well captured by the theory $r^2 = 0.57$.

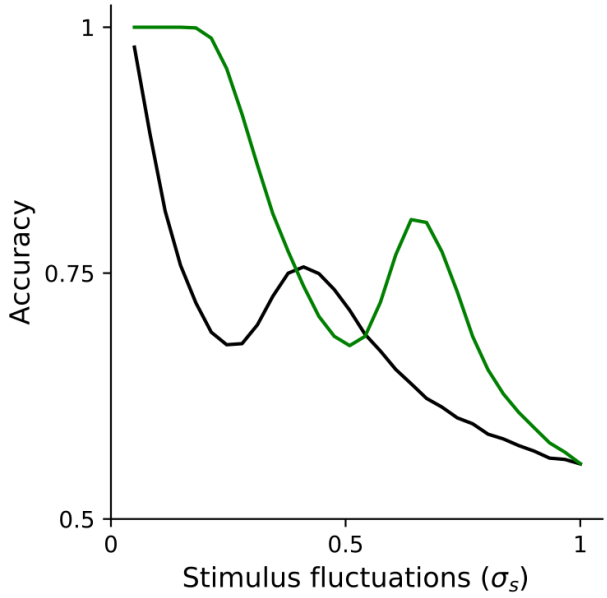

Figure S4 | Non-monotonic relation between accuracy and stimulus fluctuations with and without correlations in the stimulus.

When we introduce correlations in the stimulus such as the sample mean and the sample standard deviation are fixed to the mean and the standard deviation of the generative function, the bump in accuracy is higher. In green with stimulus correlations and in black without stimulus correlations.

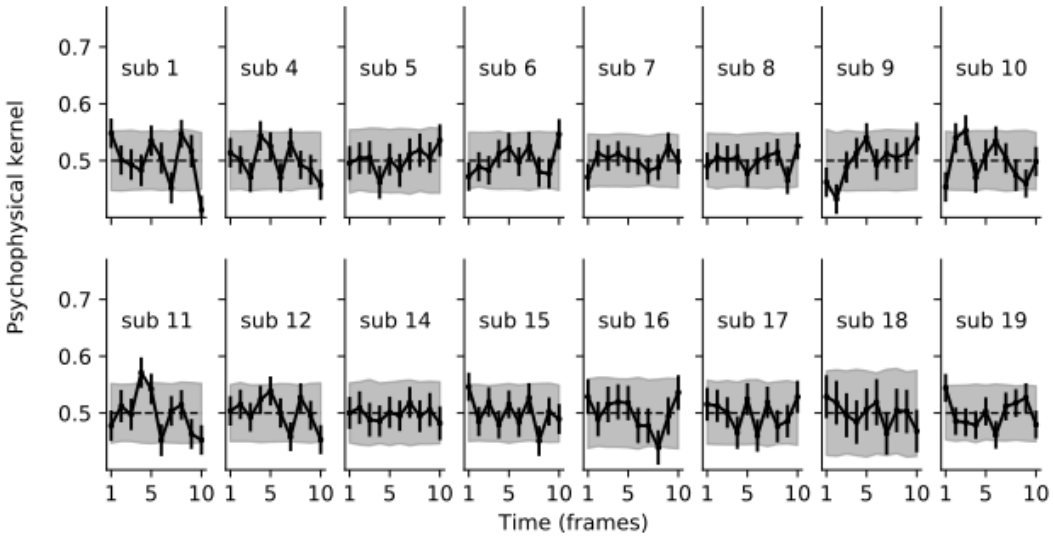

Figure S5 | Weak stimulus fluctuations have a small impact on the choice.

The weak stimulus fluctuations have a very small impact on the choice and we do not have enough trials to properly compute the psychophysical kernels. Error bars are computed with bootstrap $(N = 500)$. The grey region show two standard deviations of the distribution of psychophysical kernels computed by shuffling the decisions. Only outside this region the psychophysical kernel is significant.

Bibliography

Akaishi, Rei, Kazumasa Umeda, Asako Nagase, and Katsuyuki Sakai. 2014. “Autonomous Mechanism of Internal Choice Estimate Underlies Decision Inertia.” *Neuron* 81 (1): 195–206.

Amit, N., and N. Brunel. 1997. “Model of Global Spontaneous Activity and Local Structured Activity during Delay Periods in the Cerebral Cortex.” *Cerebral Cortex*. https://doi.org/10.1093/cercor/7.3.237.

Barth, Hilary C., Sara Cordes, and Andrea L. Patalano. 2018. “Suboptimality in Perceptual Decision Making and beyond.” *Behavioral and Brain Sciences*. https://doi.org/10.1017/s0140525x18001528.

Berg, Ronald van den, Kavitha Anandalingam, Ariel Zylberberg, Roozbeh Kiani, Michael N. Shadlen, and Daniel M. Wolpert. 2016. “A Common Mechanism Underlies Changes of Mind about Decisions and Confidence.” *eLife* 5 (February): e12192.

Bogacz, Rafal, Eric Brown, Jeff Moehlis, Philip Holmes, and Jonathan D. Cohen. 2006. “The Physics of Optimal Decision Making: A Formal Analysis of Models of Performance in Two-Alternative Forced-Choice Tasks.” *Psychological Review* 113 (4): 700–765.

Bonaiuto, James J., Archy de Berker, and Sven Bestmann. 2016. “Response Repetition Biases in Human Perceptual Decisions Are Explained by Activity Decay in Competitive Attractor Models,” December. https://doi.org/10.7554/eLife.20047.

Braun, Anke, Anne E. Urai, and Tobias H. Donner. 2018. “Adaptive History Biases Result from Confidence-Weighted Accumulation of Past Choices.” *The Journal of Neuroscience: The Official Journal of the Society for Neuroscience* 38 (10): 2418–29.

Britten, K. H., M. N. Shadlen, W. T. Newsome, and J. A. Movshon. 1992. “The Analysis of Visual Motion: A Comparison of Neuronal and Psychophysical Performance.” *The Journal of Neuroscience: The Official Journal of the Society for Neuroscience* 12 (12): 4745–65.

Brody, Carlos D., Ranulfo Romo, and Adam Kepecs. 2003. “Basic Mechanisms for Graded Persistent Activity: Discrete Attractors, Continuous Attractors, and Dynamic Representations.” *Current Opinion in Neurobiology*. https://doi.org/10.1016/s0959-4388(03)00050-3.

Bronfman, Zohar Z., Noam Brezis, and Marius Usher. 2016. “Non-Monotonic Temporal-Weighting Indicates a Dynamically Modulated Evidence-Integration Mechanism.” *PLoS Computational Biology* 12 (2): e1004667.

Brunel, Nicolas, and Xiao-Jing Wang. 2001. “Effects of Neuromodulation in a Cortical Network Model of Object Working Memory Dominated by Recurrent Inhibition.” *Journal of Computational Neuroscience* 11 (1): 63–85.

Brunton, Bingni W., Matthew M. Botvinick, and Carlos D. Brody. 2013. “Rats and Humans Can Optimally Accumulate Evidence for Decision-Making.” *Science*. https://doi.org/10.1126/science.1233912.

Burnham, Kenneth P., and David R. Anderson. 2004. “Multimodel Inference.” *Sociological Methods & Research*. https://doi.org/10.1177/0049124104268644.

Cheadle, S., V. Wyart, K. Tsetsos, N. Myers, V. de Gardelle, S. Herce Castanon, and C. Summerfield. 2014. “Adaptive Gain Control during Human Perceptual Choice.” *Journal of Vision*. https://doi.org/10.1167/14.10.1117.

Cisek, Paul, Geneviève Aude Puskas, and Stephany El-Murr. 2009. “Decisions in Changing Conditions: The Urgency-Gating Model.” *The Journal of Neuroscience: The Official*

Journal of the Society for Neuroscience 29 (37): 11560–71.
Compte, A., N. Brunel, P. S. Goldman-Rakic, and X. J. Wang. 2000. “Synaptic Mechanisms and Network Dynamics Underlying Spatial Working Memory in a Cortical Network Model.” *Cerebral Cortex* 10 (9): 910–23.
Deneve, Sophie. 2012. “Making Decisions with Unknown Sensory Reliability.” *Frontiers in Neuroscience*. https://doi.org/10.3389/fnins.2012.00075.
Drugowitsch, Jan, Rubén Moreno-Bote, Anne K. Churchland, Michael N. Shadlen, and Alexandre Pouget. 2012. “The Cost of Accumulating Evidence in Perceptual Decision Making.” *The Journal of Neuroscience: The Official Journal of the Society for Neuroscience* 32 (11): 3612–28.
Duncan Luce, R. 1991. *Response Times: Their Role in Inferring Elementary Mental Organization*. Oxford University Press.
Durrett, Richard. 2016. “Essentials of Stochastic Processes.” *Springer Texts in Statistics*. https://doi.org/10.1007/978-3-319-45614-0.
Fleming, Stephen M., Laurence T. Maloney, and Nathaniel D. Daw. 2013. “The Irrationality of Categorical Perception.” *The Journal of Neuroscience: The Official Journal of the Society for Neuroscience* 33 (49): 19060–70.
Forstmann, B. U., R. Ratcliff, and E. -J. Wagenmakers. 2016. “Sequential Sampling Models in Cognitive Neuroscience: Advantages, Applications, and Extensions.” *Annual Review of Psychology*. https://doi.org/10.1146/annurev-psych-122414-033645.
Fritsche, Matthias, Pim Mostert, and Floris P. de Lange. 2017. “Opposite Effects of Recent History on Perception and Decision.” *Current Biology: CB* 27 (4): 590–95.
Funahashi, S., C. J. Bruce, and P. S. Goldman-Rakic. 1989. “Mnemonic Coding of Visual Space in the Monkey’s Dorsolateral Prefrontal Cortex.” *Journal of Neurophysiology* 61 (2): 331–49.
Furman, Moran, and Xiao-Jing Wang. 2008. “Similarity Effect and Optimal Control of Multiple-Choice Decision Making.” *Neuron* 60 (6): 1153–68.
Gammaitoni, Luca, Peter Hänggi, Peter Jung, and Fabio Marchesoni. 1998. “Stochastic Resonance.” *Reviews of Modern Physics* 70 (1): 223.
Gold, Joshua I., Chi-Tat Law, Patrick Connolly, and Sharath Bennur. 2008. “The Relative Influences of Priors and Sensory Evidence on an Oculomotor Decision Variable during Perceptual Learning.” *Journal of Neurophysiology* 100 (5): 2653–68.
Gold, Joshua I., and Michael N. Shadlen. 2007. “The Neural Basis of Decision Making.” *Annual Review of Neuroscience* 30: 535–74.
Goldman, M. S., A. Compte, and X. -J. Wang. 2009. “Neural Integrator Models.” *Encyclopedia of Neuroscience*. https://doi.org/10.1016/b978-008045046-9.01434-0.
Groen, Onno van der, Matthew F. Tang, Nicole Wenderoth, and Jason B. Mattingley. 2018. “Stochastic Resonance Enhances the Rate of Evidence Accumulation during Combined Brain Stimulation and Perceptual Decision-Making.” *PLoS Computational Biology* 14 (7): e1006301.
Hawkins, Guy E., Birte U. Forstmann, Eric-Jan Wagenmakers, Roger Ratcliff, and Scott D. Brown. 2015. “Revisiting the Evidence for Collapsing Boundaries and Urgency Signals in Perceptual Decision-Making.” *The Journal of Neuroscience: The Official Journal of the Society for Neuroscience* 35 (6): 2476–84.
Jaramillo, Jorge, Jorge F. Mejias, and Xiao-Jing Wang. 2019. “Engagement of Pulvino-Cortical Feedforward and Feedback Pathways in Cognitive Computations.” *Neuron* 101 (2): 321–36.e9.
Kawaguchi, Katsuhisa, Stephane Clery, Paria Pourriahi, Lenka Seillier, Ralf M. Haefner, and Hendrikje Nienborg. 2018. “Differentiating between Models of Perceptual Decision Making Using Pupil Size Inferred Confidence.” *The Journal of Neuroscience: The Official Journal of the Society for Neuroscience* 38 (41): 8874–88.

Keung, Waitsang, Todd A. Hagen, and Robert C. Wilson. 2019. “Regulation of Evidence Accumulation by Pupil-Linked Arousal Processes.” *Nature Human Behaviour* 3 (6): 636–45.
Kiani, R., A. K. Churchland, and M. N. Shadlen. 2013a. “Integration of Direction Cues Is Invariant to the Temporal Gap between Them.” *Journal of Neuroscience*. https://doi.org/10.1523/jneurosci.2094-13.2013.
Kiani, Roozbeh, Leah Corthell, and Michael N. Shadlen. 2014. “Choice Certainty Is Informed by Both Evidence and Decision Time.” *Neuron* 84 (6): 1329–42.
Kiani, Roozbeh, Christopher J. Cueva, John B. Reppas, and William T. Newsome. 2014. “Dynamics of Neural Population Responses in Prefrontal Cortex Indicate Changes of Mind on Single Trials.” *Current Biology: CB* 24 (13): 1542–47.
Kiani, Roozbeh, Timothy D. Hanks, and Michael N. Shadlen. 2008. “Bounded Integration in Parietal Cortex Underlies Decisions Even When Viewing Duration Is Dictated by the Environment.” *The Journal of Neuroscience: The Official Journal of the Society for Neuroscience* 28 (12): 3017–29.
Kiani, Roozbeh, and Michael N. Shadlen. 2009. “Representation of Confidence Associated with a Decision by Neurons in the Parietal Cortex.” *Science* 324 (5928): 759–64.
Koulakov, Alexei A., Sridhar Raghavachari, Adam Kepecs, and John E. Lisman. 2002. “Model for a Robust Neural Integrator.” *Nature Neuroscience* 5 (8): 775–82.
Kramers, H. A. 1940. “Brownian Motion in a Field of Force and the Diffusion Model of Chemical Reactions.” *Physica*. https://doi.org/10.1016/s0031-8914(40)90098-2.
Lim, Sukbin, and Mark S. Goldman. 2013. “Balanced Cortical Microcircuitry for Maintaining Information in Working Memory.” *Nature Neuroscience* 16 (9): 1306–14.
Longtin, A., A. Bulsara, and F. Moss. 1991. “Time-Interval Sequences in Bistable Systems and the Noise-Induced Transmission of Information by Sensory Neurons.” *Physical Review Letters* 67 (5): 656–59.
Machens, Christian K., Ranulfo Romo, and Carlos D. Brody. 2005. “Flexible Control of Mutual Inhibition: A Neural Model of Two-Interval Discrimination.” *Science* 307 (5712): 1121–24.
MacKay, David J. C., and David J. Mac. 2003. *Information Theory, Inference and Learning Algorithms*. Cambridge University Press.
Melcher, David, Sofia Crespi, Aurelio Bruno, and M. Concetta Morrone. 2004. “The Role of Attention in Central and Peripheral Motion Integration.” *Vision Research* 44 (12): 1367–74.
Mulder, M. J., E. -J. Wagenmakers, R. Ratcliff, W. Boekel, and B. U. Forstmann. 2012. “Bias in the Brain: A Diffusion Model Analysis of Prior Probability and Potential Payoff.” *Journal of Neuroscience*. https://doi.org/10.1523/jneurosci.4156-11.2012.
Murray, John D., Jorge Jaramillo, and Xiao-Jing Wang. 2017. “Working Memory and Decision-Making in a Frontoparietal Circuit Model.” *The Journal of Neuroscience*. https://doi.org/10.1523/jneurosci.0343-17.2017.
Neri, Peter, and David J. Heeger. 2002. “Spatiotemporal Mechanisms for Detecting and Identifying Image Features in Human Vision.” *Nature Neuroscience* 5 (8): 812–16.
Neri, Peter, and Dennis M. Levi. 2006. “Receptive versus Perceptive Fields from the Reverse-Correlation Viewpoint.” *Vision Research* 46 (16): 2465–74.
Nienborg, Hendrikje, and Bruce G. Cumming. 2009. “Decision-Related Activity in Sensory Neurons Reflects More than a Neuron’s Causal Effect.” *Nature*. https://doi.org/10.1038/nature07821.
Okazawa, Gouki, Long Sha, Braden A. Purcell, and Roozbeh Kiani. 2018. “Psychophysical Reverse Correlation Reflects Both Sensory and Decision-Making Processes.” *Nature Communications* 9 (1): 3479.
Park, Il Memming, Miriam L. R. Meister, Alexander C. Huk, and Jonathan W. Pillow. 2014.

"Encoding and Decoding in Parietal Cortex during Sensorimotor Decision-Making." *Nature Neuroscience* 17 (10): 1395–1403.
Piet, Alex T., Ahmed El Hady, and Carlos D. Brody. 2018. "Rats Adopt the Optimal Timescale for Evidence Integration in a Dynamic Environment." *Nature Communications*. https://doi.org/10.1038/s41467-018-06561-y.
Ratcliff, Roger. 1978. "A Theory of Memory Retrieval." *Psychological Review*. https://doi.org/10.1037//0033-295x.85.2.59.
Ratcliff, Roger, and Jeffrey N. Rouder. 1998. "Modeling Response Times for Two-Choice Decisions." *Psychological Science*. https://doi.org/10.1111/1467-9280.00067.
Ratcliff, Roger, and Philip L. Smith. 2004. "A Comparison of Sequential Sampling Models for Two-Choice Reaction Time." *Psychological Review* 111 (2): 333–67.
Ratcliff, Roger, Anjali Thapar, and Gail McKoon. 2004. "A Diffusion Model Analysis of the Effects of Aging on Recognition Memory." *Journal of Memory and Language*. https://doi.org/10.1016/j.jml.2003.11.002.
Ratcliff, Roger, and Francis Tuerlinckx. 2002. "Estimating Parameters of the Diffusion Model: Approaches to Dealing with Contaminant Reaction Times and Parameter Variability." *Psychonomic Bulletin & Review* 9 (3): 438–81.
Ratcliff, Roger, Chelsea Voskuilen, and Gail McKoon. 2018. "Internal and External Sources of Variability in Perceptual Decision-Making." *Psychological Review* 125 (1): 33–46.
Renart, Alfonso, Pengcheng Song, and Xiao-Jing Wang. 2003. "Robust Spatial Working Memory through Homeostatic Synaptic Scaling in Heterogeneous Cortical Networks." *Neuron* 38 (3): 473–85.
Resulaj, Arbora, Roozbeh Kiani, Daniel M. Wolpert, and Michael N. Shadlen. 2009. "Changes of Mind in Decision-Making." *Nature*. https://doi.org/10.1038/nature08275.
Revels, Jarrett, Miles Lubin, and Theodore Papamarkou. 2016. "Forward-Mode Automatic Differentiation in Julia." http://arxiv.org/abs/1607.07892.
Roitman, Jamie D., and Michael N. Shadlen. 2002. "Response of Neurons in the Lateral Intraparietal Area during a Combined Visual Discrimination Reaction Time Task." *The Journal of Neuroscience: The Official Journal of the Society for Neuroscience* 22 (21): 9475–89.
Roxin, Alex, and Anders Ledberg. 2008. "Neurobiological Models of Two-Choice Decision Making Can Be Reduced to a One-Dimensional Nonlinear Diffusion Equation." *PLoS Computational Biology* 4 (3): e1000046.
Schneider, Michael. 1994. "Modelling Hobson's Underconsumption Theory." *J. A. Hobson after Fifty Years*. https://doi.org/10.1007/978-1-349-23213-0_6.
Seung, H. Sebastian, H. Sebastian Seung, Daniel D. Lee, Ben Y. Reis, and David W. Tank. 2000. "Stability of the Memory of Eye Position in a Recurrent Network of Conductance-Based Model Neurons." *Neuron*. https://doi.org/10.1016/s0896-6273(00)81155-1.
Shadlen, M. N., and W. T. Newsome. 2001. "Neural Basis of a Perceptual Decision in the Parietal Cortex (area LIP) of the Rhesus Monkey." *Journal of Neurophysiology* 86 (4): 1916–36.
Smith, Philip L., and Roger Ratcliff. 2004. "Psychology and Neurobiology of Simple Decisions." *Trends in Neurosciences* 27 (3): 161–68.
Starns, Jeffrey J., and Roger Ratcliff. 2010. "The Effects of Aging on the Speed-Accuracy Compromise: Boundary Optimality in the Diffusion Model." *Psychology and Aging* 25 (2): 377–90.
Thapar, Anjali, Roger Ratcliff, and Gail McKoon. 2003. "A Diffusion Model Analysis of the Effects of Aging on Letter Discrimination." *Psychology and Aging*. https://doi.org/10.1037/0882-7974.18.3.415.
Thura, David, Julie Beauregard-Racine, Charles-William Fradet, and Paul Cisek. 2012.

"Decision Making by Urgency Gating: Theory and Experimental Support." *Journal of Neurophysiology* 108 (11): 2912–30.
Tohidi-Moghaddam, Maryam, Sajjad Zabbah, Farzaneh Olianezhad, and Reza Ebrahimpour. 2019. "Sequence-Dependent Sensitivity Explains the Accuracy of Decisions When Cues Are Separated with a Gap." *Attention, Perception & Psychophysics*, July. https://doi.org/10.3758/s13414-019-01810-8.
Urai, Anne E., Anke Braun, and Tobias H. Donner. 2017. "Pupil-Linked Arousal Is Driven by Decision Uncertainty and Alters Serial Choice Bias." *Nature Communications* 8 (March): 14637.
Urai, Anne E., Jan Willem de Gee, Konstantinos Tsetsos, and Tobias H. Donner. 2019. "Choice History Biases Subsequent Evidence Accumulation." *eLife* 8 (July). https://doi.org/10.7554/eLife.46331.
Wald, A., and J. Wolfowitz. 1948. "Optimum Character of the Sequential Probability Ratio Test." *The Annals of Mathematical Statistics*. https://doi.org/10.1214/aoms/1177730197.
Wang, Xiao-Jing. 2002. "Probabilistic Decision Making by Slow Reverberation in Cortical Circuits." *Neuron* 36 (5): 955–68.
Wang, Xiao-Jing. 2008. "Decision Making in Recurrent Neuronal Circuits." *Neuron* 60 (2): 215–34.
Waskom, Michael L., and Roozbeh Kiani. 2018. "Decision Making through Integration of Sensory Evidence at Prolonged Timescales." *Current Biology: CB* 28 (23): 3850–56.e9.
Watson, Andrew B., and Denis G. Pelli. 1983. "Quest: A Bayesian Adaptive Psychometric Method." *Perception & Psychophysics*. https://doi.org/10.3758/bf03202828.
Wei, Ziqiang, and Xiao-Jing Wang. 2015. "Confidence Estimation as a Stochastic Process in a Neurodynamical System of Decision Making." *Journal of Neurophysiology*. https://doi.org/10.1152/jn.00793.2014.
Wimmer, Klaus, Albert Compte, Alex Roxin, Diogo Peixoto, Alfonso Renart, and Jaime de la Rocha. 2015. "Sensory Integration Dynamics in a Hierarchical Network Explains Choice Probabilities in Cortical Area MT." *Nature Communications* 6 (February): 6177.
Wimmer, Klaus, Duane Q. Nykamp, Christos Constantinidis, and Albert Compte. 2014. "Bump Attractor Dynamics in Prefrontal Cortex Explains Behavioral Precision in Spatial Working Memory." *Nature Neuroscience* 17 (3): 431–39.
Wyart, Valentin, Vincent de Gardelle, Jacqueline Scholl, and Christopher Summerfield. 2012. "Rhythmic Fluctuations in Evidence Accumulation during Decision Making in the Human Brain." *Neuron* 76 (4): 847–58.
Wyart, Valentin, Nicholas E. Myers, and Christopher Summerfield. 2015. "Neural Mechanisms of Human Perceptual Choice under Focused and Divided Attention." *The Journal of Neuroscience: The Official Journal of the Society for Neuroscience* 35 (8): 3485–98.
Yartsev, Michael M., Timothy D. Hanks, Alice Misun Yoon, and Carlos D. Brody. 2018. "Causal Contribution and Dynamical Encoding in the Striatum during Evidence Accumulation," August. https://doi.org/10.7554/eLife.34929.
Yates, Jacob L., Il Memming Park, Leor N. Katz, Jonathan W. Pillow, and Alexander C. Huk. 2017. "Functional Dissection of Signal and Noise in MT and LIP during Decision-Making." *Nature Neuroscience* 20 (9): 1285–92.
Zhang, Jiaxiang, and Rafal Bogacz. 2010. "Bounded Ornstein–Uhlenbeck Models for Two-Choice Time Controlled Tasks." *Journal of Mathematical Psychology*. https://doi.org/10.1016/j.jmp.2010.03.001.
Zylberberg, Ariel, Pablo Barttfeld, and Mariano Sigman. 2012. "The Construction of Confidence in a Perceptual Decision." *Frontiers in Integrative Neuroscience* 6. https://doi.org/10.3389/fnint.2012.00079.